UNIVERSITATEA DE ȘTIINȚE AGRICOLE ȘI
MEDICINĂ VETERINARĂ "ION IONESCU DE LA BRAD" IAȘI

LUCRĂRI ȘTIINȚIFICE
VOL. 58
MEDICINĂ VETERINARĂ

PARTEA 1

EDITURA "ION IONESCU DE LA BRAD" IAȘI 2015

ISSN: 1454-7406

CUPRINS

CAROTENOID PIGMENTS OF TOMATOES AND THEIR ANTITUMORAL POTENTIAL

DIANA CENARIU[1], ADELA PINTEA[2], EVA FISCHER-FODOR[3], MIHAI CENARIU[2], GIANINA CRISAN[1]

[1]University of Medicine and Pharmacy "Iuliu Hatieganu" Cluj-Napoca, Romania
[2]University of Agricultural Sciences and Veterinary Medicine Cluj-Napoca, Romania
[3]Institute of Oncology "Prof.Dr.I.Chiricuta", Cluj-Napoca, Romania
mihai.cenariu@usamvcluj.ro

Abstract: *The aim of this study was to show the influence of a tomato extract on hepatocellular carcinoma cells in vitro, proving their capacity to modulate the secretion of VEGF and ET-1 and thus demonstrating its inhibitory effect on tumor neovascularization. Human hepatocellular carcinoma cell line HepG2 was treated with a tomato extract, obtained from fresh tomato fruits. The expression of VEGF and Endothelin-1 by the treated cells, compared to an untreated control was assessed by ELISA. Our results proved that VEGF and Endothelin-1 expression was significantly diminished by the tomato extract, as compared to the untreated control. Therefore, our in vitro study showed that the carotenoid rich tomato extract is able to decrease tumoral neoangiogenesis in hepatocellular carcinoma and needs to be followed by clinical trials that could open new perspectives regarding the use of tomato carotenoids as adjuvant therapeutic agents.*

Key words: *carotenoids, tomato, antitumoral, neovascularization inhibition*

INTRODUCTION

One of the most frequent and dramatic neoplasm diagnosed in humans nowadays is hepatocellular carcinoma [1]. Various vegetables and fruits are recognized to contain antioxidants whose antitumoral potential was proven; carotenoid pigments of tomatoes, especially lycopene, have already been included in clinical studies [2]. Lycopene was shown to decrease proliferation of tumoral cells and inhibit neongiogenesis in some types of malignant or benign tumors: prostatic hyperplasia [3], prostate cancer [4] and colon adenocarcinoma [5]. Neoangiogenesis is one of the most frequent phenomena that occurs during the neoplasic disease and participates extensively to cancer proliferation and growth. Release of endothelin-1 (ET-1), a vascular growth factor, is inhibited by lycopene in normal endothelial cells [6, 7] and we also proved the same in colon adenocarcinoma [5]. Together with VEGF these growth factors are usually expressed by tumoral cells [8, 9] and are extremely important in modulating the activity of the vascular system.

Human HepG2 hepatocellular carcinoma cell line expresses ET-1 and VEGF and therefore was chosen for this study, in the attempt to prove that carotenoid pigments extracted from tomatoes are able to inhibit the secretion of such growth factors, and thus to decrease neoangiogenesis

The aim of this study was to show the influence of a tomato extract on hepatocellular carcinoma cells *in vitro*, proving their capacity to modulate the secretion of VEGF and ET-1 and thus demonstrating its inhibitory effect on tumor neovascularization.

MATERIALS AND METHODS

The human hepatocellular carcinoma cell line (HepG2) was obtained from the European Collection of Cell Cultures (ECACC, Salisbury, UK). The cells were grown in

Eagle's Minimum Essential Medium (EMEM) supplemented with 10% FBS (Sigma Aldrich, St Louis, MO, USA) at 37°C, 5% CO_2 and saturated humidity.

The carotenoid rich tomato extract was obtained from fresh tomatoes, using a classical method [10] characterized by HPLC and solubilized in tetrahydrofuran (THF, Sigma Aldrich), as previously described [5]. The extract had a total carotenoid content of 19.14 mg/ml.

After the cell cultures reached sub-confluence, they were trypsinized and seeded into 6-well plates where they treated with serial dilutions of the tomato extract, 0.1- 15 mg/ml, prepared with phosphate buffered saline (PBS, Sigma Aldrich). As the final ratio extract: culture media was 1:20, the active concentration was between 50 μg/ml and 950 μg/ml.

The ELISA assay was performed after 24 hours of cultivation in the presence of the extract. The supernates were collected and analyzed using a VEGF ELISA kit (BlueGene Biotech, Shanghai, China) and an Endothelin-1 kit (Cusabio Life Science, Wuhan, China). The pure protein concentrations for the standard curve were between 0 - 1000 pg/ml for VEGF and 0 - 200 pg/ml for Endothelin-1. All methods were specific for human samples and the sensitivity was below 0.7 pg. The methodology used was the one recommended by the manufacturers. Briefly, we used the antibody-coated plates from the kits; the standards and samples were pipetted into wells in triplicate. VEGF and ET-1 from the sample was allowed to bind with the specific antibody on the plate, followed by 4 subsequent wash steps. A biotin-conjugated antibody specific against human VEGF / ET-1 was added, washed, and avidin conjugated Horseradish Peroxidase (HRP) was added. After the last washing step, the substrate for HRP was added to the wells in order to develop a quantifiable color reaction, directly related to the amount of the targeted protein. The color reaction was stopped with sulphuric acid and the plate was read with an ELISA reader (Tecan Sunrise, Tecan Group, Männedorf, Switzerland), at 450nm. The results were created using the incorporated Magellan software. Normalization of the results was performed after counting the cells in each well and expressing the protein production to $5x10^5$ cells.

All experiments were performed in triplicate and the data was statistically interpreted using the Graph Pad Prism 5 biostatistics software (GraphPad Software, La Jolla, USA).

RESULTS

The amount of vascular endothelial growth factor (VEGF) was significantly lower in treated HepG2 cells, as compared to the untreated control (Fig.1) (One-way Anova test, Bonferroni post-test, in the 95% confidence interval, $p<0.01$).

The extracts also inhibited the ET-1 production in HepG2 cells treated with the carotenoid rich tomato extract, the decrease being very significant when compared to untreated control (One-way Anova test, Bonferroni post-test, in the 95% confidence interval, $p<0.01$) (Fig.2).

Antioxidants, like tomato extracted carotenoids have shown significant effects against hepatocellular carcinoma, while their great advantage when compared classical chemotherapeutic drugs is that they lack the important side effects [11]. Lycopene was shown to interfere with phosphoinositide 3-kinase (PI3K), Akt and Wnt signaling pathways in other types of tumors [12]. The tomato extract that was used in our research also had high lycopene content, as shown by our previously published data [5] and seems to act similarly against

HepG2 cells, showing a good potential to suppress neoangiogenesis by modulating vascular growth factors in vitro.

Since neoangiogenesis, the formation of new blood vessels in tumor mass is a critical step in tumor progression and metastasis; several therapeutic efforts are directed to develop new drugs which counteract this phenomenon [5]. The carotenoid rich tomato extract that was employed in the present work was able to significantly reduce VEGF and ET-1 production in HepG2 cells, therefore opening new perspectives towards its use in *in vivo* studies.

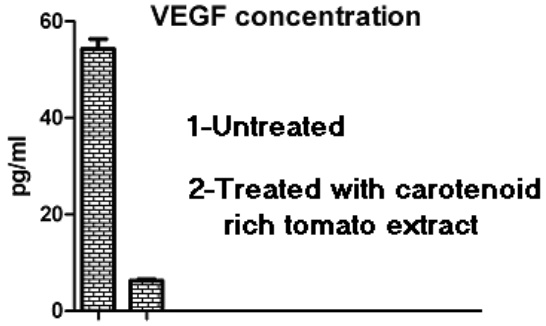

Fig. 1 VEGF concentration in untreated cells and cells treated with the carotenoid rich tomato extract; results are expressed in pg/ml and represent median values of three measurements. SEM is also shown, in the form of error bars

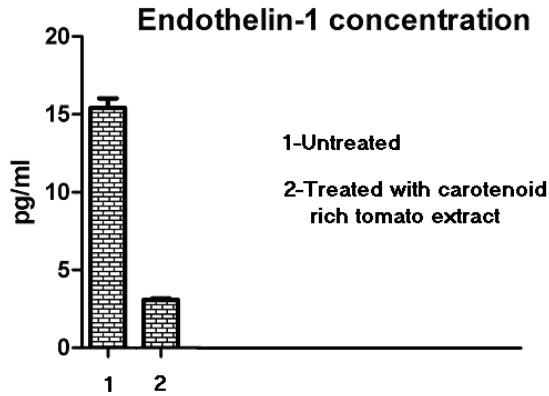

Fig. 2 Endothelin-1 concentration in untreated cells and cells treated with the carotenoid rich tomato extract; results are expressed in pg/ml and represent median values of three measurements. SEM is also shown, in the form of error bars

Endothelin-1 induces an increased DNA replication and therefore cell growth and proliferation, increasing mitosis through the activation of phosphoinositide 3-kinase signaling pathway [13]. The inhibitory effect of the carotenoid rich tomato extract shown in our study is of therefore great importance in decreasing the hepatocellular carcinoma cell growth. As our extract inhibited both VEGF and ET-1 production in HepG2 cell line *in vitro*, it is expected that PIK3 signaling pathway will be modulated as well.

CONCLUSION

Our in vitro experiments proved that the carotenoid rich tomato extract acts against hepatocellular tumor cells by reducing the tumor neoangiogenesis. It was able to significantly reduce the level of vascular growth factors VEGF and ET-1, therefore proving a significant antitumoral effect. The in vitro studies need to be followed by clinical trials that could open new perspectives regarding the use of tomato carotenoids as adjuvant therapeutic agents in hepatocellular carcinoma.

ACKNOWLEDGEMENTS

This paper was published under the frame of European Social Found, Human Resources Development Operational Programme 2007-2013, project no. POSDRU/159/1.5/S/136893.

REFERENCES

1. Cicalese L (2014). Hepatocellular Carcinoma. Medscape References. Drugs, Diseases and procedures. Available at: http://emedicine.medscape.com/article/197319-overview.
2. Breemen R.B, Pajkovic N. Multitargeted therapy of cancer by lycopene. Cancer Lett. 2008 Oct 8; 269(2): 339–351.
3. Minutoli L, Bitto A, Squadrito F, Marini H, Irrera N, Morgia G, Passantino A, Altavilla D. Serenoa Repens, lycopene and selenium: a triple therapeutic approach to manage benign prostatic hyperplasia. Curr Med Chem. 2013;20(10):1306-12.
4. Prauchner CA (2014). Angiogenesis inhibition by antioxidants. International Journal of Biomedical Science and Engineering. Special Issue: Cancer Research. Vol. 2, No. 6-1, 2014, pp. 7-19.
5. Cenariu D, Fischer-Fodor E, Virag P, Tatomir C, Pintea A, Cenariu M, Mocan A, Crişan G (2015). The in vitro effects of a tomato extract on neoangiogenesis-controlling molecules in colon carcinoma cells. SPASB 48(1):112-117.
6. Armoza A, Haim Y, Bashiri A, Wolak T, Paran E. Tomato extract and the carotenoids lycopene and lutein improve endothelial function and attenuate inflammatory NF-κB signaling in endothelial cells. J Hypertens. 2013 Mar;31(3):521-9. doi: 10.1097/HJH.0b013e32835c1d01.
7. Liu X, Qu D, He F, Lu Q, Wang J, Cai D. Effect of lycopene on the vascular endothelial function and expression of inflammatory agents in hyperhomocysteinemic rats. Asia Pac J Clin Nutr. 2007;16 Suppl 1:244-8.
8. Aktas SH, Akbulut H, Akgun N, Icli F. Low dose chemotherapeutic drugs without overt cytotoxic effects decrease the secretion of VEGF by cultured human tumor cells: a tentative relationship between drug type and tumor cell type response. Cancer Biomark. 2012-2013;12(3):135-40.
9. Takahashi K, Totsune K, Kitamuro T, Sone M, Murakami O, Shibahara S. Three vasoactive peptides, endothelin-1, adrenomedullin and urotensin-II, in human tumour cell lines of different origin: expression and effects on proliferation. Clin Sci (Lond). 2002;103 Suppl 48:35S-38S.
10. Breithaupt D.E., Schwack W. 2000. Determination of free and bound carotenoids in paprika (Capsicum annuum L.) by LC/MS. Eur Food Res Technol 211: 52–55.
11. Kasdagly M, Radhakrishnan S, Reddivari L, Veeramachaneni DN, Vanamala J. Colon carcinogenesis: influence of Western diet-induced obesity and targeting stem cells using dietary bioactive compounds. Nutrition. 2014;30(11-12):1242-56
12. Tang FY, Shih CJ, Cheng LH, Ho HJ, Chen HJ. Lycopene inhibits growth of human colon cancer cells via suppression of the Akt signaling pathway. Mol Nutr Food Res. 2008;52(6):646-54.
13. Kanwar SS, Yu Y, Nautiyal J, Patel BB, Majumdar AP. The Wnt/beta-catenin pathway regulates growth and maintenance of colonospheres. Mol Cancer. 2010;9:212.

RESEARCH MICROSCOPIC MORPHOLOGY OF LUNG IN SMALL RUMINANTS

VALERICA DANACU, STEFANIA RAITA, CARMEN IONITA, ANCA SEICARU
FMV Bucharest
valericadanacu@yahoo.com

Abstract: *Goat lungs contain within their structure intrapulmonary airways consisting of intrapulmonary bronchi, bronchioles and terminal bronchioles composed of pulmonary lobules, respiratory alveolar ducts and alveoli of the lungs. In the pulmonary stroma the parenchymal gap is made up of loose connective tissue and outside the pulmonary alveoli.*

Extra-lobular bronchi within pulmonary stroma have the following histological structure: mucosa, lamina propria, muscular mucosal tunic and the fibrocartilagenous adventitia. The terminal bronchioles wall is formed by an epithelium that is simple cubic and Clara cell secretory granules that present the apical pole.

Lamina propria is composed of smooth muscle and elastic fibers that gradually decrease and adventitia is reduced to extinction. Intralobular bronchioles or bronchi are located in the respiratory parenchyma lumen presents a characteristic festooned with pleats or folds mucosa showing longitudinal ciliated columnar epithelium simple with few goblet cells. In the respiratory bronchioles we find simple cubic epithelium and the alveolar epithelium is the ducts flattens. Alveoli presents a very thin wall papered by simple squamous epithelium.

Noted that the interalveolar septum consists of two layers of squamous cells separated by thin elastic fibers, fiber cross-linking, typically the capillaries, connective matrix and cells of alveolar septal cells or macrophages. Alveolar macrophages are located between alveolar epithelial cells or inside the alveoli and presents an oval-shaped nucleus placed excentric.

Alveolar epithelium shows cells arranged in a single row and consists of: First order pneumocytes or membranous pneumocytes, order II pneumocytes or pneumocytes granulosa with a brushed edge and alveolar macrophages. In the First-order alveolar cells they appear extremely flattened, with a heterochromatic nucleus that protrufes in the lumen and covers the alveoli. The second order alveolar cells appear interspersed among the first-order alveolar cells and appear clustered in interavleolar septa.They cubical spheroid core is centrally located and acidophile cytoplasm.

Keywords*: intrapulmonary bronchi, lung alveoli.*

MATERIAL AND METHODS

The research was conducted on permanent histological preparations made from sheep lung parenchyma from clinically healthy. For this purpose initiated an experiment examined microscopic lung morphology in small ruminants.

Histological specimens were prepared as follows: 10% formalin fixing, paraffin embedding and sectioning inclusion microtome. Large sections were stained on slides after staining following methods: hematoxylin eosin, hematoxylin eosin methylene blue staining and Mallory.

Histological preparations obtained were examined by light microscopy Labophot type 2 shooting device equipped with Nikon DX AFK-making photomicrographs.

RESULTS AND DISCUSSION

On histological examination is observed pulmonary stroma consisting of lung parenchyma and lax connective tissue outside the pulmonary alveoli (Figure 1).

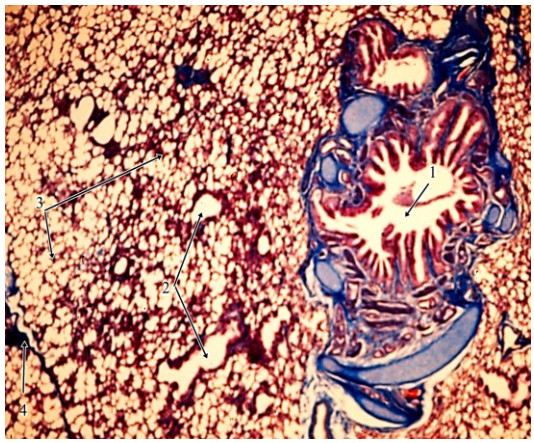

Figure 1. Sheep lung. (Mallory, ob.4x);
1-the extra-lobular bronchus; 2-terminal bronchioles;
3-pulmonary alveoli; 4-blood vessels.

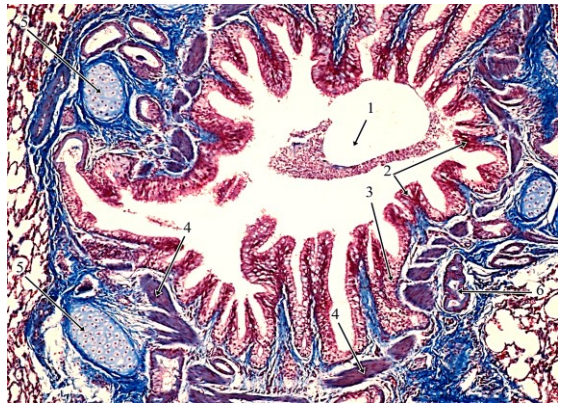

Figure 2. Extra-lobular bronchi. (Mallory, ob.10x)
1-lumenul bronchus; 2-pseudostratified ciliated columnar epithelium;
3-lamina propria; 4-bronchial muscle;
5-insule cartilage (nodules);

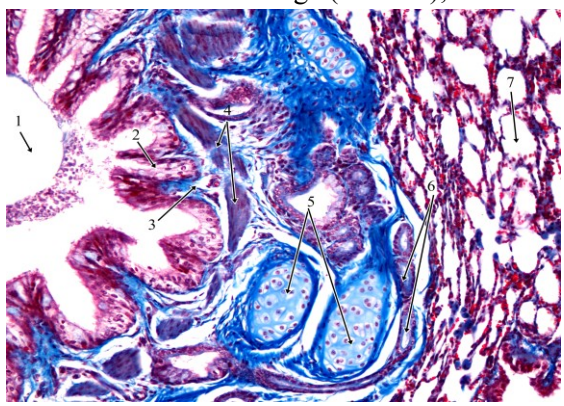

Figure 3. Extra-lobular bronchi. (Mallory, ob. 20x)
1-lumenul bronchus; 2-Pseudostratified ciliated columnar epithelium ; 3-lamina propria;
4-bronchial muscle; 5-islands of cartilage (nodules); 6-mucous glands.

Extra-lobular bronchial mucosa shows formed pseudostratified prismatic ciliated epithelium. Lamina propria consists of loose connective tissue fibers rich in elastic fibers, infiltration and lymphatic glands seromucoase. Muscular lining is composed of smooth muscle fibers arranged in circular or spiral, located between epithelial and cartilaginous skeleton and represents the continuation of tracheal muscle (Figure 3). Tunica fibrocartilaginosă is made up of the islands of cartilage tissue (Figure 6).

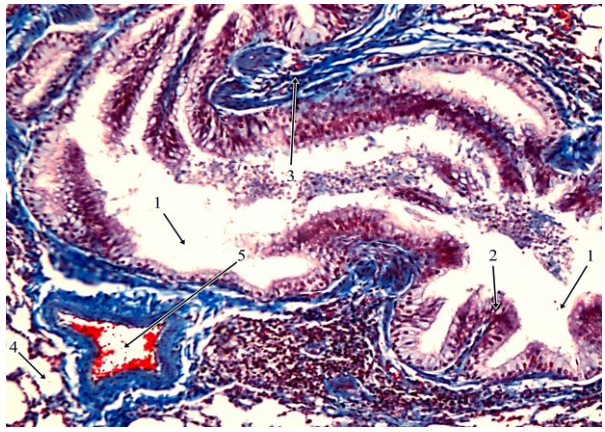

Figure 4. Sheep lungs. (Mallory, ob.20x)
1. intralobular bronchus; 2. epithelium; 3. bronchial muscle;
4. wafers; 5. blood vessel

Intralobular bronchi presents longitudinal folds mucosa, being composed of ciliated columnar epithelium simple, with few goblet cells (Figure 4). Bronchiolus terminal wall is formed of a simple cubic epithelium is located and Clara cells (Figure 5). Lamina propria is composed of smooth muscle and elastic fibers gradually decrease and adventitia is reduced to extinction (Figure 7). Respiratory bronchioles wall shows interrupted here and there by opening alveoli. The epithelium is simple cubic nonciliated simple squamous epithelium and alternate with alveolar type around the opening alveoli. Under the epithelium is a layer composed of smooth muscle and the elastic fibers arranged spiral.

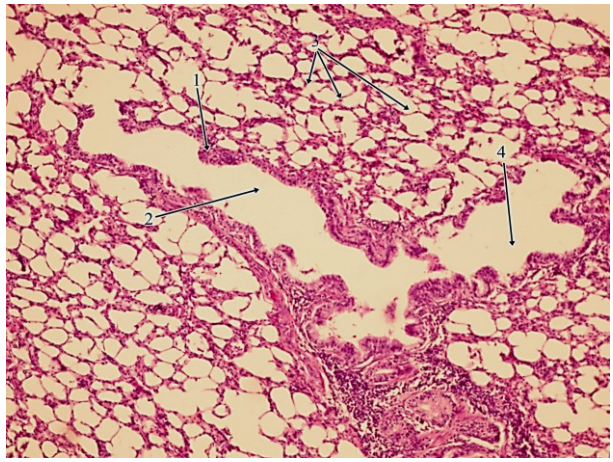

Figure 5. Sheep lung (HE, 10x)
1. epithelium terminal bronchiolitis; 2. alveolar duct.
3. pulmonary alveoli; 4. alveolar sac.

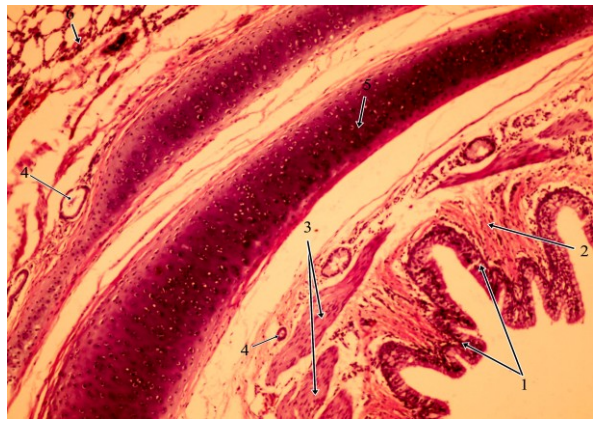

Figure 6. Extra-lobular bronchi. (HE, ob.20x)
1-pseudostratified ciliated columnar epithelium; 2-lamina propria;
3-bronchial muscle; 4-blood vessels; 5-islands of cartilage hialn; 6-adventitia.

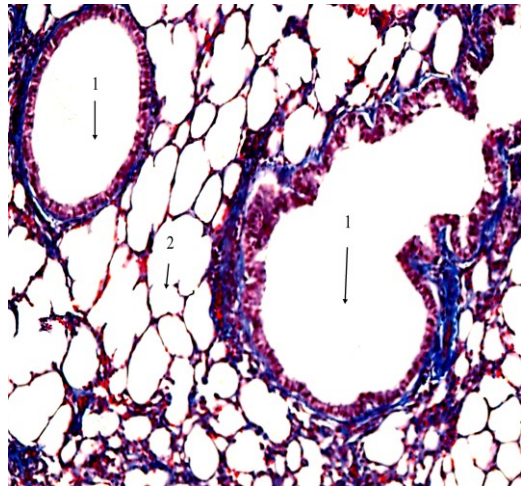

Figure 7. Sheep lungs. (Mallory, ob. 10x) 1. The terminal bronchioles; 2. pulmonary alveoli.

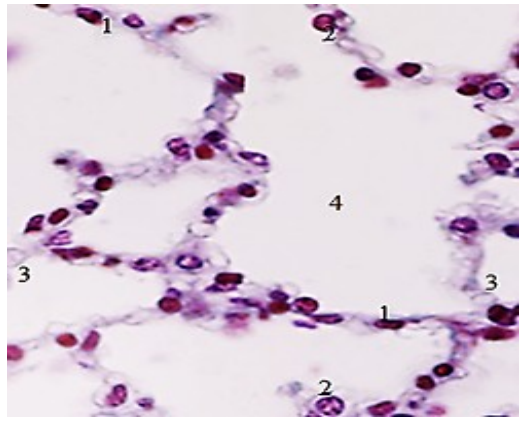

Figure 8.Detailed picture of lung alveoli (Mallory, ob.40x)
1-I pneumocytes order; 2-II pneumocytes order;
3-capillary; 4-alveolar sac;

Observe the respiratory bronchioles, alveolar ducts that continue representing narrow cylindrical space in which the wall of the pulmonary alveoli open.

Alveolar ducts are lined by simple squamous epithelium and lamina propria is extremely low. Smooth muscle fibers are arranged in a fine network interalveolar. It is noted that the alveolar sacs open orifices in the alveoli. Epithelium and the alveoli is similar in their walls and the elastic fibers are present cross-linking fibers arranged around the opening of the alveoli. Alveoli presents a very thin wall papered the squamous epithelium simple. Between two adjacent wafers is observed Interalveolar septum made up of two thin layers of squamous cells separated by elastic and reticular fibers, capillaries, connective matrix and alveolar macrophages.

Alveolar epithelium consists of pneumocytes of I, II pneumocytes or pneumocytes order granulosa edge pneumocytes and alveolar macrophages brush. I order pneumocytes were extremely flattened squamous having heterocromatic nuclei that protrude in the lumen. II pneumocytes are interspersed among pneumocytes order-order and appear clustered in two or three septumurile interalveolar (Figure 8). They cubical, spheroidal nucleus is centrally located and acidophile cytoplasm.

Pneumocytes with brush border are closely surrounded by pneumocytes of I realizing a contact surface and alveolar macrophages appear on the surface and inside the alveoli septa interalveolar.

CONCLUSIONS

1. The histological structure of the extra-lobular bronchi enter: mucosa, lamina propria, muscular mucosal tunic and adventitia fibrocartilaginoasă.
2. Extra-lobular bronchi mucosa epithelium is composed of ciliated pseudostratified prismatic
3. Lamina is made up of lax connective tissue fibers, while the muscle lining consists of circularly arranged smooth muscle fibers or spiral.
4. Islands of cartilage are present in the extra-lobular bronchi. They disappear instead of entering the lung lobe.
5. Adventitia consists richly vascularized connective tissue with numerous lymphoid infiltration in the bronchial branching.
6. Intralobular bronchi presents longitudinal folds mucosa, being composed of ciliated columnar epithelium simple, with few goblet cells.
7. In the respiratory bronchioles, lamina propria or chorionic presents lax connective tissue fibers that are willing diffuse lymphoid tissue.
8. Respiratory bronchioles wall shows interrupted here and there by opening alveoli, and this is where gas exchange is performed.
9. Acinar pulmonary respiratory lung parenchyma is the unit and consists of all pipes aerifere and respiratory cavities from one terminal bronchus.
10. Alveoli presents a very thin wall papered the squamous epithelium simple. Between two adjacent wells is a wall called interalveolar septum.

11. Alveolar epithelium consists of cells arranged in a single row and is formed by pneumocytes of I, II pneumocytes order, with pneumocytes and alveolar macrophages brush border.

REFERENCES

Cornila, N., Raita Stefania Mariana-Cell biology, histology and embryology, Vol II, Ed.Ceres Bucharest, in 2013.

1. Danacu Valerica-Histology and Embryology animal, Publishing Ars Docendi, Bucharest 2015
2. J. Elia, 2000. Response of bronchiolar Clara cells induced by the domestic insecticides. Analysis of CC10 kDa protein content. Histochem Cell Biol, Maldonado CA.
3. Fawcett DW., Jensh RP., 2002. Concise Histology, 2th. Ed. Arnold, London.
4. Gartner LP, Hiatt JL, JM Strum, Cell Biology and Histology 2011. BRS, 6th edition. Lippincott Williams & Wilkins, Philadelphia.
5. Ionita, L.,et.al. 2010 Research on variation of haematological parameters, blood chemistry and protein in horses with respiratory disease fractions, after taking herbal extract year (2010). ARS Docendi, Romanian Biotechnological Letters.
6. Mariana Pencheva Panayotova-Stancheva, Tsvyatkov Marin Alexandrov, 2010 Some Pathological Features of Lungs from Domestic and Wild Ruminants with Single and Mixed Protostrongylid Infections; Veterinary Medicine International
7. Hunter, K. S., et al. ,2010 In vivo measurement of proximal pulmonary artery elastic modulus in the neonatal calf pulmonary hypertension model of: development and validation ex vivo. Journal of Applied Physiology. 108, 968-975.
8. Mitchell GB, Clark ME, Caswell JL 2007. Alterations in the bovine bronchoalveolar lavage proteome induced by dexamethasone. Veterinary Immunology and Immunopathology.

RESEARCH ON SHEEP KIDNEY HISTOLOGICAL STRUCTURE

VALERICA DANACU, STEFANIA RAITA, ANCA SEICARU, CARMEN IONITĂ, ROSU PETRONELA
FMV Bucharest
valericadanacu@yahoo.com

Abstract: *Differential renal parenchyma into two distinct Areas: the cortex and medulla the. Cortical area is located in the external capsule, known as renal cortex is composed of: the narrow area adjacent to the renal capsule, called cortical area, corticis subcapsular or cortex; Called cortical area the labyrinth That is the cortical portion of the pyramids Ferrein; Bertin renal cortical columns That has extensions Between renal tissue is adjacent pyramids.*

The area contains cortical kidney renal corpuscles, distal convoluted tubules, proximal convoluted tubules. The area surrounded by the renal cortex is the medullary cortical areas and the layout of the pyramids Malpighi is uniform. The gap is made up of renal tissue rich in cells that CAN BE distinguished: fibroblasts, pericytes mononuclear bone marrow Located in the loops along the Henle, Vessels That supply. There is interstitial bone marrow Located in the cells Which is made up of cytoplasmic extensions That capillaries and tubules extend to the medulla. Located in Renal corpuscles have kidney and renal cortical columns HAVING relatively spheroidal aspect.

Proximal tubule nuclei have unequal compared to distal tubule arrangement has Numerous nuclei, WILLING equidistant. Medullary conical or pyramidal area consists of structures with aspect Called renal pyramids or pyramids Malpighi targeted to the renal hilum top and the base is directed Towards the cortex. The base of each pyramid to start overtime Malpighi tubules just look Entering the renal cortex and has Ferrein Called pyramids.

Cortical collecting tubules has papered of a simple cubic epithelium Which comprises two types of cells: clear cells that have the principal or many, have round nuclei and cells interspersed centrally located and dark, with cytoplasmic vesicles Numerous rare localized in the apical area. Medullary tubules collectors show columnar cell wall composed of small renal papilla cells and the level is high.

Keywords: *renal parenchyma, renal columns, Ferrein pyramids, pyramids Malpighi*

MATERIAL AND METHODS

Research on the kidney's histological structure were performed on histological to continuous from the renal parenchyma at the age of 9 months sheep. Histological specimens were prepared as follows: 10% formalin fixing, paraffin embedding and sectioning inclusion microtome.

Large sections were stained on slides after staining following methods: hematoxylin eosin, hematoxylin eosin methylene blue staining and Mallory. Histological preparations obtained were examined by light microscopy Labophot type 2 shooting device equipped with Nikon DX AFK-making photomicrographs.

RESULTS AND DISCUSSION

On histological examination it is noted that renal parenchyma differentiate into two distinct areas namely the cortex and the medulla (Figure 1). In the renal cortex observed cortical area consists of the cortex or cortex subcapsular corticis labyrinth renal cortical columns Bertin(Figure2).According to the literature, the meddular zone is made up of conical

or pyramidal structures with aspect called renal pyramids or pyramids Malpighi. From the base of each pyramid Malpighi start looking for straight tube extensions, which penetrate renal cortical and are called pyramids Ferrein (Figure 3).Renal pyramids conical or pyramidal structures are oriented toward the base to the tip of the capsule and the renal hilum.

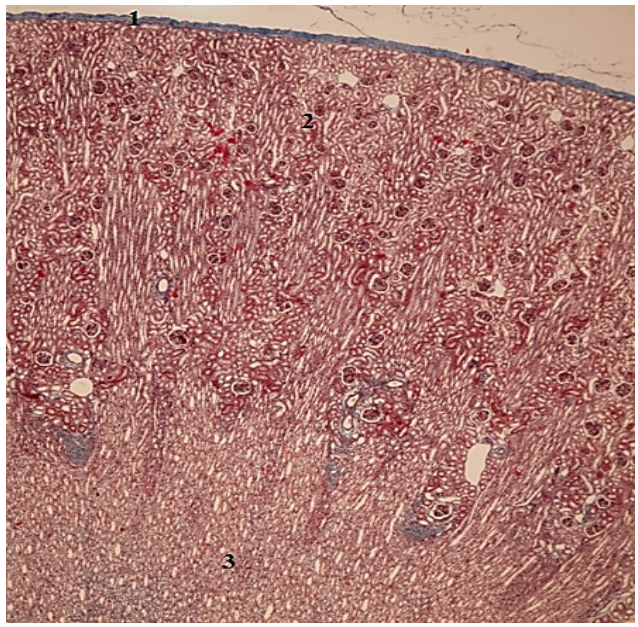

Figure 1. Histological structure kidney, Mallory stain, ob.4x.
1-the capsule; 2-cortical area; 3-medulla area

Proximal convoluted tubule is the longest segment of the nephron, being located in cortical labyrinth. It is coated by a single layer of epithelial cells, cubic or prismatic protruding microvilli conducting brush border.

On cross sections, proximal convoluted tubules shows 5-6 centrally located nuclei. At the apical pole of these cells are present ducts at the base of microvilli, pinocytosis vesicles, lysosomes merging with realizing complex role in endocytosis with low protein absorption.
Show a distal convoluted tubule lumen wider than proximal convoluted cells are smaller and less high acidofile weak(Figure 4).

Distal convoluted tubules significant differences proximal convoluted tubules compared namely the apical pole no brush border, nuclei are more cross-sectional surfaces and tubule lumen diameter and is larger than the proximal convoluted tubule.

The front of the tube distal convoluted shows a close association with glomerular afferent arteriole and efferent in the vascular pole of the renal glomerulus and the wall undergoes changes that achieve dense macula, part of the juxtaglomerular apparatus.

The collecting tubules are: cortical collecting tubule which are along the labyrinth pyramids Ferrein and medullary cortex and the collecting tubules which join together and form of the papillary channels, the urine drained by the tip of renal papilla, and then potassium basin.

Cortical collecting tubules are papered of a simple cubic epithelium which comprises two types of cells: the principal or clear cell and intercalated cells or dark cells.
The main cells or cells are numerous and show clear round centrally located nuclei.

Interleaved or dark cells, containing many rare and cytoplasmic vesicles located within the apical. Medullary tubules collectors show columnar cell wall composed of small renal papilla cells and the level are high with little organelles in the cytoplasm.

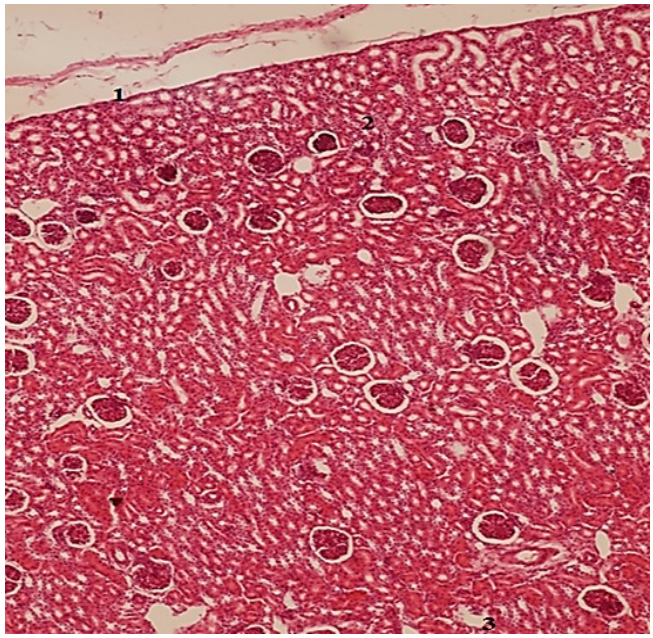

Figure2. Histological structure kidney-overview,
HE staining, ob.10x
1-the capsule; 2-cortical area; 3-medulla area.

Renal corpuscles present a vascular pole, consisting of arteriole efferent and afferent arteriole and urinary pole in the area of origin of the proximal convoluted tubule where parietal foil portion continues with proximal convoluted tube.

Podocytes are squamous epithelial cells that form the visceral layer of Bowman capsule.The cytoplasm of these cells show Golgi complex abundant mitochondria and RER rare underrepresented. Podocytes are heavily modified, presents a more complex form of overtime or primary processes, branching andforming secondary processes known pedicle surrounding the glomerular capillaries.

Podocytes were instrumental in phagocytosis and basement membrane regeneration.

The renal glomerulus is comprised of a cluster of capillaries that form vascular capillary mat located within the Bowman's capsule.The structure can differentiate glomerular endothelial cells that form the lining of the capillary. Preferring presents a fine and cytoplasm contains large fenestration.

The basal membrane is located between endothelial cells and podocytes. It is thick and contains three distinct areas: foreign rare lamina adjacent epithelium of foot; Lamina is an area thick dense, rich in type IV collagen fibers; domestic rare capillary endothelium adjacent lamina.

Mesangial interstitial tissue is present between glomerular capillaries. In its structure enters mesangial cells and extracellular matrix developed by these cells.

Mesangial cells present cytoplasmic extensions that protrude into the lumen through the endothelial cells. They provide support to podocytes where the basement membrane is missing or incomplete. They are also involved in phagocytosis large protein molecules.

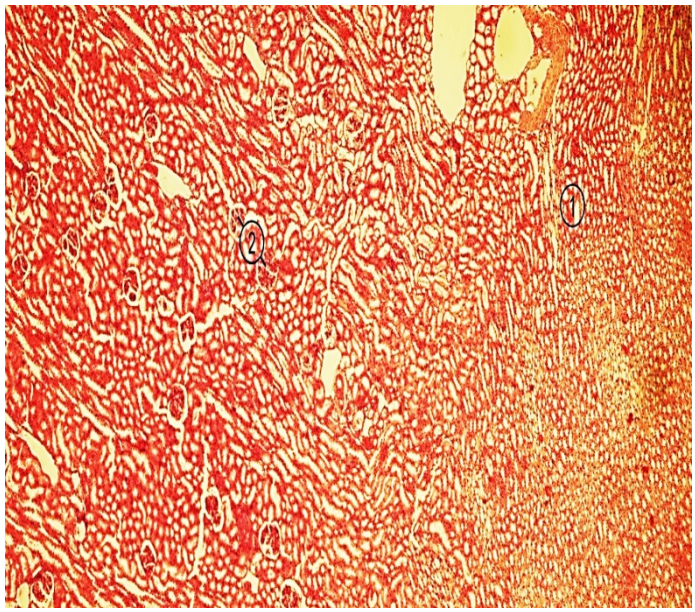

Figure 3. Section through the kidneys, HEstaining , ob.4x.
the cortex and the medulla:
1-Tubes straight; 2-Malpighi pyramids.

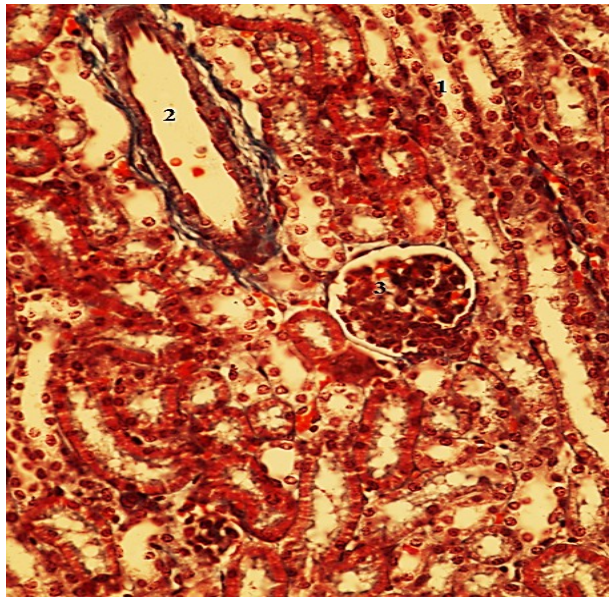

Figure 4. Kidney-cortical area, Mallory staining, ob. 20x
1-tubules collectors; 2 blood vessel; 3-renal corpuscle.

Renal corpuscle circumscribed formation, which is found in cortical labyrinthine zone. Renal corpuscles consists of two components: Bowmann capsule wall made of double epithelial and vascular glomerulus consists of a ball of capillaries (Figure 5).

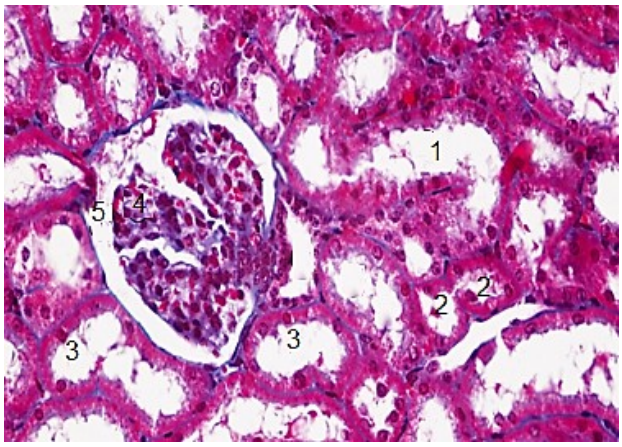

Figure 5. Kidney sections staining Mallory-cortical area,ob.40x;
1-tube collector; 2-proximal convoluted tubules;3-distal convoluted tubules; 4-renal corpuscle; 5-Bowman capsule

Bowmann capsule is the initial portion of the nephron, which delimits the renal glomerulus. It has a double wall showing two skins: an external parietal foil and visceral internal foil. External parietal foil bounding renal corpuscles and presents simple squamous epithelium. Wrap foil internal visceral glomerular capillaries consisting of glomerular epithelium, simple squamous amended, consisting of podocytes (Figure 6).

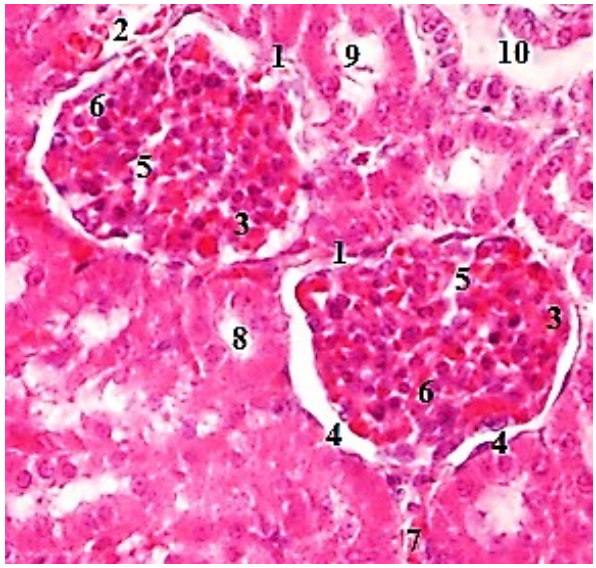

Figure 6 Parenchymal renal cortical area,HEstaining ob.40x;
1-renal corpuscle; 2-Bowman capsule; 3 glomerulus vascular; 4-podocytes; 5-glomerular capillary; 6- cell mesangial; 7-arteriole; 8- proximal convoluted tube; 9-distal convoluted tubules; 10-tubules collectors.

CONCLUSIONS

1. Cortical and medullary area of the two kidneys appears normal limits and stains used have revealed structures that traverzează two areas.
2. Glomeruli occurred to normal size, clutter inside the capillary vascular capillaries that make up ghemeul arranged inside the capsule Bowman.
3. The region of Bowman capsule constitutes the initial portion of the nephron and limit the renal glomerulus is formed by a double wall.
4. Malpighi pyramids were characterized by the conical structure of the base facing the inner periphery presenting mesangial cells which act as support for the glomerular capillaries.
5. In the proximal convoluted tubule nuclei were identified with the level of which appear uneven arrangement which carries brush border microvilli.
6. Distal convoluted nuclei consists of many and has a wider lumen compared to the proximal convoluted tubule.
7. Tubii collectors cortical are papered of a simple cubic epithelium which comprises two types of cells: the principal or clear cells are numerous, have round nuclei and cells interspersed centrally located and dark, with numerous rare cytoplasmic vesicles located within the apical .
8. Tubii collectors marrow wall composed of columnar cells shows small renal papilla cells and the level are high with little organelles in the cytoplasm.

REFERENCES

1. Aughey E.,Free F.L. - Comparative VeterynaryHistology with Clinical Correlatees, Manson publishing, 2010.
2. Cornilă, N., Raita Ștefania Mariana-Biologie celulară, histologie și embriologie, Vol II, Ed.Ceres Bucuresti, 2013.
3. CiocalteuA -Treaty of Nephrology. National Publisher., 2006, 17-31
4. Eleanor K L Mitchell et. all. -Nephron Endowment and Filtration Surface Area in the Kidney after Growth Restriction of Fetal Sheep, 2004
5. Dănacu Valerica- Histology and Embryology Animal Docendi Ars Publishing, Bucharest 2015
6. Gartner I P.,Hiatt J.L.-Concise Histology,Saunders Elsevier,2011
7. Ioniță L, Ionita C, Ivana S, Ipate I., Toba G. F, Tanase A, Danacu V, Trambitas B., Retea , 2011-The role and the place of nutritional-metabolic pathology in ruminants, in the context of world food crisis**,** Scientific Works - University of Agronomical Sciences and Veterinary Medicine, Bucharest Series C, Veterinary Medicine.
8. Kierszenbaum A.,-Histology and Cell Biology:An introduction to Pathology .Ed.Elsevier Healt Sciences, 2011.
9. Solcan Carmen- Histology and Embryology, Ed.Performantica, Iasi, 2006.

MORPHOPATHOLOGICAL STUDY OF MYXOMATOSIS IN RABBITS

GRIGORE DUMITRAȘ, NICOLAE NAFORNIȚA
State Agrarian University of Moldova
Chisinau, Republic of Moldova
grigore.dumitras@gmail.com

Abstract: Morphopathological study of myxomatosis in rabbits
Myxomatosis in rabbits develops in two main forms: edematous and nodular. Edematous form is characterized by inflammation of the eyelid and conjunctiva. The head of a rabbit suffering from myxomatosis is like a lion's head. Nodular form grows on the head, ears, eyelids, representing some growths that can merge with other parties giving ugly rabbit form.

Key words: *myxomatosis, myxoma, edematous, form, nodular*

INTRODUCTION

Myxomatosis description was made for the first time by Sarelli in 1896, which signaled the disease in wild rabbits in Uruguay [1]. Later it was recorded in Brazil, Mexico and USA. It seems that in Australia and Europe the disease remained unknown in the first half of the twentieth century, although there are opinions according to which it should be reported in these countries, but not expand. Then the disease spread to many countries in the world [2, 3, 5]. It was shown that myxomatosis is a disease caused by a virus that attacks only rabbits, both the domestic and wild rabbit population. There are several strains of the virus that manifest themselves in a different way. Most often the disease is transmitted by the bite of mosquitoes, fleas, lice or ticks and in many cases is fatal. This disease can also be transmitted through direct contact between rabbits or by air. In some cases, transmission is carried out indirectly through food or bedding vessel, their master can transmit the virus from infected to the healthy rabbit. Animal exhibitions are just another important source of infection, there is a possibility that a carrier rabbit pass on the virus [2, 3].

The evolution of the disease progression can be slow in case of very well cared rabbits and sometimes there are chances of healing them by intensive care. However, myxomatosis can be a very serious and long-term disease and, most often, it is recommended euthanasia of the sick animal [4, 7].

Republic of Moldova is like those European countries in which myxomatosis has caused a great damage. Currently it is trying to control the spread of myxomatosis by vaccinating rabbits flock. However, the disease often occurs in individual sectors, causing great damage to peasants. In our country myxomatosis was poorly studied in terms of pathology and therefore we proposed morphopathological study of this disease.

MATERIAL AND METHODS

The morphological study of myxomatosis in rabbits was conducted on pathological material obtained from 5 corpses of rabbits aged from 4 to 6 months belonging to Soldanesti town residents. The autopsy was performed in the necropsy room of veterinary clinic in the town.

After macroscopic examination of internal organs, modified visceral portions of which were cut for histopathological research. Initially organ portions were washed for a day under running tap water to remove the substrate fixer.

Subsequently, the concentration and dehydration of the portions of the tissue pieces were passed through alcoholic solutions with concentrations from 60 ° to 100 °, for each 24 hours. This was followed by the passage of pathological material through the portions of the alcohol-chloroform for 12 hours, then the pieces of organs were embedded in paraffin liquid.

After pouring pathological material in paraffin blocks, the latter were installed in sliding microtome. As a result of sectioning the paraffin block histopathological pieces with a thickness of 8-10 microns were obtained which were stained with hematoxylin-eosin.

RESULTS AND DISCUSSION

Macroscopically, we determined that myxoma tumor appears as a single, circular or lobular, which can reach considerable size in deep soft tissues. The tumor is not encapsulated or only partially encapsulated, enclosed in the surrounding tissues or infiltrative and often relapsing after surgical removal. Tumor mass has a soft consistency, and the translucent section presents a swollen aspect, sometimes with cystic and hemorrhagic areas, our data are consistent with the results observed by Marlier D. and colleagues in experimental infection [4].

By our observations, myxomatosis quickly disseminate, mortality hovering at a level of 95-100%. According to the literature, the animals passed through the disease become immune, being carrying and eliminating the virus [3]. After an incubation period of 4-5 days, the disease begins with fever, rhinitis and serous conjunctivitis, which then becomes mucopurulent, followed by swelling of the eyelids, scalp (especially the nose), then appear myxomas of the ears, eyelids, nose, genitals and limbs.

Myxomatosis in rabbits develops in two forms: edematous and nodular. Of the five dead bodies of myxomatosis rabbits, two showed changes of edematous form and three – of the nodular form. Edematous form is characterized by inflammation of the eyelids and conjunctivitis. As a result, the eyelids become mate, ocular secretions appear, develops serous rhinitis. On the surface of the head, in the region of the anus, the external reproductive organs there are present masses of gelatinous edema as 3-5 cm size formations. Sick animals are diverging, and the temperature of their bodies rises to 41.4 ° C. Rabbits, usually refuse feed, and as a result, decrease in the weight. Visible mucous membranes are cyanotic, breathing becomes more difficult. Head sick rabbit myxomatosis is that „a lion head". Malignant disease is manifest and lasts 4-10 days, sometimes five weeks, ending with the death of animals.

If in the beginning of the disease fever and anorexia install, then further progression of the disease may take the form of nodular usual form. Nodular form develops on the head, ears, eyelids, constituting some growths that can merge with other parties giving ugly rabbit form. After about 2 weeks of nodules formation foci of necrosis appear which in case of a benign evolution, usually heal.

Nodular form can be acute, subacute, or benign. The disease begins with the appearance conjunctival secretions, initially serous then mucopurulent. Secretions are followed by subcutaneous connective tissue edema in the head, especially the muzzle and

myxomatous pseudotumor formation. In the next phase of tumor nodules can be generalized by their spreading to limbs, scrotum, lungs and thorax and as a result, the animal is weak and often presents serious respiratory disorders.

In the acute form the animal death occurs in most cases in 2-10 days. In subacute form myxomas are less numerous, sick animals weaken significantly and present respiratory abnormalities. Duration of the disease is 2-4 weeks. In the fatal case the skin covering the myxoma forms crusts and then fall off with the pseudotumoral tissue [2].

Benign forms are found in more resistant animals from a genetic point of view or in those descending from immune mothers. In these animals the disease is characterized by easy development with unchanged general condition, with few pseudotumors, located mostly on the head, which are necrotized and then quickly blistered. The disease, in most cases, ends with a complete healing of the animal.

Edematous form, as well as nodular forms, begins with conjunctivitis and mucopurulent discharge, then blepharitis and dyspnea can add, sometimes hidden papules on the ears. The female rabbits abortion or infertility may occur. In all cases of disease bacterial complications are quite common. The overlapping of secondary infections, particularly Pasteurella, is characterized by fibrinous pneumonia lesions. At necropsy of rabbit corpse there are few characteristic lesions. It highlights splenomegaly, swollen lymph nodes, subcutaneous connective tissue, especially at the level of pseudotumors, is edematous.

Pseudotumors are of different sizes, with characteristic appearance, non-adherent to the underlying subcutaneous tissue, smooth surface on section, yellowish, gelatinous, with intensely vascularized peripheral area. Lymph nodes, lungs, gonads and other internal organs are congested. In the histopathological study it was determined that mesenchimatous pseudotumors consist of mucoid connective tissue, similar to that of Warton gelatin from umbilical cord, no cases in adult tissues.

Myxoma is made of rare cells, stellate or spindle-shaped, with extra long, thin, apparently anastomosed, spread in a basic substance, which is amorphous, mucoid, rich in mucopolysaccharides, in particular in hyaluronic acid, metachromatic to toluidine blue staining. Cells have cytoplasm in a moderate amount, clear, with fine vacuoles and nuclei that are relatively large, round or oblong, with a well defined chromatin network. The fundamental substance mucoid can highlight reticulin fibers and collagen. The blood vessels are rare. In some areas of tumor and perivascular areas tumor cells may be more numerous and round, without processes.

Microscopically, we determined baloon degeneration of the spinous layer of skin epithelium, hyperacantosis and in the cytoplasm of epithelial cells we found inclusions or Splendore's bodies. In the dermis and hypodermis histopathological investigation revealed hyperplasia and swelling of endothelial of capillaries with lumen obliteration, with fibrinoid degeneration and thrombosis of capillaries, a fact noted by P. Marcato and colleagues [3]. Simultaneously pericytes proliferate takes place that are located like bulb onions.

We noticed a serous exudation and bleeding with excess of eosinophils in dermohypodermic foci like in the research of J. Patterson-Kane [6]. Collagen fibers are fluidified and present cells are big with cytoplasmic extensions and bulky looking brindle cores. In myxomatous cells Splendore bodies can be identified.

In the lymph nodes hyperplasia of reticular cells with epithelial transformation and giant polynucleic cells (polykariocytosis), regression of lymphoid tissue (kariorexis and atrophy), proliferation of hyperbasofile immature cells, hyperplasia of capillary endothelium, bleeding and necropurulent microfoci are found.

Our observations are consistent with literature data, according to which certain histopathological changes should be applied for differential diagnosis of myxomatosis with pastereulosis, staphylococcal disease, spirochetosis, oral papillomatosis, Shope papilloma and rabbits infectious rhinitis [7]. Like in our study, they indicate systemic nature, rabbits polyorganic damage of the rabbits with dystrophic changes and bleeding in vital organs - the myocardium, liver, kidney, brain, involving small caliber vessels of panvasculitis type. Therefore, we have not only histopathological confirmation of systemic inflammatory response syndrome, but also morphological substrate of multiple organ failure syndrome, which explains the high mortlality described by several authors in myxomatosis [1, 4, 5, 7] .

CONCLUSIONS

1. Myxomatosis is a viral very serious infectious disease of rabbits, especially those domestic and some species of the wild ones, mainly characterized by mucosal swelling and the presence of pseudotumors called myxomas. Nodular form of myxomas grows mainly on scalp and genitals. Edematous form is characterized by blepharoconjunctivitis with dead eyelid, eye discharge and rhinitis.
2. Histopathological lesions of myxomatosis in rabbits include: mesenchimatous pseudotumors consisting of mucoid connective tissue, similar to umbilical cord; tumor cells with moderate cytoplasm and fine vacuoles, with the relatively large round or oblong nucleum; dermohypodermic foci with serous exsudation, bleeding, fluidifying of collagen fibers; hyperplasia of reticular cells, giant polynucleic cells, bleeding and necroopurulent microfoci in the lymph nodes.

BIBLIOGRAPHY

1. Calvete C., Estrada R., Villafuerte R., Osacar J.J., Lucientes J. Epidemiology of viral haemorrhagic disease and myxomatosis in a free-living population of wild rabbits. Vet Rec. 2002; 150 (25): 776-782.
2. Kerr P. J., Best S. M. Myxoma virus in rabbits. Rev Sci Tech Off Int Epizoot. 1998; 17: 256–268.
3. Marcato P.S., Simoni P. Ultrastructural researches on rabbit myxomatosis. Lymphnodal lesions. Vet Pathol. 1977; 14 (4): 361-367.
4. Marlier D., Cassart D., Boucraut-Baralon C., Coignoul F.,Vindevogel H. Experimental infection of specific pathogen-free New-Zealand white rabbits with five strains of amyxomatous myxoma virus. J Comp Path. 1999; 121: 369–384.
5. Merchant J.C., Kerr P.J., Simms N.G., Robinson A.J. Monitoring the spread of myxoma virus in rabbit Oryctolagus cuniculus populations on the southern tablelands of New South Wales, Australia. Natural occurrence of myxomatosis. Epidemiol Infect. 2003; 130 (1): 113-121.
6. Patterson-Kane J. Study of localised dermatosis in rabbits caused by myxomatosis. Vet Rec. 2003; 152(10): 308.
7. Wunderwald C., Hoop R.K., Not I., Grest P. Myxomatosis in the rabbit. Schweiz Arch Tierheilkd. 2001; 143(11): 555-558.

DEOXYRIBONUCLEIC ACID INTERACTIONS SPECIFIC TO BIOCHEMICAL INJURY INDUCED BY SOME CARCINOGENIC XENOBIOTICS

ZENO GÂRBAN[1,2], NICOLAE MANOLESCU[3,4], GHEORGHE DĂRĂBUŞ[5], ADINA AVACOVICI[2],FLORIN MUSELIN[5], JELENA SAVICI[5], ROBERT UJHELYI[2,6], SERGIU MICLOŞONI[5]

1. University of Agricultural Sciences and Veterinary Medicine of Banat "King Michael I of Romania" Timişoara, Faculty of Food Products Technology, Romania
2. Working Group for Xenobiochemistry, Romanian Academy-Branch Timişoara,
3. University of Agronomic Sciences and Veterinary Medicine Bucharest, Institute of Comparative Medicine, Romania
4. "Al. Trestioreanu" Institute of Oncology, Bucharest, Romania
5. University of Agricultural Sciences and Veterinary Medicine of Banat "King Michael I of Romania" Timişoara, Faculty of Veterinary Medicine, Romania
6. S.C. CaliVita International, Medical Department, Timişoara, Romania

zeno.garban@yahoo.com

Abstract: *At the origin of the neoplastic processes in which deoxyribonucleic acid is involved, one can mention as trigger factors a great number of xenobiotics which are present in the air, feedstuffs, foodstuffs and water having harmful effects on animals and humans. Xenobiotics of various sources : chemical (organic and inorganic compounds), physical (ionizing radiations, UV radiation) and biological (oncoviruses) can become carcinogenic agents.Submitted as a review the aim of this paper is to give data on the molecular mechanisms inducing biochemical injuries as a consequence of the interaction of deoxyribonucleic acid (DNA) with various chemical compounds. The interactions of DNA with the following organic compunds are discussed : aflatoxins (AF), polycyclic aromatic hydrocarbons (PAH), aromatic amines and the following inorganic compounds : some metal ions (M^{n+}) with toxicogene potential; nitrates (NO_3^-) and nitrites (NO_2^-). These interactions are of interest for comparative medicine due to their pathobiochemical and pathophysiological aspects. All the above mentioned adducts are frequently discussed in pathology being at the origin of the biochemical injury which can evolve to a carcinogen process. Initially the nuclear DNA is damaged and further on the cell. If the pathological process develops the result is the formation and growth of a neoplasm.*

Key words*: deoxyribonucleic acid, biochemical injury, xenobiotics*

INTRODUCTION

Deoxyribonucleic acid (DNA) is a macromolecule that contains the genetic information which controls the biological development of all cellular forms of life. In the environment (air, water, foods) there are numerous substances considered as chemical xenobiotics which can interact with DNA, altering its structure, and giving rise to adduct genesis. As a result of such interaction mutagen, carcinogen and teratogen processes can be triggered (Knudsen, 1989; Ames et al., 1993; Nassar, 2010).

Such chemical xenobiotics (organic or inorganic) can get into the organism by food along with nutrients and water intake as well as by air breathing or skin contact (Arcos et al., 1996; Kohlmeier, 2003; Creppy et al., 2005; Gârban, 2007). Among the organic chemical xenobiotics the most discussed for their carcinogenic effects are those with cyclic structure,

like: polycyclic aromatic hydrocarbons (PAH), mycotoxins, monomethyl aminoazobenzene (MAB), steroidic compounds (Bannett and Klich, 2003; Manolescu, 2003; Luck, 2005) and organic pesticides (Brooks and Roberts, 1999). All the chemical xenobiotics mentioned before give rise to adducts with DNA, e.g.: the benzo(a)anthracene, a well-known PAH, by binding to the adenine of DNA forms an adduct of type DNA-B(a)P ; MAB forms with DNA the adduct DNA-MAB; aflatoxins, especially AFB_1 , by binding to guanine forms the DNA-AFB_1 type adduct. Regarding the inorganic chemical xenobiotics it is known that potentially toxicogen metal ions like Cd^{2+}, Hg^{2+}, Sn^{2+} can bind to DNA giving rise to adducts of the DNA-M^{n+} type while nitrates converted into nitrites generate (in vivo) nitrozamines which further on form intermediate compounds and finally one of them alkylate to DNA.

In the present review issues related to pesticides, compounds of great importance in xenobiochemistry, are not approached because of their very extended domain. Data concerning organochlorine and organophosphorus compounds as well as carbamate and thiocarbamate will be exposed in a next work dealing with their interactions and biomedical effects. Knowledge on the structural peculiarities of DNA can allow a better understanding of the appearance of DNA adducts and carcinogenesis.

1. Structural characteristics of DNA - general aspects

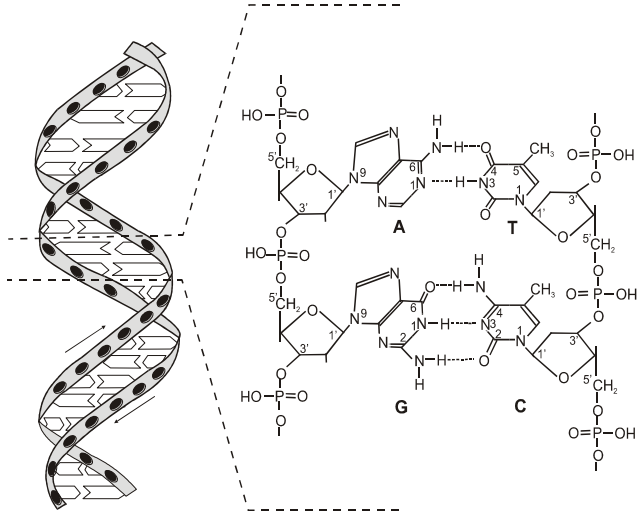

Fig. 1. DNA macromolecule (structural formula)

DNA is a macromolecular biopolymer ubiquitously spread in the animal and vegetal reign and constitute the genetic material of micro- and macroorganisms. This macromolecule is composed of building blocks called nucleotides. Each nucleotide consists of deoxyribose, a phosphodiesteric group and one of four nitrogen containing bases – adenine (A), thymine (T), guanine (G) and cytosine (C). Phosphates and deoxyribose of the adjacent nucleotide link to form a monostrand. In the DNA macromolecule there are two strands (fig.1) .

The nucleobases from one strand bind to the nucleobases from another opposite strand to form a double-stranded structure. The binding takes places according to the Watson

– Crick model: adenine forms two hydrogen bonds with thymine on the opposite strand, and guanine forms three hydrogen bonds with cytosine on the opposite strand.

2. Chemical injury of DNA and biogenesis of adducts

Experimental investigations initiated in 20th century regarding the interaction between DNA and small molecules of chemical xenobiotics revealed the appearance of some biologically non-compatible structures that, initially were named "molecular complexes". This denomination was considered inadequate and, later on, due to years of physical-chemical investigations and mechanic-quantum calculations over the electronic density they were named "molecular associations". Studying more thoroughly the donor-acceptor relationship between DNA and small molecules, the term "adducts" was preferred (Phillips, 2005). One of the major challenges in biochemical pathology (pathobiochemistry) was to define the structural and chemical basis for carcinogenesis and mutagenesis induced by DNA injuries (Wassom, 1980; Ames et al., 1993).

A great number of molecules present in our environment, i.e. water, foods, air can interact with the DNA macromolecule and give rise to adducts which are biologically non-compatible and will disturb the structure-activity relationship, alter the genetic information transmission and lead to mutagen, carcinogen or teratogen processes. Such interactions may affect the DNA template during replication, as well as mRNA, tRNA or one of their nucleotide precursors. Disturbances in the transmittance of genetic information, in the biosynthesis of amino acids – constituents of specific proteins – will lead to possible oncogen and teratogen effects. Damage to mitochondrial DNA (adducts and mutations), mitochondrial membranes, increased cell death (thanato-citosis) and disruption of ATP production can be produced, too. Biogenesis of DNA adducts occurs not only during the metabolization of nutrients but also in the case of the biotransformation of chemical xenobiotics (Poirier and Beland, 1992; Gârban, 2011). In fact, DNA adducts may be formed with various organic and inorganic compounds considered as xenobiotics of nutritional, pharmacological and toxicological interest. Further on structural data is presented on various xenobiotics and on structures of certain adducts formed after interactions.

3. Interactions with organic compounds

3.1. Interaction with aflatoxins

Data of FAO/WHO show that the number of known mycotoxins counts over 200 types, are the secondary metabolites of different varieties of moulds and highly toxic for both animals and humans (Bannett and Klick, 2003). These toxins are produced when moulds grow on agricultural products or after harvest or during transportation or storage.

Aflatoxins as secondary metabolites of fungi have been identified and isolated in the period 1961-1962. Aflatoxins – the most toxicogen mycotoxins, are produced by different species of *Aspergillus* as well as members of the species *Penicillium* and *Rhizopus*. *Aspergillus flavus* produces aflatoxins B_1 and B_2 while *Aspergillus parasiticus* produces aflatoxins B_1, B_2, G_1 and G_2. The interest for the knowledge of the chemical structure-biological activity as well as of the aspects related to the pathobiochemistry and

pathophysiology concerning mycotoxins generally, and aflatoxins especially, focused the theoretic and applicative scientific preoccupations on the environment, food quality and safety in relation with their effects on public health (Podar et al., 1982; Gârban and Daranyi, 2000). Aflatoxins are present in the food chain. They have been found in human cord blood and can enter into the developing fetus in humans and animals. Exposure to mycotoxins is mostly by ingestion (contaminated grain and cereals as well as contaminated animal products) but also occurs by the dermal and respiratory routes. Food contamination has been implicated in both animal and human aflatoxicosis. The toxic response varies in relation to species, sex, age, nutritional status, duration of intake and level of aflatoxin in the ration.

In the structure of aflatoxins (Fig. 2) one can remark monoheteroatomic heterocycles (furan, pyran), partially hydrogenated, where oxygen is the heteroatom. Structural formulas have been established by spectroscopy and crystallography. Aflatoxins belong to more structural types designated depending on: the blue fluorescence and noted AFB_1, AFB_2; the green fluorescence AFG_1, AFG_2 in ultraviolet light; according to the source of origin: milk AFM_1, AFM_2 and others: AFQ_1, AFP_1 .

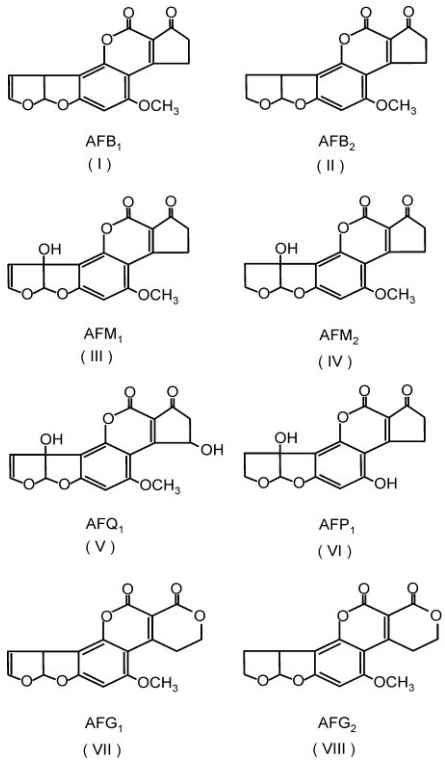

Fig. 2. Aflatoxins – structural formula

Beside the mentioned structures there have been isolated oxydrilated and methoxylated derivatives in various positions of the polycycles. Sometimes these have been considered new types of aflatoxins, but in fact they represent steps of the metabolization of initial compounds.

Predilectly AFB_1 and AFG_1 present high reactivity, which have an unsaturated side heterocycle (of furanic type). The biologic activity and toxicity decrease in the series: $AFB_1 > AFG_1 > AFG_2 > AFB_2$

Aflatoxin B_1 (AFB_1) is the major mycotoxin produced by most species under culture conditions. Because of this and its toxicity, B_1 is the most frequently studied. AFB_1 is a potent toxin ivolved in the ethiology of hepatocarcinoma. It is relatively non-reactive until it is ingested and converted by liver enzymes to the reactive intermediate AFB_1 8,9-oxide.This metabolite reacts with DNA and forms DNA-AFB_1 type adducts at the N_7 position of guanine.

The mechanism of action of aflatoxins consists in their interaction with the nucleic acids. During interaction, the extension and distorsion of the double helix takes place and, finally, the breaking of hydrogen bonds between the nucleobases A-T and G-C. Due to the high electron density of some atoms such as N_7 of guanine and O from C_4 of thymine, these ones present a high reactivity and accesibility for the interaction with an external chemical agent – see fig.3 .

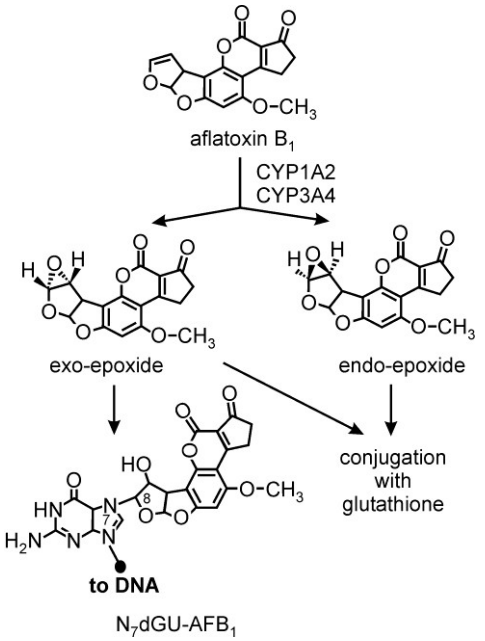

Fig. 3. Biotransformation of AFB_1 – genesis of glutathione-conjugates and DNA- AFB_1 adduct (type N_7dGu-AFB_1)

Human organisms metabolize AFB_1 to an 8,9-epoxide forming DNA and albumin adducts by the same activation pathways as susceptible animal species. Glutathione-S-transferase-mediated conjugation of glutathione 8,9-epoxide reduces DNA damage and this mechanism is important in reducing tumors.

These adducts formation explained by molecular pathology (pathobiochemistry), a complementary domain of cellular pathology, may be considered as precursory step of

morphofunctional changes observed in living organisms as a consequence of the action of mycotoxins.

3.2. Interaction with polycyclic hydrocarbons

Polycyclic aromatic hydrocarbons (PAH) have two important characteristics that influence their biological activity: a planar molecule and π delocalized electrons (Luch, 2005; Gârban, 2007). Deviations of the planar form can severely alter the chemical structure – biological activity relation. The structural formulas for polycene (I-XII) are presented in fig.4.

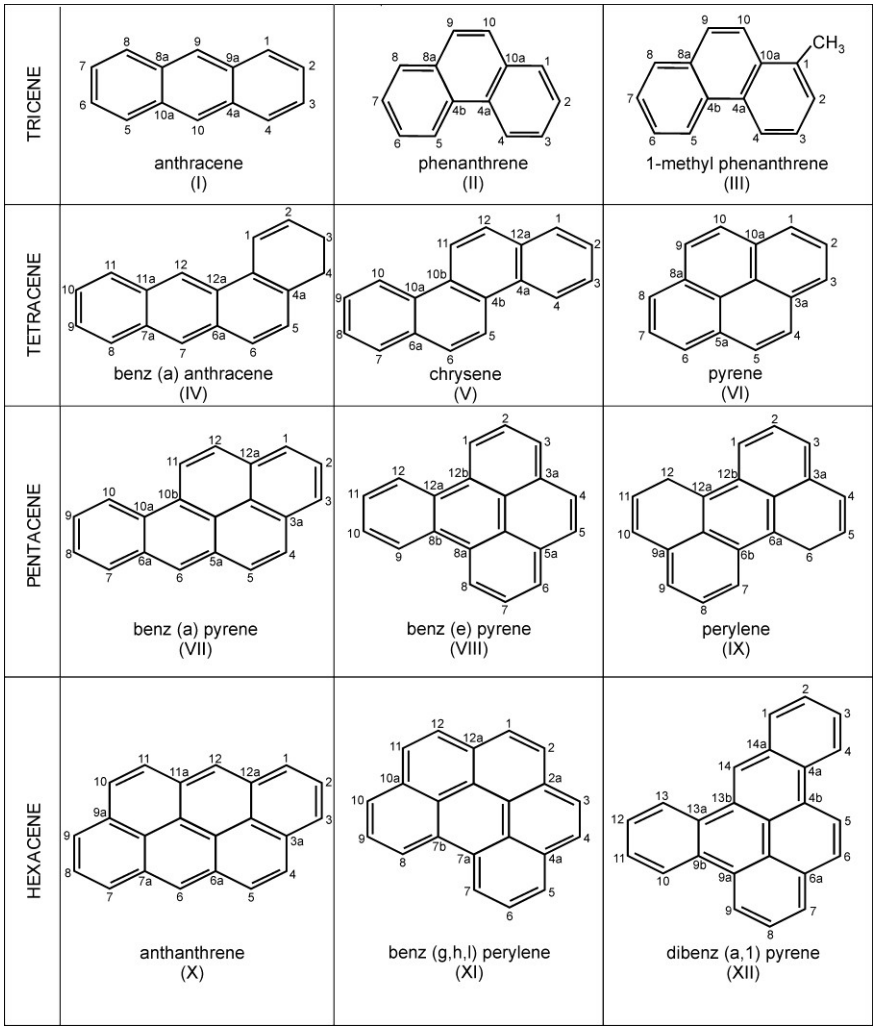

Fig.4. Polycyclic aromatic hydrocarbons – chemical structure

As a result of the DNA macromolecule interaction with PAH adducts of type DNA-HPA are formed (Arcos, 1996; Avacovici, 2005). Benz(a)anthracene (IV) – B(a)A and benz(a)pyrene (VII) – B(a)P are most often incriminated for their carcinogenic effects. In the case of B(a)P the binding to the DNA macromolecule usually takes place at N_2 of

deoxyriboguanine (N_2dGu) and at N_6 of deoxyriboadenine (N_6dAd) and in the case of MB(a)A the binding may appear at N_4 of deoxyribocytosine (N_4dCi) – see fig.5.

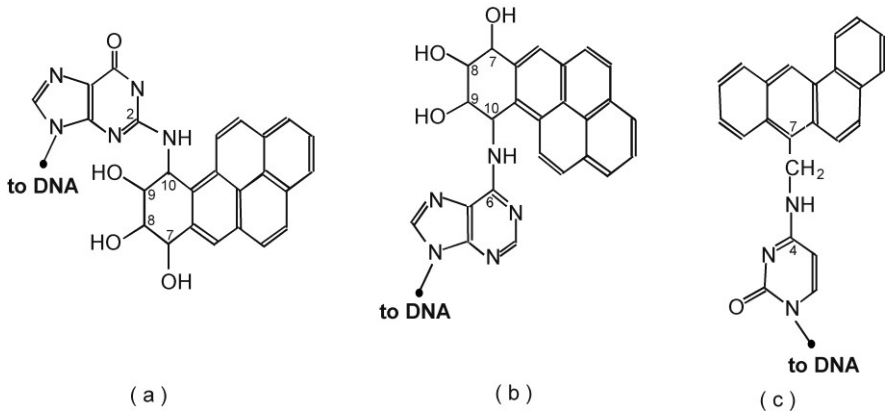

Fig.5. Structure of adducts DNA-PAH0 by bindings to nucleobases
(a)N_2dGu-B(a)P ;(b) N_2dAd-B(a)P; (c) N_2dCi-MB(a)A

Appearance of DNA-PAH adducts is followed by the destabilization of the DNA macromolecule which contributes to the perturbation of genetic information during the replication-transcription-translation processes, leading to the appearance of mutagenic and/or carcinogenic processes.

3.3. Interaction with aromatic amines

a) Interaction with aminobenzene

Aminobenzene ia an "azo dye" used in textile industry but in the past it has been used also in the food industry. It is known a monomethylated derivative (MAB) and a dimethylated derivative (DAB). Metabolization of MAB, for example, occurs at the level of hepatic ribosomes, giving rise to the biologically non-compatible adduct DNA-MAB. The binding is made at the C_8 of the deoxyguanosine of DNA, usually noted C_8dGu. Structure of the monoaminobenzene (MAB) and it adduct with DNA is given in fig.6.

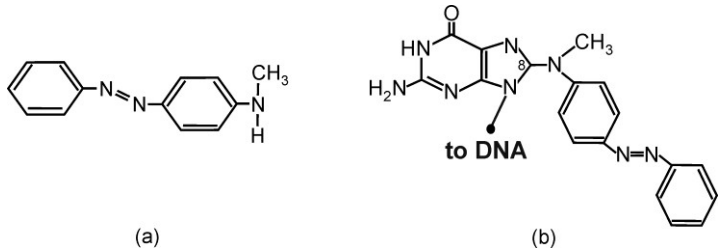

Fig.6. Structure of the monoaminobenzene – MAB (a) and of the adduct DNA-MAB (b)

b) Interaction with aminofluorene and with quinoleine

Aromatic amines are amines with an aromatic substituent – that is –NH_2, –NH – or nitrogen group(s) attached to an aromatic hydrocarbon, whose structure usually contains one or more benzene rings (Gârban, 2007). Human exposure to aromatic amines is made especially through industrial pollution and cigarette smoke. The biotransformation process

that activates the aromatic amines consist mainly in N-oxidation which generates N-hydroxy-arylamines that can interact directly with DNA, thus resulting DNA adducts.

Two of the most representative compounds from this class are 2-aminoflouren (2-AF) and 2-amino-3-methylimidazo[4,5-f]quinoline (IQ) . Their chemical structures are given in fig.7.

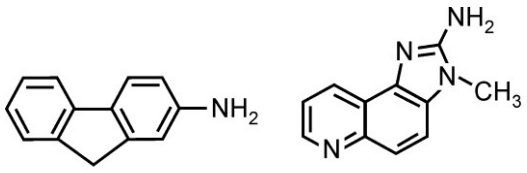

2-aminofluoren 2-amino-3-methylimidazo [4,5-f]quinoline

Fig.7. Chemical structure of 2-aminoflouren and 2-amino-3-methylimidazo[4,5-f]quinoline

By metabolic activation of aromatic amines electrophilic arylnitrenium ions are generated ultimately. These will attack DNA giving rise to specific adducts by binding to the DNA guanine and which will impede replication and induce mutations that underlie tumorigenesis.

One of the most recently discussed aromatic amines is 2-amino-3-methylimidazo-[4,5-f] quinoline (IQ), a carcinogenic compound found especially in cooked food. After a previous activation IQ interacts with DNA and generates especially N-(deoxyguanosine-8-yl)-2-amino-3-methylimidazo- [4,5-f] quinoline (C_8dGu-IQ) and 5-(deoxyguanosin-N_2-yl)-2-amino-3-methylimidazo- [4,5-f]quinoline (N_2dGu-IQ). Their chemical structure is given in figure 8.

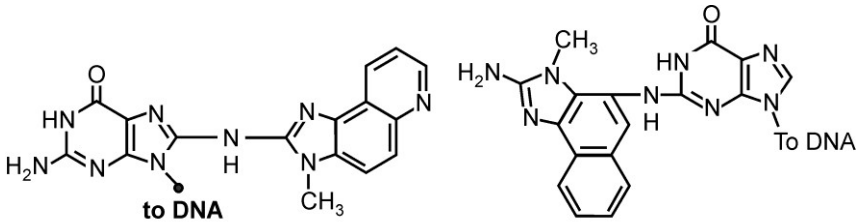

(a) (b)

Fig. 8. Structure of some adducts between DNA nucleobases and IQ
a)C_8dGu-IQ; b) N_2dGu-IQ

The DNA-IQ adducts are incriminated especially for colon cancer and the structural formulas shown above were determined on lab rats after the administration of IQ.

4. Interactions with inorganic compounds

In this category the most discussed xenobiotics are the metallic compounds which may generate through biotransformation metallic ions that interact with the DNA macromolecule. Also in this category one can mention nitrates and nitrites which generate by biotransformation organic compounds like nitrosamines that interact with DNA.

4.1. Interaction with some metals

One of the most discussed and studied category of chemical xenobiotics are the potentially toxicogen metals, known for their carcinogenicity, and metals present in the environment as pollutants (especially of industrial origin) which can accidentally reach feedstuffs, food or tap water (Williams,1997; Merian et al., 2004; Haiduc, 2006). Among those metals the most common are: cadmium (Cd), lead (Pb), mercury (Hg) and tin (Sn).

Cadmium is used especially in the battery industry and in the pigments manufacturing, e.g. cadmium sulfide (CdS). Lead is found as an environmental contaminant, especially tetraethyl lead – $Pb(CH_2H_5)_4$ – from the emissions of auto vehicles. Mercury is an industrial pollutant – mostly discussed as a contaminant of sea food, especially as methyl mercury radicals (CH_3Hg^+) – e.g.: chloromethylmercury (CH_3HgCl).

After the interaction between DNA and metallic ions (M^{n+}), the resulted adducts severely alter the duplex stability. In some cases, when the metal ions are intercalated between nucleobases, the strand can be broken. The newly formed DNA-M^{n+} type adducts affect the structure-activity relationship of DNA macromolecule and the protein synthesis.

Divalent metal ions (M^{2+}) give rise to adducts with DNA by the binding to a nucleobase at N_7 position and O from C_6 of guanine and at N_7 and N from C_6 of adenine. An example of such adducts are those formed by the attachment of cadmium to guanine and adenine (fig. 9). Also, in case of Hg^{2+} and Cu^{2+} and the binding can appear at N_7 and O from C_6 of adenine or guanine.

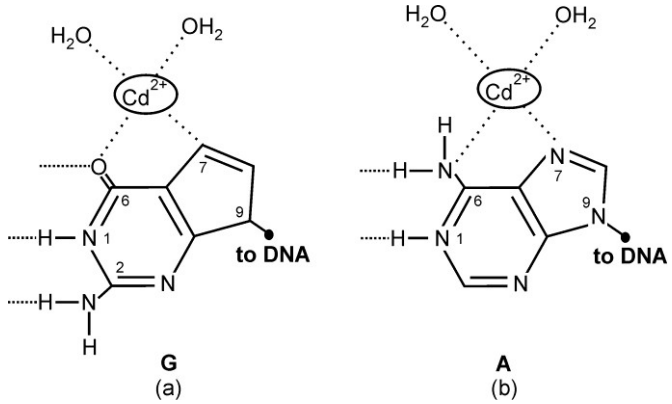

Fig.9. Binding of Cd^{2+} to purinic nucleobases of DNA:
a)Cd^{2+}-guanine; b) Cd^{2+}-adenine

The complexes formed by the interaction of DNA with divalent metal ions (M^{2+}) present various binding types: a) to the phosphodiesteric groups; b) between a phosphodiesteric group and nucleobases; c) between two complementary intrastrand nucleobases; d) between two vicinal nucleobases; e) at different positions of the same purine nucleobases. The first three binding modes are predilectly characteristic for biometallic ions.

4.2. Interaction with nitrates and nitrites

The nitrosamines may appear from the interaction with nitrates and nitrites. This interaction takes place usually during the digestion process. The formed nitrosamines have

non-cyclic (e.g.: N-nitrosodimethylamine, N-nitrosodiethyl-amine) or cyclic structure (e.g.: N- nitrosopyrolidine, N-nitrosopiperidine).

A special class of nitrosamines that is more and more studied these days due to their carcinogenicity and also due to their magnitude of impact on humans is the tobacco specific nitrosamines (Hecht, 1998; Mensinga et al., 2003). These nitrosamines are formed during the processes of curing and maturation of tobacco when nitrates are reduced to nitrites which act as nitration agents for the present secondary and tertiary amines. The most studied compound from this class is 4-(methyl-nitrosamino)-1-(3-pyridyl)-1-butanone also named N-nitroso ketone (NNK) which can form adducts with DNA. Among the resulted adducts the most common were those at the N_7 of deoxyguanine (N_7dG), N_2 of deoxycytosine (N_2dC) and N_2 of deoxythymine (N_2dT) – see fig. 10.

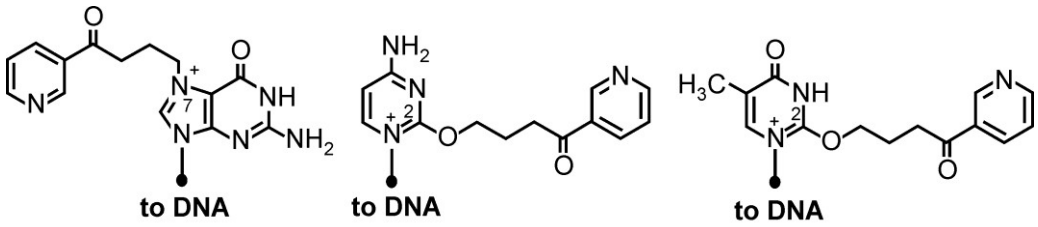

Fig.10. Chemical structure of some adducts between DNA and NNK:
a) N_7dG-NNK; b) N_2dC-NNK; c) N_2dT-NNK

These adducts were identified using mass spectrometric analysis and their presence is correlated with the initiation of carcinogenesis. Such adducts have been found in tissues and cells of rodents that have been exposed to NNK, and often in the blood and urine of smokers.

Compounds with adduct structure resulted from the interaction of DNA with various xenobiotics are non-biocompatible. In the organism such structures disturb the cell division and are followed by neoplastic processes. Aspects related to neoplastic processes will be discussed in another paper.

CONCLUDING REMARKS

Interactions of chemical xenobiotics with the DNA macromolecule are of importance both for fundamental studies – involving the molecular mechanisms and the applicative research - regarding the biochemical injury.

As a result of the biochemical injury is the formation of some biologically non-compatible “molecular complexes” known as DNA adducts. These compounds are at the origin of some processes which can affect the animal and human organisms. The effects are conditioned by the type of the xenobiotic, physiological status of the organism, access route a.o. In time, the pathobiochemical changes followed by pathophysiological modifications may lead to mutagen, oncogen and carcinogen processes.

In the domain of the carcinogen pathobiochemical processes the adduct formation of various chemical xenobiotics with DNA are of special interest. Investigations focused on the DNA adducts might help to improve diagnosis in the early stages of a carcinogenic process.

***Note**: The present paper was elaborated within the activity of the «Romanian Society of Comparative Oncology » Bucharest (Manolescu) and of the Working Group for Xenobiochemistry Timişoara (Gârban). Studies in the same domain were extended (after February 14, 2015) in the framework of the collaboration with the Faculty of Veterinary Medicine Timişoara.*

This work was communicated at the Jubilee Session of 70 yrs from the foundation of the University of Agricultural Sciences Timişoara (1945-2015).

References

1. Ames B.N., Shigenaga M.K., Gold L.S. – DNA lesions, inducible DNA repair and cell division: three key factors in mutagenesis and carcinogenesis, *Environ. Health Perspect*., 1993, 5, 35-44.
2. Arcos J.C., Argus M., Woo Y. (Eds.) – *Chemical induction of cancer: Modulation and Combination Effects*, Birkhauser, Boston, 1996.
3. Avacovici Adina, Gârban Gabriela, Ghibu G.-D., Gârban Z. – Adducts of deoxyribonucleic acid with polycyclic aromatic hydrocarbons and acridinic derivatives, *"Scientifical researches: Agroalimentary Processes and Technologies"*, Timişoara, 2005, XI (1), 129-138.
4. Bannett J.W., Klich M. – Mycotoxins, *Clinical Microbiology Reviews*, 2003, 16, 3, 497-516.
5. Brooks G.T., Roberts T.R. - *Pesticide Chemistry and Bioscience, The Food-Environment Challenge*, Publ. by The Royal Society of Chemistry, Cambridge, 1999.
6. Creppy E.E., Serge Moukha S., Bacha H., Carratu Maria Rosaria - How much should we involve genetic and environmental factors in the risk assessment of mycotoxins in humans? *Int. J. Environ. Res. Public Health,* 2005, 2(1), 186–193.
7. Gârban Z., Daranyi Gabriela - Biomedical implications of the adducts biogenesis resulted by the interaction of deoxyribonucleic acid with aflatoxins, *Central European Journal of Occupational and Environmental Medicine,* 2000, 6 (2-3), 161-167.
8. Gârban Z. - *Tratat comprehensiv de biochimie. Vol.IV. Xenobiochimie*, ediţia 2-a, Editura Didactică şi Pedagogică R.A., Bucureşti, 2007.
9. Gârban Z. - *Xenobiochimia în ştiinţele agricole şi ştiinţa alimentului*, Editura Solness, Timişoara, 2011.
10. Haiduc I. – Metals in our food, pp.15-20, in "*Metal Elements in Environment, Medicine and Biology",* Tome VII (Gârban Z., Drăgan P., Eds.), Publishing House Eurobit Timişoara, 2006.
11. Hecht S.S. – Biochemistry, biology and carcinogenicity of tobacco-specific N-nitrosamines, *Chem. Res. Toxicol*., 1998, 11, 559-603.
12. Knudsen I. – Animal Studies in the Evaluation of Carcinogens - Anticarcinogens in Food, *Biol. Zent. bl*., 1989, 108, 423-450.
13. Kohlmeier M. – *Nutrient metabolism, Chap. 5, Xenobiotics* (pp.85-110), Academic Press, Amstedam-Boston-Heidelberg-London-New York, 2003.
14. Luch A. - *The Carcinogenic Effects of Polycyclic Aromatic Hydrocarbons*, Imperial College Press, London, U.K., 2005.
15. Manolescu N. (Ed.) - *Introducere în oncologia comparată*, Editura Universitară "Carol Davila" Bucureşti, 2003.
16. Mensinga T.T., Speijers G.J.A., Meulenbelt J. – Health implications of exposure to environemental nitrogenous compounds. Review article, *Toxicological Reviews*, 2003, 22(1), 41-51.
17. Merian E., Anke M., Stoeppler M. (Eds.) – Elements and their compounds in the environment. Vol.I, General aspects (2nd edition,Viley-VCH Verlag, Weinheim, 2004.
18. Nassar A.F. (Ed.) - *Biotransformation and Metabolite Elucidation of Xenobiotics: Characterization and Identification*, J.Wiley and Sons Inc., Chichester, UK, 2010.
19. Phillips D.H. – DNA adducts as markers of exposure and risk, *Mutat. Res.,* 2005, 577(1-2), 284-292.
20. Podar C., Gârban Z., Silvaş E., Roman M., Ciorlăuş A.T., Ştef L. - Poluarea micotică şi implicaţiile acesteia în patologia tineretului taurin, *Rev. Creşt. Anim.,* Bucureşti, 1982, 2, 2, 46-50.

21. Poirier M.C., Beland F.A. – DNA adducts measurements and tumor incidence during chronic carcinogen exposure in animal models: implications for DNA adducts-based human cancer risk assessment, *Chem.Res.Toxicol*., 1992, 5, 749-755.
22. Wassom J.S. - *Mutagenesis, carcinogenesis and teratogenesis information system*, Information Center Complex, Oak Ridge, 1980.
23. Williams R.J.P. - Bioinorganic Chemistry and Cancer, pp.19-83, in "*Carcinogenicity of inorganic substances: Risks from Occupational Exposure"* (Chief Duffus J.H., Ed.), Publ. by The Royal Society of Chemistry, Cambridge, 1997.

MORPHOMETRIC ANALYSIS OF JAGUAR (*PANTHERA ONCA*) AND TIGER (*PANTHERA TIGRIS*) SKULLS - SPECIES ON THE "RED LIST" OF THE INTERNATIONAL UNION FOR CONSERVATION OF NATURE (IUCN)

BOGDAN GEORGESCU[1], GABRIEL PREDOI [1], CRISTIAN BELU[1], ȘTEFANIA MARIANA RAITA[1], LETIȚIA PURDOIU[1], OANA-MĂRGĂRITA GHIMPEȚEANU[1], FLORICA BĂRBUCEANU[2],ȘERBAN PURDOIU[1]

[1] University of Agronomical Sciences and Veterinary Medicine, Faculty of Veterinary Medicine, Bucharest, Romania

[2] Institute for Diagnosis and Animal Health, Bucharest, Romania

georgescubogdi@gmail.com

Abstract: *In Romania, the two species covered by this study - the jaguar (Pantheraonca) and the tiger (Pantheratigris) are species found only in zoos or circuses. Romania, as an European Union border state, may be transited or used by collectors or by smugglers of exotic species, especially since the two species are subject to an extremely strict control. The tiger (Pantheratigris) according to the IUCN Red List is an endangered species and the jaguar (Pantheraonca) is nearly endangered. These species have a common ancestor - Proailuruslemanensis - but have evolved in different environments, Indian jungles and the Siberian taiga (the tiger), all North and South American habitats (the jaguar). In order to perform the morphometric analysis there were used skulls of three adults tigers (Pantheratigris) and from a jaguar male (Pantheraonca), skulls found under administration of the discipline's museum. Description, identification and homologation were made according to N.A.V .2005. Following the studies and measurements carried out, it appears that there is a little difference in size of the skulls of the two species, especially as the jaguar, unlike the tiger, is climbing, and the whole body must be lighter and smaller. The described and used graphics and reference points allow performing complex measurements, both on anatomically prepared skulls and on radiological images. It is observed that the jaguar's skull is slightly smaller than the tiger's one. The measurements that make the differences between the two skulls are those of the jaw. There are also differences on the dorsal and ventral facets of the skull as on the lateral side. There were identified eight reference points on which it can be determined to which species the skull being analyzed belongs.*

Keywords*: jaguar, tiger, skull, species, measurements*

INTRODUCTION

The studied two species are present in Romania only in zoos and circuses. We consider that is of interest because one of the two species –the tiger (*Panthera tigris*) - is an endangered species (according to the Red List of the International Union for Conservation of Nature / IUCN), and also, in some Asian countries, it is the raw material for the production of herbal remedies. Our country, as an European Union border state,may be transited or used by collectors (declared or not) or by the Asian people established in the EU to traffic (legally or less legally) this species. The jaguar (*Panthera onca*) is less put at risk and it is possible to used it as species to replace (if only declarative) as a trophy (or raw material for remedies) the tiger in this type of traffic. Therefore we wanted to establish some differential dimensional criteria between the two species, criteria that can be used by customs officials in situations of uncertainty (especially with the lack of supporting documentation).

MATHERIAL AND METHOD

In order to perform the morphometric analysis there were used skulls of three adults tigers (*Panthera tigris*), 9, 11, and 12 years old,donated by Bucharest-Baneasa Zoo and by N & Variete Globus Circusfor teaching purposes,and from a jaguar male (*Panthera onca*)with melanism, 24 years old, donated for teaching purposes by Bucharest Zoo.

Measurements were performed and the most interesting aspects were photographed.Description, identification and homologation were made according to Nomina Anatomica Veterinaria (N.A.V) 2005. For measurement there were used zootechnical compass, ruler and beam compass.

RESULTS AND DISCUSSION

Following the carried out studies and measurements, it appears that there is alittle dimensional difference between the skulls of the two species, especially as the jaguar, unlike the tiger, is climbing, and its whole body must be lighter. But it appears that the jaguar has a stronger bite than the tiger, proved by a deeper masseteric fossa.

The described plans and reference points allow the performance of complex measurements, both on anatomically prepared skulls and on radiological images (with a modern imaging system, as the one of Bucharest Faculty of Veterinary Medicine Clinic, which is equipped with automatic program for morphometry) (figure no 1).

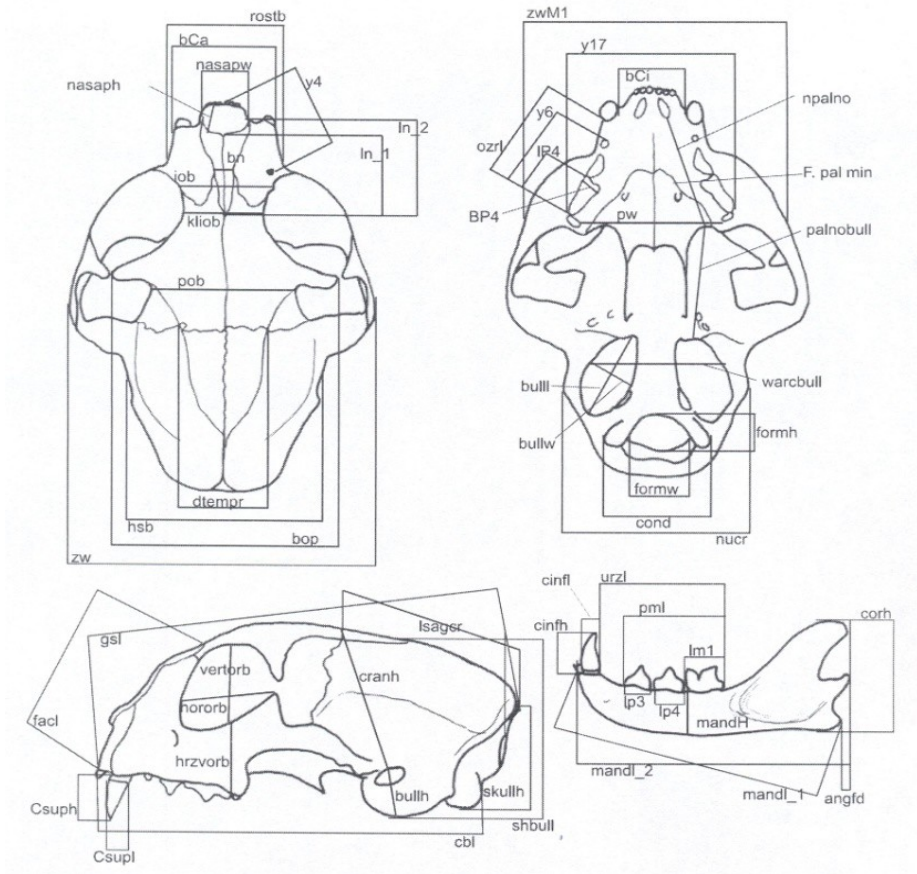

Fig. 1. Reference points for feline skull measurements (Clara Stefen and D. Heideck, 2012).

The results of carried outmeasurements are shown in the tablesbelow (table no 1, 2, 3, 4, 5).

Table 1.Measurements of the ventral facet of the jaguar (*Panthera onca*) skull, and tiger (*Panthera tigris*) skull

Measurements	Species - Values (cm)			
	Jaguar (*Panthera onca)*	Tiger (*Panthera tigris*)		
		Specimen 1	Specimen2	Specimen3
bCi (distance between canines)	4,3	4,5	5,8	6,1
y17(the largest width measured at the maxillary PM4)	8,2	10,0	13,0	14,0
pw (palatine width between molars 1)	7,1	10,6	10,6	11,0
ozrl (maxilla length from canine to premolar 4)	5,9	7,8	8,0	9,0
y6 (dental arch length from premolar 2 to premolar 4)	5,7	6,0	7,0	7,0
lP4 (premolar 4 alveolar length)	3,0	3,0	3,5	3,0
BP4 (premolar 4 alveolar width)	1,3	2,0	2,0	2,1
zwM1 (maximum width of the skull at the molar 1)	12,9	15,0	16,0	16,0
npalno (distance from the nasal cavity to the palatine anterior suture)	6,5	7,0	10,0	11,0
palnobull (distance from the palatine anterior suture to the tympanic bulla notch at the styloid process base)	8,2	9,0	11,0	10,0
warcbull (width of the skull at the tympanic bulla)	7,5	8,0	10,0	10,0
bullw (tympanic bulla width)	2,7	2,0	3,8	3,0
bulll (tympanic bulla length)	4,1	3,6	4,7	4,0
formh (the large occipital foramen height)	2,1	3,0	3,1	3,0
formw (maximum width of the large occipital foramen)	2,4	3,0	3,1	3,0
cond (maximum width at the occipital condyles)	5	5,8	11,0	10,0
nucr (maximum width at the nuchal crest)	10,7	12,0	14,5	14,0

Table 2. Measurements of the dorsal facet of the jaguar (*Panthera onca*) skull, and tiger (*Panthera tigris*) skull

Measurements	Species - Values (cm)			
	Jaguar (*Panthera onca)*	Tiger (*Panthera tigris*)		
		Specimen 1	Specimen2	Specimen3
y4 (distance from the incisive to the center of the infraorbital foramen)	7,0	10,0	12,0	11,0
ln_1 (nasal cavity length at the median suture)	6,0	8,0	9,0	9,0
ln_2 (maximum length of nasal bones)	7,1	9,8	14,0	14,0
bn (width of nasal bones in the incisor-maxilla-frontal sutures)	2,0	3,0	3,2	3,0
iob (interorbital width at the angular vein of the eye)	5,3	6,7	6,0	6,0
kliob (interorbital width measured at the smallest distance between the orbits)	5,6	6,1	7,0	7,0
pob (width at the posterior of the orbital processes)	5,4	4,8	12,0	12,0
nasaph (maximum height of the internal nasal aperture)	4,4	4,4	6,5	6,0
nasapw (maximum width of internal nasal aperture)	3,9	4,9	4,2	4,0
bCa (width at the right maxilla canines)	7,3	8,0	9,5	8,0
rostb (maximum width of the snout)	7,0	10,0	10,0	8,7
dtempr(distance between the fronto-parietal edges at the intersection with frontoparietal sutures)	2,8	4,6	4,5	5,0
hsb (maximum width of the skull at the temporal scale)	9,7	7,0	7,8	8,7
bop (width at the orbital processes)	7,4	11,0	14,0	11,0
zw (maximum width of the skull at the zygomatic arch)	17,0	20,5	24,0	20,0

Table 3. Measurements of the lateral facet of the jaguar (*Panthera onca*) skull, and tiger (*Panthera tigris*) skull

Measurements	Species - Values (cm)			
	Jaguar (*Panthera onca)*	Tiger (*Panthera tigris*)		
		Specimen 1	Specimen2	Specimen3
Csuph (maxillary canine crown height)	3,5	5,0	5,0	5,0
Csupl (thickness of maxillary canine at the dental isthmus)	2	2,9	3,1	3,0
facl (facet length)	11,3	8,7	14,0	13,0
gsl (the longest length of the skull)	29,8	32,9	37,5	37,0
lsagr (sagittal crest length)	11,8	14,0	13,0	12,0
vertorb (maximum vertical diameter of the orbit)	4,8	6,0	5,8	6,0
hororb (horizontal diameter of orbit)	3,9	4,8	7,0	6,5
hzvorb (the vertical distance from the orbit to the maxilla between premolar 4 and molar 1)	5	10,0	11,2	12,1
cranh (skull height at the dorsal auditory meatus point to the sagittal intersection of frontoparietal sutures)	7,9	12,0	14,0	14,0
bullh (tympanic bulla height)	2,6	2,8	2,9	3,1
cbl (condyle basilar length)	23,3	26,0	28,0	29,0
skullh (skull height from the condyles to the nuchal crest)	6,2	6,5	9,5	9,0
shbull (skull height measured vertically from the tympanic bulla)	9,1	12,0	12,0	13,0

Table 4. Measurements of the mandible to the jaguar (*Panthera onca*), and tiger (*Panthera tigris*)

Measurements	Species - Values (cm)			
	Jaguar (*Panthera onca)*	Tiger (*Panthera tigris*)		
		Specimen 1	Specimen2	Specimen3
cinfh (mandibular canine height)	5,9	4,5	4,5	4,3
cinfl (mandibular canine socket length)	2,2	2,2	2,6	3,0
lp3 (premolar 3 width)	1,5	1,5	1,5	2,0
lp4 (premolar 4 width)	2,1	2,0	2,5	2,2
lm1 (molar 1 crown width)	2,3	2,0	3,0	2,3
pm1 (molars arch alveolar length)	6,0	6,0	7,5	7,5
urzl(mandible dental arch length from the distal edge of the canine to the distal edge of molar 1)	7,5	8,7	10,0	10,0
mandH (mandibular height between premolar 4 and molar 1)	3,2	3,8	6,0	4,0
mandl_2 (jaw length from the incisor socket to the condiloid process. parallel to the ventral edge of the mandible)	19,3	22,0	24,0	24,0
mandl_1 (jaw length from the incisor socket to the aboral edge of angular process, sagittal plan)	16	20,0	23,0	23,0
angfd (imaginary line that starts from the condiloid process to the coronoid process)	1,8	2,1	2,2	2,0
corh (jaw height at the coronoid process)	7,7	10,0	11,0	10,5

Table 5. Measurements of the skull and cranial cavity volume to the jaguar (*Panthera onca*), and tiger (*Panthera tigris*), according to the irregular ellipsoid formula (4/3∏abc)

Measurements	Species - Values (cm)			
	Jaguar (*Panthera onca)*	Tiger (*Panthera tigris*)		
		Specimen 1	Specimen2	Specimen3
a (half of the maximum length of the skull - from the incisive to the nuchal crest)	14,9	16,45	18,75	18,5
b (half of the maximum length of the skull - the skull height from the dorsal auditory meatus point to the intersection of sagittal frontoparietal sutures	3,95	6,0	7,0	7,0
c (half of the maximum width of the skull - measured at the zygomatic arch)	8,5	10,25	12,0	10,0
Skull volume according to the formula: 4/3∏abc (cm^3)	2412,59	4237,69	6597,34	5424,48
a (half of the anterior-posterior diameter of the cranial cavity)	4,6	4,45	5,35	5,75
b (half of the dorso-ventral diameter of the cranial cavity)	3,15	2,75	3,15	3,35
c (half of the transverse diameter of the cranial cavity)	3,75	3,5	4,5	5,0
The volume of the cranial cavity according to the irregular ellipsoid formula (4/3∏abc)(cm^3)	227,49	179,41	316,66	403,43

CONCLUSIONS

1. It is observed that the jaguar skull is slightly lighter than the tiger one.
2. Measurements that may be considered differences between the two skulls are those of the mandible, respectively **mandl_1** and **mandl_2** (the mandible length from the incisor socket to the aboral edge of the angular process, the sagittal plan, and the mandibular length from the incisor socket to the condiloid process, parallel to the ventral edge of the mandible).
3. There are also differences on the dorsal facet, respectively **zwM1** (maximum width of the skull at molar 1).
4. On the ventral facet, there are differences at**y17** (the largest measured width at maxillary PM4) **ozrl** (maxilla length from canine to premolar 4) and **pw** (palatine width between molars 1).

5. On the lateral side, the reference point of difference is the **hzvorb** (the vertical distance from the orbit to the maxilla between premolar 4 and molar 1) and **cranh** (skull height at the dorsal auditory meatus point to the sagittal intersection of frontoparietal sutures).
6. Based on the measurements of the eight reference points we can determine to which species the skull belongs.

REFERENCES

1. Barone R. (1966). Anatomie comparée des mammiferes domestiques, Tome premier - Osteologie, Imprimerie des Beaux – Arts s.a. - J. Tixier & fils, Lyon.
2. Bertrand, Anne-Sophie, Morisot, A. (2012). Neotropical Spotted Cat Species Discrimination Using Morphometrics. Natureza & Conservação, 10 (1): 40-44.
3. Christiansen, P., Adolfssen, J.S. (2005). Bite forces, canine strength and skull allometry in carnivores (Mammalia, Carnivora). J. Zool. Lond. 266: 133-151.
4. Driesch von den, Angela (1976). A guide to the measurement of animal bones from archaeological sites. Peabody Museum Bulletin 1/1976 – Peabody Museum of Archaeology and Ethnology, Harvard University, USA.
5. Feiler, A., Clara Stefen (2009).Tigers (*Pantheratigris, P. sondaica*and *P. sumatrae*) in the Collection of the Museum fürTierkunde Dresden (Carnivora: Felidae). Lynx, n.s. (Praha), 40: 153-162.
6. Garcia, Karla, Ortiz, J.C., Marcela Vidal, Rau, J.R. (2010). Morphometric of the Tracks of *Puma concolor*: Is It Possible to Differentiate the Sexes Using Measurements from Captive Animals? Zoological Studies, 49 (4): 577-582.
7. Georgescu B., Predoi G., Belu C., Letiția Purdoiu, Mărgărita Ghimpețeanu, Marilena Chereji, Petronela Mihaela Roșu, Ancuța Elena Oprea, Vișoiu C., Florica Bărbuceanu (2014). Biodiversitatea morfometrică a craniului la jaguar (*Panthera onca*). Studiu de caz. Revista Română de Medicină Veterinară, 24 (4): 29-42.
8. Georgescu, B., Predoi, G., Belu, C., LetițiaPurdoiu, Tudor, N., ȘtefaniaRaita, Dumitrescu, I., Ciobanu, M.L., FloricaBărbuceanu (2015). Caracterelemorfologice ale craniului la tigru (*Pantheratigris*).RevistaRomână de MedicinăVeterinară, 25 (1): 27-44.
9. Tudor, N., Vlăgioiu, C. (2015).Radiologieveterinară – Aparatullocomotor. ArsDocendi, București.
10. Predoi, G., Georgescu, B., Belu, C., Dumitrescu, I., AncaȘeicaru, PetronelaRoșu (2011). Anatomiacomparatăaanimalelordomestice. OsteologieArtrologie, Miologie, Editura CERES, București.
11. *** - Nomina Anatomica Veterinaria, Fifth edition, Published by the Editorial Committee Hannover, Columbia, Gent, Sapporo, 2005.

RESEARCHES ON NUTRITIVE VALUES ON ROE DEER *(CAPREOLUS CAPREOLUS)* MEAT

M. LAZĂR[1*], P.C. BOIȘTEANU[2], G. LAZĂR[3], ROXANA LAZĂR[2]
[1] UASVM of Iasi, Faculty of Veterinary Medicine, Romania
[2] UASVM of Iasi, Faculty of Animal Science Iasi, Romania
[3] CSV Crăcăoani, Neamt, Romania
* Faculty of Veterinary Medicine "Ion Ionescu de la Brad" University, Iasi, Romania
mlazar@uaiasi.ro

Abstract: *One of the species of cynegetic interest well represented numerically in the north of Moldavia, the roe deer (Capreolus capreolus) (Linnaeus, 1758) is a hunt species with high demand. Researches were developed on four roe deer: two males and two females, harvested in the north area of Moldavia (counties Suceava and Iaşi). The assessment of meat quality represents a process which includes the analyses of physico-chemical and organoleptic parameters, the establishment of nutritional, biological, food and culinary values. Samples were processed in order to determine proteins collagen, fat, water, and the pH, known as that the nutritional value of meat is given by these parameters and expression of the sensorial characteristics based on relationships in which they are found. The obtained results reflect the high nutritional value of meat from deer, and from an alimentary point of view the meat came from females situates in consumers top preferences.*

Keywords*: deer, meat, nutritive values*

INTRODUCTION

The quantitative and qualitative level of human nutrition is an essential indicator in assessing the welfare degree of a population.

In the food quality is feeling increasingly the tendency to return to nature and to monitor the achievement of products with physicochemical parameters as close to those of naturally derived products.

The continuing concern represented by the early appearance of the obesity and diabetes in young population as well as rapidly ascending dynamics of their frequency compels finding an alternative healthier food, by ingestion of foods low in fat but with high protein content. This correlated with the food diversity in continuing expansiveness represent important elements on the decision to purchase and consumption, the ultimate goal to achieve a balance between the producer - the quality principles - consumer concomitant with the correct information (Postolache et col., 2013).

In the reference literature, there are many debates on the nutritional properties of game meat, by age, sex and degree of development of animals. All these researches highlight the interest increasingly higher of consumers for game meat because of the low amount of fat and cholesterol of meat, but with high protein content, essential amino acids and vitamins (Daszkiewicz et col., 2012; Hutchison et col., 2010; Pollard et col., 2002, Wiklund et col., 2003).

Game meat represents an alternative food in continuing expansiveness, due to its high nutritional properties, of particular taste and continued interest in the livestock industry, as well as for the consumer, by diversification (exploitation) of cynegetic resources at an industrial level.

MATERIAL AND METHOD

The investigations were conducted in the Pathological anatomy and Forensic Laboratory, Faculty of Veterinary Medicine Iaşi, and in Meat quality control and Experimental and Applied Physiology, Faculty of Animal Sciences Iaşi, on deer corpses harvested from hunting fund Frasin, Suceava county and hunting fund Turia Perieni, Iaşi.

As a biological material was used 4 deer (*Capreolus capreolus*) individuals (2 males and 2 females).

The protein, fat, water and beffe quantity from meat were determined with the use of Food Check automatic analyzer.

Automatic meat analyzer (Fig. 1) is a near-infrared spectrometer which is used to analyze the composition, using the infrared absorbance characteristics of the sample spectra.

Fig.1. Food–Check Automatic meat analyzer

The operating principle of the method is as follows: the light of a tungsten halogen lamp illuminates the entrance slit of the monochromator. Inside the monochromator, the light is diffracted by an optical grating. For each grating angle, a different NIR wavelength is obtained at the exit slit. The monochromator NIR light leaving the monochromator strikes the meat placed into the sample compartment. After interaction with the grain meat sample, the remaining light leaves the sample. A large portion of this light is collected under a wide angle on a silicon detector underneath the sample plate to generate a corresponding photometric signal.

From the ratio values read by the analyzer and those of reference, are established calibration constants for each wavelength, which is the basis for calculation of the values of parameters analyzed. The measurement time is approximately 50 seconds, the spectral range having limits between 730 - 1100 nm.

The display is located on the upper part of the front panel. It is the user interface for the integrated Omega software and displays menu options, dialogs, measurement results, error messages etc. The display serves as a touch screen at the same time. Meat samples thorough grounded are located on a glass plate that ulterior will be introduced in the analyzer for analyzing. The obtained results will be displayed on the screen.

RESULTS AND DISCUSSIONS

Were determined the main biochemical constituents from the same four muscle categories taken in study, respectively *M. Longissimus*, semitendinosus muscle (*M. Semitendinosus*), triceps brachii muscle (*M. Triceps brachii*) and trapezius muscle (*M. Trapezius cervicalis*).

Table 1

Protein value in deer *Capreolus capreolus* males

Nr. crt.	Protein value % ♂			
	Semitendinosus muscle	Triceps brachii muscle	*Longissimus dorsi* muscle	Trapezius muscle
1	21,3	21,5	20,9	21,3
2	21,7	21,6	21,7	21,4
x(average)	21,50	21,55	21,30	21,35
sx(mean standard deviation)	0,200	0,050	0,400	0,050
s(standard deviation)	0,28	0,07	0,57	0,07
v%(coefficient of variation)	1,32	0,33	2,66	0,33
min	21,30	21,50	20,90	21,30
max	21,70	21,60	21,70	21,40

Concerning the overall image of each muscle group highlighted slightly superior content of total proteins for all muscles harvested from the second carcass towards the muscles from the first carcass, establishing percentage differences that ranged from 0.1% for trapezius muscle and triceps brachii muscle, up to 0.8% for *Longissimus dorsi* muscle.

For the first carcass is noticed a constant in total protein value by 21.3% corresponds to semitendinosus and trapezius muscles, which is preceded by a difference of 0.2% the gross protein maximum (21.5%), it also constitutes the minimum protein for the triceps brachii muscle harvested from the two carcasses (Table 1).

The values for standard deviation and also for mean standard deviation are numerically constant for triceps brachii and trapezius muscle (0.07 respectively 0.05) (Table 1). The maximum of total protein substances (21.7%) corresponds both to *Longissimus dorsi muscle* as well as for semitendinosus muscle belonging to the carcass of the second male (Table 1).

Table 2

Collagen value in deer *Capreolus capreolus* males

Nr. crt.	Collagen value % ♂			
	Semitendinosus muscle	Triceps brachii muscle	*Longissimus dorsi* muscle	Trapezius muscle
1	19,5	19,8	19	19,7
2	20,1	19,9	19,9	19,8
x(average)	19,80	19,85	19,45	19,75
sx(mean standard deviation)	0,300	0,050	0,450	0,050

s(standard deviation)	0,42	0,07	0,64	0,07
v%(coefficient of variation)	2,14	0,36	3,27	0,36
min	19,50	19,80	19,00	19,70
max	20,10	19,90	19,90	19,80

Concerning the overall image of each muscle group highlighted slightly superior content of total collagen for all muscles harvested from the second carcass towards the muscles from the first carcass, establishing percentage differences that ranged from 0.1% for trapezius muscle and triceps brachii muscle, up to 0.9% for *Longissimus dorsi* muscle (Table 2).Total muscular collagen registers a maximum value of 20.1% corresponding to semitendinosus muscle harvested from the second carcass, value counterweighted by the minimum percentage of superior limits (19.7%) corresponding to trapezius muscles from the first carcass (Table 2). For standard deviation and for mean standard deviation were found numerically constant values for triceps brachii muscle and also for trapezius muscle (0.07 respectively 0.05), while the coefficient of variation framed between a minimum of 0.36 for trapezius and triceps brachii muscles and a maximum of 3.27 corresponding to *Longissimus dorsi* muscle (Table 2).The average of total collagen is highlighted through the difference of 0.4% between the maximum (19.85%) corresponding to triceps brachii muscle and minimum value (19.45%) calculated for *Longissimus dorsi* muscle, between intermediary values determined for this statistical indicator, taken two by two, with differences between 0.05% and 0.35% (Table 2).

From the analysis of the total lipid content of the muscle of the two carcasses, it is found the downward slope of the parameter for each muscle group, the maximum being represented by the values of the muscles that have their origin in the first carcass. Within this carcass, is noted the variation of gross lipid content between a minimum of 3.3% corresponding to triceps brachii muscle and a maximum of 5.4% *Longissimus dorsi* muscle, value that represents the absolute superior limit of the item for all muscles subjected to analyses (Table 3).

Table 3

Lipid value in deer *Capreolus capreolus* males

Nr. crt.	Lipid value % ♂			
	Semitendinosus muscle	Triceps brachii muscle	*Longissimus dorsi* muscle	Trapezius muscle
1	3,9	3,3	5,4	4
2	2,5	2,8	2,9	3,8
x (average)	3,20	3,05	4,15	3,90
sx(mean standard deviation)	0,700	0,250	1,250	0,100
s(standard deviation)	0,99	0,35	1,77	0,14
v%(coefficient of variation)	30,94	11,59	42,60	3,63
min	2,50	2,80	2,90	3,80
max	3,90	3,30	5,40	4,00

The minimums parameter variations highlights the difference 1.4% between their extremes (superior 3.9% and inferior 2.5% - recorded in muscles of the second carcass) (Table 3).

The mean values highlight the maximum of total fat content in *Longissimus dorsi* muscle (4.15%), followed at a difference of 0.25% by the content of trapezius muscle (3.90%), the limit of decrease of this statistical parameter being about 3.05% corresponding to triceps brachii muscle (Table 3).

The coefficient of variation presents superior values to its correspondent, of the same parameter studied in common deer, framing limits for values being superior of 42.6 for *Longissimus dorsi* muscle and inferior of 3.63 for trapezius muscle (Table 3).

The amount of water had percentage variations for semitendinosus muscle of the first carcass (74.2%) and is also maintained constant for trapezius muscle of the same carcass. The minimum value (73.1%) corresponding to the *Longissimus dorsi* muscle it is counterweighted by the maximum moisture content (74.8%) recorded in Triceps brachii muscle (Table 4).

For carcass number 2 is distinguished the superiority of all values for each muscle towards the moisture content of the first carcass, highlighting a difference of 1.2% between the minimum of 74.4% for trapezius muscle and the maximum of 75.6% for semitendinosus muscle (Table 4).

Table 4

Water content identified in meat of deer *Capreolus capreolus* males

Nr. crt.	Water value % ♂			
	Semitendinosus muscle	Triceps brachii muscle	*Longissimus dorsi* muscle	Trapezius muscle
1	74,2	74,8	73,1	74,2
2	75,6	75,3	75,2	74,4
x(average)	74,90	75,05	74,15	74,30
sx(mean standard deviation)	0,700	0,250	1,050	0,100
s(standard deviation)	0,99	0,35	1,48	0,14
v%(coefficient of variation)	1,32	0,47	2,00	0,19
min	74,20	74,80	73,10	74,20
max	75,60	75,30	75,20	74,40

Concerning the statistical measures is noticed a maximum value (2.0) of the coefficient of variation in *Longissimus dorsi* muscle while in the trapezius muscle registered a minimum value of 0.19 (Table 4). For minimum values, the water content fluctuates between the following limits: 73.1% in *Longissimus dorsi* muscle of the first carcass and 74.8% for Triceps brachii muscle of the same carcass (Table 4).

Table 5

Protein value in deer *Capreolus capreolus* females

Nr. crt.	Protein value % ♀			
	Semitendinosus muscle	Triceps brachii muscle	*Longissimus dorsi* muscle	Trapezius muscle
1	21,7	21,6	21,5	21,3
2	21,6	21,3	21,6	21,4
x(mean)	21,65	21,45	21,35	21,55
sx(mean standard deviation)	0,050	0,150	0,050	0,050
s(standard deviation)	0,07	0,21	0,07	0,07
v%(coefficient of variation)	0,33	0,99	0,33	0,33
min	21,60	21,30	21,30	21,50
max	21,70	21,60	21,40	21,60

Total protein content varies between an inferior limit of 21.3% corresponding to the trapezius muscle harvested from the first carcass and to triceps brachii muscle from the second carcass (Table 5). Calculating the mean of the parameter, is distinguished that this average is framed by the minimum measure (21.35%), corresponding to *Longissimus dorsi* muscle and the maximum of 21.65% for Semitendinosus muscle (Table 5).

The coefficient of variation is framed between two strict values, a minimum of 0.33 for semitendinosus muscle, *Longissimus dorsi* muscle and Trapezius muscle, with a maximum of 0.99 for Triceps brachii muscle (Table 5).

Table 6

Collagen value in deer *Capreolus capreolus* females

Nr. crt.	Collagen value % ♀			
	Semitendinosus muscle	Triceps brachii muscle	*Longissimus dorsi* muscle	Trapezius muscle
1	20,1	19,9	19,9	19,7
2	19,9	19,7	20	19,7
x(average)	20,00	19,80	19,95	19,70
sx(mean standard deviation)	0,100	0,100	0,050	0,000
s(standard deviation)	0,14	0,14	0,07	0,00
v%(coefficient of variation)	0,71	0,71	0,35	0,00
min	19,90	19,70	19,90	19,70
max	20,10	19,90	20,00	19,70

By processing and analyzing the samples was highlighted the same content in total collagen (19.7%) for trapezius muscle harvested from both carcasses, a value that is maintained also in triceps brachii muscle from the second carcass. However, this represents the minimum numerical value of this compositional index, while the superior limit of 20.1% is indicated in semitendinosus muscle from the first carcass (Table 6).

The mean value of 19.8% is maintained for triceps brachii muscle, and the calculated maximum (20%) is attributed to semitendinosus muscle. The value for the standard deviation (0.14) and coefficient of variation (0.71) remain constant for two muscles: semitendinosus and triceps brachii muscles, and for trapezius muscle these are null (Table 6).

Table 7

Lipid value in deer *Capreolus capreolus* females

Nr. crt.	Lipid value % ♀			
	Semitendinosus muscle	Triceps brachii muscle	*Longissimus dorsi* muscle	Trapezius muscle
1	2	3,2	3,7	4,4
2	3	4,2	2,9	3,9
x(average)	2,50	3,70	3,30	4,15
sx(mean standard deviation)	0,500	0,500	0,400	0,250
s(standard deviation)	0,71	0,71	0,57	0,35
v%(coefficient of variation)	28,28	19,11	17,14	8,52
min	2,00	3,20	2,90	3,90
max	3,00	4,20	3,70	4,40

The content of total lipids for semitendinosus muscle presents a unitary difference between registered values for the two carcasses, value of 2% being also the inferior limit of all the values that characterize the total lipid content of the two carcasses. The maximum of 4.4% was registered for trapezius muscle harvested from the first carcass (Table 7).

Calculated, the parameters mean fits between a minimum of 2.5% for semitendinosus muscle and a maximum of 4.15% for trapezius muscle. The values of the standard deviation and mean standard deviation are represented thus: 0.71 respectively 0.5 for semitendinosus and triceps brachii muscles and 0.35 for trapezius muscle (Table 7).

The percentage of total water from muscles from the two carcasses fits between a minimum of 74.1% triceps brachii muscle and a maximum of 76% corresponding to semitendinosus muscle (Table 8).

Maximum mean values (75.5%) corresponding semitendinosus muscle, it correlates to mean standard deviation by 0.5 and to a maximum coefficient of variation (0.94), while the standard deviation maintains the value of 0.35 for *Longissimus dorsi* muscle (Table 8).

Table 8

Water content identified in meat of deer *Capreolus capreolus* females

Nr. crt.	Water value % ♀			
	Semitendinosus muscle	Triceps brachii muscle	*Longissimus dorsi* muscle	Trapezius muscle
1	76	74,8	74,6	73,9
2	75	74,1	75,1	74,3
x(average)	75,50	74,45	74,85	74,10
sx(mean standard deviation)	0,500	0,350	0,250	0,200
s(standard deviation)	0,71	0,49	0,35	0,28

v%(coefficient of variation)	0,94	0,66	0,47	0,38
min	75,00	74,10	74,60	73,90
max	76,00	74,80	75,10	74,30

CONCLUZII

The study highlights that the features of chemical composition of deer meat are similar to meat from domestic ruminants under poor fattening condition;

The ratio between analyzed parameters reflects higher values for nutritional, biological and alimentary quality of meat obtained from deer, this being found in the actual preferences of consumers (the fat content reported to a low content of collagen)

The harvesting period of the studied specimens should be considered, given that the males were in the breeding period, which was reflected in lower organoleptic properties of meat obtained from males, a fact demonstrated also by different results for chemical composition of meat between sexes. The report of the chemical constituents is more favorable in females, determined by a higher percentage of fat with beneficial consequences on the energy value and culinary qualities.

ACKNOWLEDGMENT

This paper was published under the frame of European Social Fund, Human Resources Development Operational Programme 2007-2013, project no. POSDRU/159/1.5/S/132765.

BIBLIOGRAFIE

1. Daszkiewicz T., Kubiak D., Winarski R., Koba-Kowalczyk M. - *The effect of gender on the quality of roe deer (*Capreolus capreolus *L.) meat*. Small Ruminant Research, Vol. 103, Issuees 2-3, April 2012, Pages 169–175, doi:10.1016/j.smallrumres
2. Hutchison C.L., Mulley R.C., Wiklund E., Flesch J.S. - *Consumer evaluation of venison sensory quality: Effects of sex, body condition score and carcase suspension method*, Meat Sci., 2010, 86: 311–316.
3. Pollard J.C., Littlejohn R.P., Ashera G.W., Pearse A.J.T., Stevenson-Barry J.M., McGregor S.K., Manley T.R., Duncan S.J., Sutton C.M., Pollock K.L., Prescott J. - *A comparison of biochemical and meat quality variables in red deer (Cervus elaphus) following either slaughter at pasture or killing at a deer slaughter plant*, Meat Sci., 2002, 60: 85–94.
4. Alina Narcisa Postolache, P.C. Boişteanu, Roxana Lazăr - *Red deer meat (Cervus elaphus l.): between hunting and necessity*. USAMV Iași - Lucrări Ştiinţifice - Seria Zootehnie, vol. 55, pg. 507-511, 2013, Iași
5. Wiklund E., Manley T.R., Littlejohn R.P., Stevenson-Barry J.M. - *Fatty acid composition and sensory quality of musculus longissimus and carcass parameters in red deer (Cervus elaphus) grazed on natural pasture or fed a commercial feed mixture*, J. Sci. Food Agric., 2003, 83:419–424.

XENOBIOCHEMIC SPECIFICITY OF THE DEOXYRIBONUCLEIC ACID INTERACTION WITH SOME CYTOSTATIC CHEMOTHERAPEUTICS

NICOLAE MANOLESCU[1,2], ZENO GÂRBAN[3,4], VIOREL HERMAN[5], LUDOVIC SAYTI[6], FLORIN MUSELIN[5], CORNEL BALTĂ [4], SORIN MARINESCU[6]

1. University of Agronomic Sciences and Veterinary Medicine Bucharest, Institute of Comparative Medicine, Romania
2. "Al. Trestioreanu" Institute of Oncology, Bucharest, Romania
3. University of Agricultural Sciences and Veterinary Medicine of Banat "King Michael I of Romania" Timişoara, Faculty of Food Products Technology, Romania
4. Working Group for Xenobiochemistry, Romanian Academy-Branch Timişoara, Romania
5. University of Agricultural Sciences and Veterinary Medicine of Banat "King Michael I of Romania" Timişoara, Faculty of Veterinary Medicine, Romania
6. Institute of Chemistry Timişoara of the Romanian Academy, Romania

manolescunicolae@yahoo.com

Abstract:*The mostly recommended methods in oncotherapy are the surgical intervention, chemotherapy, radiotherapy, immunotherapy or a combination between them. The chemotherapy consists in the use of various drugs among which the most important are : the alkylating agents, antimetabolites, steroid hormones, antibiotics, phyto alkaloids, metal based drugs.*

In this review there are discussed the molecular mechanisms of the interaction of an alkylating cytostatic, i.e. cyclophosphamide (2 bis(β-chloroethyl) amino-1-oxa-3-aza-2-phosphocyclohexan-2-oxide) – Cp and of a metal based cytostatic, i.e. cis-platinumum (cis-dichlorodiammineplatinum) - cDDP with deoxyribonucleic acid (DNA). Cyclophosphamide and cis-platinum present similar mechanism of interaction with DNA. Interacting with DNA these cytostatics give rise to mono- and bidentate adducts. The topics are of interest for comparative medicine (veterinary and human medicine).

A particular importance arising from the appearance of the DNA-chemotherapeutic adducts is that these compounds can be detected analytically and can provide information on the consequences of the biochemical injury. Detection of DNA adducts is useful not only for the diagnosis of neoplastic diseases, but also for biomonitoring the evolution during chemotherapy.

Key words *: deoxyribonucleic acid, xenobiotics, cytostatic chemotherapeutics*

INTRODUCTION

In cancer treatment the mostly recommended solutions are the surgical intervention, chemotherapy, radiotherapy, immunotherapy or a combination between them (Ghilezan, 1992; Price and Sikora, 2002; Manolescu, 2003). Chemotherapy consists in the use of chemical substances among which the most important are : the alkylating agents, antimetabolites, steroid hormones, antibiotics, phyto alkaloids, metal based drugs (Price and Sikora, 2002). The approached thematic in this review is of interest for comparative medicine. More exactly, there are presented data regarding the cytostatic drugs cyclophophosphamide (Cp) and cis-platinum (cDDP) which can be considered as chemical xenobiotics of pharmaceutical interest, from the point of view of comparative oncology.

Cyclophosphamide due to its chloroethyl group may become a bifunctional alkylating agent (Lindemann and Harbers, 1980; Gârban, 1986 a; Johnson et al., 2012).

Binding either to the phosphodiesteric groups of the DNA strands or to the guanine nucleobase of DNA a monoalkyl- or dialkyl guanine derivative is resulting which will generate adducts of type DNA-Cp.

Cis-platinum having in its structure a divalent platinum atom may also realize two bifunctional bonds (Gârban, 1986 b ; Lippert, 1999). The binding occurs particularly to the guanine (G) nucleobases of DNA and a lesser extent to the nucleobases adenine (A), thymine (T) and cytosine (C).

Generally it is considered that chemical xenobiotics are represented by organic/inorganic substances which belongs to various classes of compounds. In the acceptation of Biochemistry/Xenobiochemistry the chemical xenobiotics could be of food interest (e.g. additives, contaminants), of pharmaceutical interest (chemotherapeutics obtained by synthesis or by extraction) and of toxicological interest (biocides). The subject of this paper circumscribes two xenobiotics of pharmacological interest often used both in veterinary and human medicine for treatment (Martin, 1989; Gârban et al., 1990; Manolescu, 1997; Summers, 2014).

1. Chemical structure of cyclophosphamide and *cis*-platinum

One of the most frequently used antitumor compound is cyclophosphamide (fig.1-a, fig.1-b), an alkylating agent. Its pharmacologically active group is 2-bis (β-chloroethyl)-amino-2-oxo-1,3,2-ozazaphosphorinan often called nitrogen mustard (Lindemann and Harbers, 1980; Gârban et al., 1986 a).

Cis-platinum (fig.1-c) is a synthetic anticancer agent that belongs to the group of the metal-based alkylating agents (Haiduc and Silvestru, 1989; Reedijk, 2008).

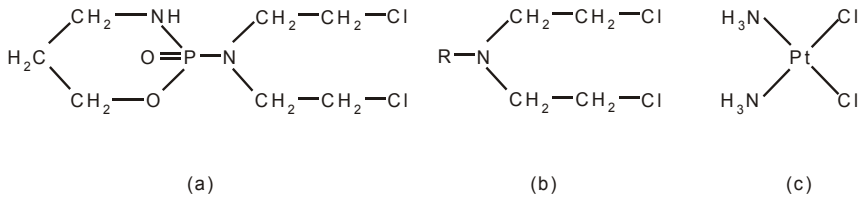

Fig.1. Chemical formula of cyclophosphamide and cis-platinum :
a) Cp - structural formula; (b) Cp- general formula; (c) cDDP - structural formula

From the chemical point of view *cis*-platinum is an inorganic coordination compound. It was synthetised by Peyrone in 1845 and the separation of its *cis* and *trans* isomers was made by Werner in 1889 (Lippert, 1999). Since the investigation of its cytostatic action by Rosenberg (1985), various pharmacological studies were performed. It was concluded that the receptor substratum in the interaction of *cis*-platinum with biological systems is represented by nucleic acids and particularly by the DNA macromolecule which conveys the genetic information (Reedijk, 2008).

In this context the molecular mechanisms of interaction for the alkylating agent cyclophosphamide and the metal-based drug cis-platinum (Pană et al., 1983; Johnson et al.,

2012; Galuzzi et al., 2014) will be exposed. Hereinafter will be discussed the chemical structure of the mentioned chemotherapeutics and details on their interaction with DNA.

A general mention is made with respect to that in case of Cp administration the cytotoxic effect target mainly the liver functions and in case of cDDP the renal functions.

A particular aspect in cytostatic chemotherapy is the fact that the DNA adducts make possible the biomonitoring of cases. In such circumstances there are discussed the investigations extended to biomarkers (Hemminki et al., 1998).

2. Mechanisms of action

2.1. Interaction of cyclophosphamide with DNA

The main target of Cp in biologic systems is represented by the nucleic acids, especially DNA. While the final alkylation targets of Cp are the guanine and cytosine bases of tumor cell DNA, it is activated in the liver to hydroxy-Cp, which enters tumor cells and converts to phosphoramide mustard (Gârban et al., 2000; Wolkenberg, 2001). The highly reactive metabolites of Cp interact with DNA, disturbing the structure – biologic activity relationship of the macromolecule, with dramatic effects on the cell life.

The mechanism of the interaction between Cp and DNA, which explains the antitumoral effects, is determined by the capacity of nitrogen mustards to bind to the N_7 atom of guanine, the most nucleophilic center, accessible from a steric point of view within the framework of the helical structure (Gârban, 2009). The interaction results in the formation of mono- or di-alkylated derivatives of the guanylic residue (the latter are typical for Cp). The attack of the alkylating agent Cp can lead to the appearance of both intrastrand and interstrand links. The interstrand links affect the guanines from different DNA strands, determining cross-linking which rapidly can block the replicative process of DNA. Whatever the linking manner, the final effect is the same: the modification of the chemical structure of the DNA macromolecules, followed by the disturbance of the biological activity – fig.2.

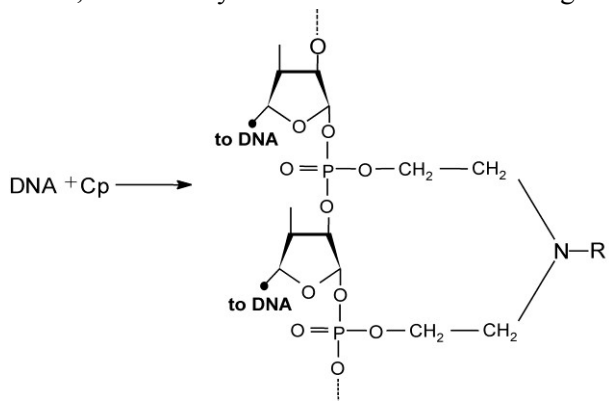

Fig 2. Binding mode of Cp to the phosphoric groups of DNA

The interaction of Cp with DNA, macromolecule which bears the genetic information, also implies the possibility that replication-transcription and translation processes could be affected (Johnson, 2012). As a result, the influence of protein synthesis is possible.

Cyclophosphamide is used in clinic to treat non Hodgkin lymphoma, Burkitt's lymphoma, chronic lymphocytic leukemia, various visceral solid tumors with rapid

proliferation tendency; Cp is often used in combination with surgical treatment, radiotherapy and other cytostatics. The indications of Cp in benign diseases include chronic evolutive arthritis, systemic lupus erythematosus, nephrotic syndrome, Waldenström disease, multiple sclerosis. Due to its immunoablation activity Cp is also used in preparative regimens for allogenic transplantation. Many studies have been made up to the present concerning the biologic effects of Cp, existing an extensive literature in the area.

Biogenesis of DNA-Cp adducts (fig.3) occurs by the cyclophosphamide binding to DNA after releasing one Cl^- atom and generating a monodentate derivative (monoalkylated) and after releasing two Cl^- atoms giving rise to a bidentate derivative (dialkylated)

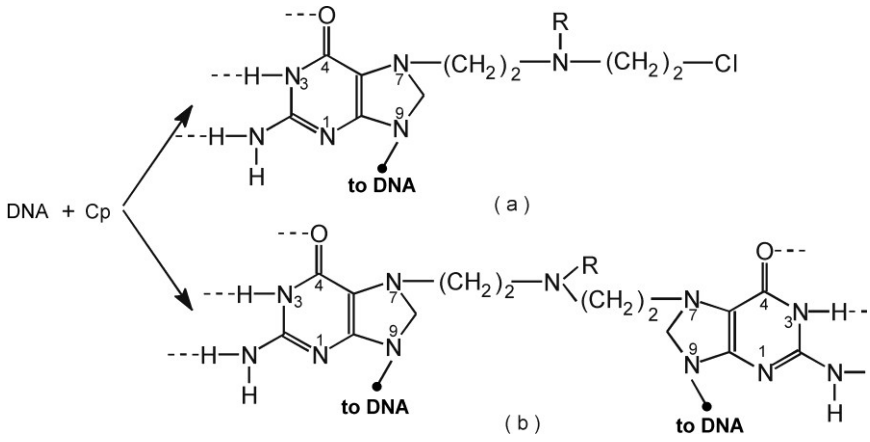

Fig. 3. Binding of Cp to the guanine nucleobase of DNA
a) mono(alkyl)guanine-derivate; b) di(alkyl)guanine-derivate

2.2. Interaction of cis-platinum with DNA

In the antitumoral chemotherapy different metallic compounds containing Pt, Pd, Ru etc. were studied. Among them *cis*–dichlorodiammineplatinum (abbreviated *cis*-platinum, *cis*-DDP or cDDP) is mainly used as a component of various drugs, such as: Cysplatyl, Neoplatin, Platidiam, Platinex a.o.

Cis-platinum is characterised by a planar geometry, has two inert ligands ($2NH_3$) and two labile ligands ($2Cl^-$) which are released during the hydrolysis (Rosenberg, 1985; Dasari and Tchounwou, 2014). Hydrolysis, developed in two steps, implies the mono- or diaquated platinum species formation (fig.4).

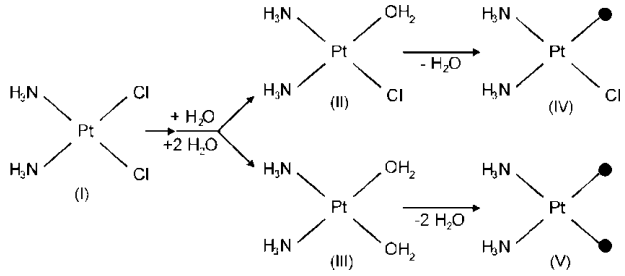

Fig.4. Formation of mono- and diaquated species of *cis*-platinum

Both species can form bindings with the nucleobases of DNA and, in some cases, with DNA (polyheteronucleotidic macromolecule) and protein (polyheteroaminoacid molecule) – symbolized by the amino acid chain (-aa-aa-). The bindings to the DNA nucleobases are made in the preferential order: guanine > adenine > cytosine, observing that thymine is not so often involved (Reedijk, 2008; Gârban et al., 2014; Manolescu et al., 2014). The binding may be homomacromolecular (DNA–cDDP) or heteromacromolecular (DNA–cDDP–Protein). As a result of the binding different derivatives with mono- or bidentate ligands are formed (fig.5)

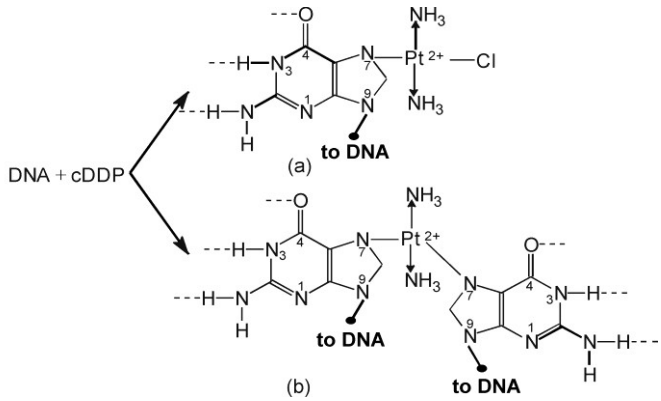

Fig. 5. Binding of cDDP to guanine nucleobase of DNA
a) fixing of monodentate ligand; b)) fixing of bidentate ligand

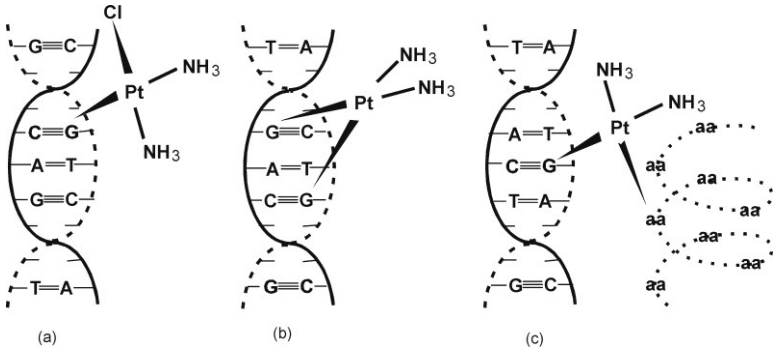

Fig.6. Binding of cDDP to DNA or to DNA and proteins:
a) monofunctional binding to a nucleobase; b) binding to different nucleobases;
c) heteromacromolecular binding between DNA strand and a polypeptide

Cis-platinum binding to the DNA can be made to the intrastrand nucleobases resulting adducts of type DNA-cDDP (i.e. homomacromolecular) or to nucleobases and protein generating adducts of type DNA-cDDP-Protein (i.e. heteromacromolecular) – see fig.6.

Generally, the usage of cis-platinum in the cytostatic chemotherapy is based on its interaction with DNA when various adducts of type DNA-cDDP result (Gârban, 2004). Adducts are formed by different bindings: (a)interstrand cross-link to different nucleobases; (c) interstrand cross-link to identic nucleobases; (b) intrastrand cross-link to identic

nucleobases; (d) intrastrand cross-link to different nucleobases; (e) intrastrand cross-link to nucleobase-monoadduct; (f) hetero-macromolecular cross-link DNA-cDDP-Protein.

Thus, the resulted DNA-cDDP adducts limit the division of cells and especially of the cancer cells. This means that cis-platinum, as a frequently used chemotherapeutic drug, affects mostly the cancer cells which a higher growth rates. In the organism the presence of the adducts DNA-cDDP can be detected analytically and can provide information about the efficiency of the anti-cancer action of the applied chemotherapeutic.

Discussing aspects related to the interactions of the DNA with cyclophosphamide (biogenesis of DNA-Cp adduct) and with cis-platinum (biogenesis of DNA-cDDP adduct) as well as their use in chemotherapy it is necessary to mention similarities and distinctions (Gârban et al., 1990; Gârban et al., 2009).

Similarities consist in the formation of adduct type complexes which reduce the multiplication of cells (having a more rapid rate in case of neoplasic cells) by disturbing their DNA biosynthesis . By this way the metastatic processes are limited, too.

Distinctions consist in their therapeutic efficiency in various types of neoplasis. In this regard it is known that cyclophosphamide is used with good results in the treatment of lymphomas, leukemia, breast cancer, malignant pheochromocytoma, Ewing's sarcoma a.o. Cis-platinum is more efficient in the therapy of testicular cancer, ovarian cancer, cervical cancer, sarcomas etc.

CONCLUDING REMARKS

Assessment of the adducts formation activity of Cp and cDDP – chemical xenobiotics of pharmacological interest - led to the knowledge of the specific molecular mechanisms and allowed to understand their cytostatic/cytotoxic effects.

In this context the structural characteristics, molecular speciation of Cp and cDDP as well as their interaction with the DNA macromolecule have been defined. The interaction is followed by the biogenesis of DNA-Cp, DNA-cDDP and DNA-cDDP-Protein adducts types. In the oncotherapy of humans and animals it is important to know also the neoplastic disease forms with better response to the use of these cytostatics

Presently, a domain of excellence in the cytostatic chemotherapy consists in the detection of DNA adducts useful in the biomonitoring of cases. But, in order to personalize the chemotherapy it must be taken into consideration the specificity of the resulting dyshomeostasis in metabolomics, too.

***Note**: The present paper was elaborated within the activity of the «Romanian Society of Comparative Oncology » Bucharest (Manolescu) and of the Working Group for Xenobiochemistry Timişoara (Gârban). Studies in the same domain were extended (after February 14, 2015) in the framework of the collaboration with the Faculty of Veterinary Medicine Timişoara.*

This work was communicated at the Jubilee Session of 70 yrs from the foundation of the University of Agricultural Sciences Timişoara (1945-2015).

REFERENCES

1. Dasari S., Tchounwou P.B. – Cisplatin in cancer therapy : molecular mechanisms of action, *Eur.J.Pharmacol*., 2014, 740, 364-378
2. Galluzzi L., Vitale I., Michels J., Brenner C., Szabadkai G., A Harel-Bellan A, M Castedo M., Kroemer G. - Systems biology of cisplatin resistance: past, present and future, *Cell Death and Disease*, 2014, 5, e1257. doi:10.1038/cddis.2013.428
3. Gârban Z., Roth L., Ion N., Mărculescu E., Brazdă Maria, Siniteanu A., Neda G. – Medicamente azotiperitice utilizate în chimioterapia antitumorală. Particularităţi structurale, mecanism de acţiune.,*Timişoara Medicală,* 1986 a 3, 71-84.
4. Gârban Z., Maurer Ana, Miklos J, Repanovici Rodica, Daranyi Gabriela, Precob V., Sayti L., Popeţi Doina - Some considerations concerning the action of cis-platinum on deoxyribonucleic acid. I. Investigations in vitro and in vivo*, Rev. roum. Biochim.,* 1986 b, 23(4), 293-302.
5. Gârban Z., Drăgan P., Daranyi Gabriela, Riviş I., Mareş A., Eremia Iulia - The effects of cis-platinum and cyclophosphamide on deoxyribonucleic acid, p.52, in *XIth International Symposium on Medicinal Chemistry*, Jerusalem-Israel, September 2-7, 1990
6. Gârban Z., Moldovan I., Avacovici Adina, Daranyi Gabriela - Structure-activity relationships in case of interaction between cis-platinum and deoxyribonucleic acid, pp.517-522, *Current Problems in Cellular and Molecular Biology* (Crăciun C., Ardelean A., Eds.), Publishing House Risoprint, Cluj-Napoca, 2000.
7. Gârban Z. - Influence of metals on deoxyribonucleic acid, Chap. 7. pp.401-414, in *"Elements and their Compounds in the Environment: Occurrence, Analysis and Biological Relevance"* Vol. I General Aspects, (Merian E., Anke M., Ihnat M., Stoeppler M., Eds.), 2nd edition, Wiley-VCH Verlag GmbH & Co KgaA, Weinheim, 2004
8. Gârban Z. (Ed.) - *Biologie moleculară: concepte, metode, aplicaţii*, ediţia 6-a, Editura Solness, Timişoara, 2009.
9. Gârban Z., Manolescu N., Herman V., Avacovici Adina, Ioniţă Hortensia, Muselin F., Ahmadi-Vincu Mirela - Characteristics of the structure - activity relationship in case of platinum compounds: theoretical and applicative aspects, *Scientifical Papers: Veterinary Medicine Timişoara*, 2014, Vol.XLVII(1), 136-146.
10. Ghilezan N. - *Oncologie generală*, Editura Medicală, Bucureşti, 1992.
11. Haiduc I., Silvestru C. - *Organometallics in cancer chemistry, Vol.I,* CRC Press Boca Raton, Fl., 1989.
12. Hemminiki K., Byhov V., Yang K., Rajaniemi H. – Use of DNA adducts in Biomonitoring, pp. 133-135, in *Biomarkers: Medical and Workplace Applications* (Mendelson L., Mohr L.C., Peeters J.P., Eds.), Joseph Henry Press, Washington DC, 1998.
13. Johnson L.A., Malayappan B., Tretyakova N.Y., Campbell C., Macmillan M.L., Wagner J.E., Jacobson P.A. - Formation of cyclophosphamide specific DNA adducts in hematological diseases. *Pediatr. Blood Cancer,* 2012, 58, 708-714.
14. Lindemann H., Harbers E. - In vitro - Reaktion der drei alkylierenden Pharmaka Cyclophosphamid, Ifosfamid und Trofosfamid mit DNS und DNS Bausteinen, *Drug. Res*., 1980, 30, 12, 2075-2080.
15. Lippert B. (Ed.) - *Cisplatin : Chemistry and Biochemistry of a Leading Anticancer Drug*, Verlag Helvetica Chimica Acta Zurich, Wiley VCH, Weinheim-NewYork-Chichester-Brisbane-Singapore-Toronto, 1999.
16. Manolescu N. (Ed.-Coord.) - *Aspecte de patologie celulară comparată. Vol.1*, Editura Ceres, Bucureşti, 1997.
17. Manolescu N. (Ed.) - *Introducere în oncologia comparată*, Editura Universitară "Carol Davila", Bucureşti, 2003.
18. Manolescu N., Gârban Z., Herman V., Balint Emilia, Gârban Gabriela, Dărăbuş Gh., Nicola Tr., Muselin F., Avacovici Adina, Savici Jelena - Effects of cis-platinum on the biochemical homeostasis in rats Note I. Investigations on the hepatic DNA and on serum proteins, *Scientific Works Series C, Veterinary Medicine Bucharest*, 2014, Vol. LX(2), 43-47.

19. Martin R,J. – Small animals therapeutics, J. Wright, Butterworth and Co. (Publishers) Ltd, London-Boston-Durban-Singapore-Sydney-Toronto-Wellington, 1989
20. Pană I., Gârban Z., Mihalca Victoria, Brazdă Maria, Sayti L. - Aspecte comparative privind acţiunea radiaţiilor X şi a ciclofosfamidei., *Radiologia,*1983, XXI, 4, 285-296.
21. Price P., Sikora K. (Eds.) – Treatment of cancer, 4th edition, Arnold, London, 2002.
22. Summers Alleice – *Common diseases in companion animals*, 3rd edition, Elsevier/Mosby, Philadelphia, 2014
23. Reedijk J. – Significance for effectiveness as anticancer drugs, *Platinum Metals Rev*., 2008, 52(1), 2-11
24. Rosenberg B. – Fundamental studies with cisplatin, *Cancer*, 1985, 55(10), 2303-2316
25. Wolkenberg S.E., Boger D.L. - Mechanisms of in situ activation for DNA-targeting antitumor agents. *Chem Rev*., 2002, 102, 2477–2495

THE MORPHOPATHOLOGICAL PREVALENCE OF INFLAMMATORY CARDIOMYOPATHIES IN DOGS

ADRIAN OLARIU-JURCA
Banat's University of Agricultural Sciences and Veterinary Medicine „King Michael I of Romania" from Timisoara, Romania
olariujurca_adrian@yahoo.com

Abstract: *The research was conducted during the period October 2013-May 2015 and it consisted of the necropsic exam of 30 dog bodies of different ages, sexes and breeds. It was completed with a microscopic exam of the histopathological preparations which were obtained from heart samples coming from 19 cases which presented lesions. Eight cases were diagnosed with inflammatory cardiomyopathies (42.09%). The diagnosed cardiac lesions, of the cases taken into study were multiple and complex, they developed in the same time or successively in several structures (pericardium, myocardium and endocardium as well as in blood vessels). They were exteriorized through pericarditis (5.26%), myocarditis (21.5%) and endocarditis (10.52%) as well as parasitic pulmonary arteritis (5.26%). Fibrinous pericarditis, chronic evolution, signaled in one of the cases was histopathologically exteriorized through the presence of fibrin networks with leukocytes and erythrocytes, attached to the swollen and infiltrated with inflammatory cells epicardium.*

The myocarditis which was morphopathologically identified, was represented by the parenchymatous myocarditis in one case, lymphohistiocitary myocarditis in two cases and fibrous interstitial myocarditis in one case.

The endocarditis we diagnosed morphopathologically was represented by the verrucous or thrombotic endocarditis (5.26%) as well as by ulcero-polypous endocarditis (5.26%).

In one case with cardiopulmonary dirofilariosis, we anatomopathologically diagnosed wormy pulmonary arteritis, expressed through lesions of several degrees, intensities and extensions of the arterial wall. They were translated through erosions of the intima as consequence of the contact with dirofilaria larvae.

Key words: *morphopathological prevalence, inflammatory cardiopathies, dogs*

The heart, respectively the myocardium, is the biggest energy consumer in the animal organism during their entire lives. In this purpose, the cardiomyocytes, despite the fact that in essence they are only muscular fibers, possess an ultrastructure which is orientated towards the oxidative processes. It is considered that the number of the mitochondrias is around 250 billion/ myocardium gram. They are big oxygen consumers, 5 times bigger than the cells in the liver (7).

Under the influence of numerous aggressors, cathecolamines accumulate in large quantities and cause a short intensification of the metabolic activity. This generates and oxygenation deficit, morphopathologically translated through fuchsinephile degeneration, myocytolisis followed by the activation of the active mezenchyma, hyperplasia and differentiation in the directions of cellular and humoural defense with the apparition of a reactive complex with different influences on the vital functions (2, 4, 9, 10).

The lesions of the myocardium start in the shape of relatively simple modifications which amplify and complicate in time, leading to more or less serious heart failure (1, 2, 4, 7).

Heart diseases generally have circulatory disorders as pathomorphic substrate (thrombosis, ischemic necrosis), atrophies, specific and unspecific inflammations, processes

that do not differ significantly from the ones located in other places. The only differences regard etiological conditions and specific clinical manifestations (3, 5, 6, and 10).

MATERIALS AND METHODS

The research of the present study was conducted in the period October 2013-May 2015, through an anatomopathological examination of hearts taken from 30 dog bodies of different ages, breeds and sexes, 19 cases presented cardiac lesions. The bodies came from private owners, kennels and animal shelters and they were necropsied and examined at the Forensics discipline in the Faculty of Veterinary Medicine.

The bodies were put in dorsal position and then they were necropsied. After the external and internal examination of the bodies we performed the evisceration according to the specific technique (5, 6). The evisceration of the heart was made by sectioning the sterno-pericardial ligament and the big vessels. This was followed by the macroscopical examination of the heart through inspection, palpation and sectioning in order to identify the physic-structural modifications of the heart 9 shape, size, colour, aspect, and shine, thickness of the pericardium, myocardium, and cavity ratio.

After a detailed examination of the heart, 19 samples were taken from the bodies which presented cardiac lesions, from the: pericardium, myocardium, endocardium and pulmonary artery for the histopathological exam. The samples were processed using the paraffin technique; they were cut at 6 μm and stained using the HEA method in order to identify microscopic cardiac lesions. The histopathological preparations thus obtained were examined using a research microscope MC 5 A with ocularies of 10 and higher and the photographing was done using an Olympus CX41 microscope (acquired through POS CCE, DICES-MVT 2669-145). After the examination and interpretation of the histopathological preparations, microphotographs were taken to illustrate the most characteristic histological modifications.

RESULTS AND DISCUSSIONS

The research regarding cardiomyopathies in dogs was systemized intro four groups: pericarditis, , myocarditis, endocarditis and arteritis (Table 1, Fig.1.).

The inflammatory cardiomyopathies were diagnosed in 4 cases out of which one was parenchymatous.

Myocarditis, two cases were lymphohistiocitary myocarditis and one was fibrous interstitial myocarditis.and with friable consistency. The serous pericardial surfaces (visceral and parietal are thickened, opaque, dull, harsh due to fibrin deposits (hairy heart). Fibrinous pericarditis with chronic evolution was diagnosed in the case which presented interstitial fibrous myocarditis.

Macroscopically, the pericardial sack is distended and slightly adherent to the epicardium due to the fibrinous exudate, of grey-yellowish colour, with an aspect similar to greaves Myocarditis, two cases were lymphohistiocitary myocarditis and one was fibrous interstitial myocarditis.and with friable consistency. The serous pericardial surfaces (visceral and parietal are thickened, opaque, dull, harsh due to fibrin deposits (hairy heart). Microscopically, using the x10, x20, x40 objectives we noticed: the myocardium in transversal section, subepicardial conjunctive tissue, swollen epicardium, infiltrated with leukocytes and erythrocytes, fibrin network attached to the epicardium,

with leukocytes and erythrocytes in its holes, with fibrinoidosis and coagulation necrosis of the valvular endocardium (Fig. 2.).

The parenchymatous myocarditis or the acute toxic myocarditis was identified in one case, a stray, 4 year old, male dog from a kennel. Macroscopically, the heart was enlarged, of grey-yellowish color, even both at inspection and on section, with the aspect of a boiled organ. This type of inflammation is hard to differentiate macroscopically from the granular myocardosis, the only exam capable of differentiating them being the histopathological exam. Microscopically, we noticed granular degeneration in the myocardiocytes, hyalinosis in the myocardial fibers, sero-leukocytic interstitial exudate and rare fibrilar hyperplasia of the local mezenchyma in the perifibrilar and peri-fascial spaces (Fig. 3.). This inflammation is the consequence of various intoxications and also of canine parvovirus and herpesvirus. Lymphohistiocitary myocarditis, found in two cases, was exteriorized macroscopically through the enlargement of the heart, even grey-yellowish color and on section the myocardium had a fatty aspect and high consistency. Microscopically, we could notice interstitial, lymphohistiocitary hyperplasia, located perifibrilar and perifascial, fallowed by atrophies and dystrophies and necrosis of the myocardial fibers (Fig. 4.). It is signaled in parvovirus encephalo-myocarditis in puppies. It is more frequent in young puppies from unvaccinated others and in dogs up to the age of 8 weeks is caused by a parvovirus.

Fibrous interstitial myocarditis, diagnosed in one case, is a predominantly productive inflammation that appers either as a consequence of necrotic, parenchymatous or lymphohistiocitary myocarditis or as an irrigation disorder of the myocardium. Macroscopially, on inspection and on section, diffuse white areas of fibrosis, of high consistency, can be noticed on the red-brownish background of the myocardium. Microscopically, there are exudates, infiltrations of inflammatory cells, mostly eosinophils and peri-fibrilar and peri-fascial fibro-conjunctive hyperplasia which lead to atrophies, dystrophies, and necrosis of the myocardial fibers (Fig. 5.).

Verrucous endocarditis (thrombotic) diagnosed in one case, is macroscopically exteriorized through the apparition on the tricuspid valvular endocardium of deposits with an irregular surface, isolated or confluated, of various dimensions (Fig. 6.).

Microscopically, we noticed endothelial desquamation, agglutination of thrombocites and deposition of fibrin in the shape of polyps (Fig.7.). Ulcero-polypous endocarditis was identified in one case, with right cardiac dilation. Macroscopically, one can notice voluminous polyps on the valve endocardium, with an irregular surface, altenated with ulcerative areas (Fig. 8.). Microscopically, the process starts with an ulceration, with abundant fibrin and cellular deposits on its surface (mixed thrombi). One can notice: sero-fibrinous and leucocitary infiltration of the endocardium, polyps made of fibrin, leukocytes and red blood cells, fibrinoidosis and coagulation necrosis ; reduced unspecific mesenchymal reaction which justifies the high friability of the polyps (Fig. 9.).

Verminous pulmonary arteritis was identified in one case which presented cardiac dirofilariosis (Fig. 10.). Microscopically, there are lesions of different degrees of intensity or extension in the arterial wall. They are translated through erosions of the intima as consequence of the contact with dirofilaria larvae (L5). Vascular lesions are represented by endothelial denudation, larvae thromboembolisms, endarteritis with

leukocitary infiltrate, mostly eosinophils, intimal hyperplasia with intraluminal focal appearance, giving it its rough aspect and in several areas, there are also granulomatous reactions in the arterial wall (Fig. 11.). The vascular lesions are the effect of mechanic trauma caused by parasites, but also of the intervention of several cytokins, especially the growth factor derived from the plates. This hypothesis is also mentioned in the consulted specialty literature. The intimal roughness favors obliterant thrombo-embolisms which cause pulmonary infarctions. The acute inflammatory reaction lasts as long as the larvae are present, and are accompanied by proliferation of the conjunctive tissue which will organize the superficial thrombus.

Table 1

Frequency of cardiomyopathies

No.	Necropsied dogs	Total of cases with cardiomyopathies	Inflammatory cardiomyopathies								%
			Pericarditis		Myocarditis		Endocarditis		Arteritis		
			%		%		%		%		
1	30	19	5,26	1	21,05	4	10,52	2	5,26	1	42,09

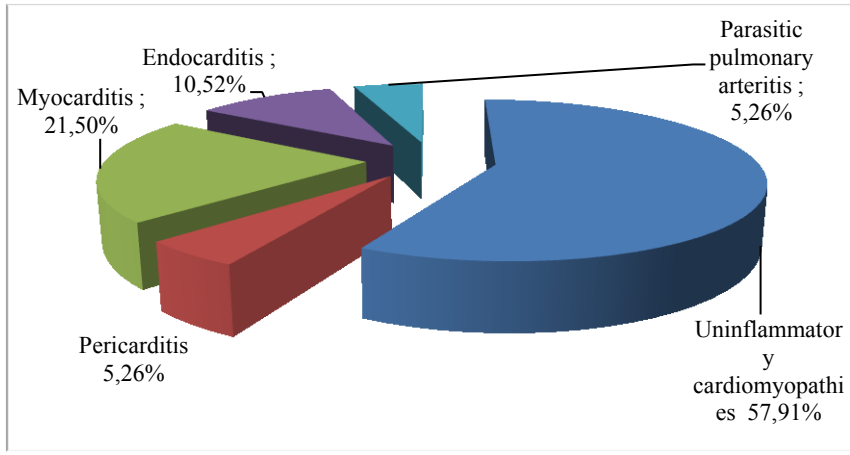

Fig. 1. Graphic representation of the prevalence of inflammatory cardiomyopathies.

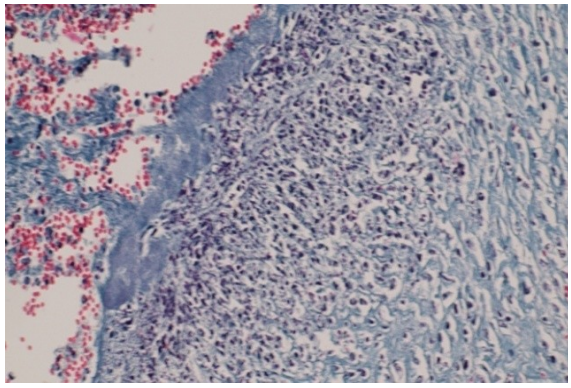

Fig. 2. Fibrinous pericarditis: swollen epicardium, infiltrated with leukocytes and erythrocytes, fibrin network attached to the epicardium, with leukocytes and erythrocytes. Col. HE x 10.

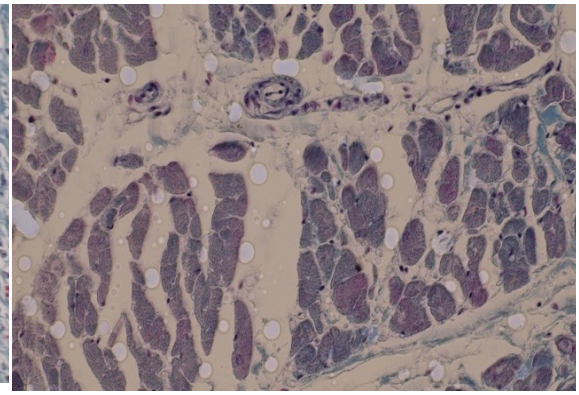

Fig. 3. Parenchymatous myocarditis: granular degeneration in the myocardiocytes, hyperplasia of the local mezenchyma in the perifibrilar and peri-fascial spaces. Col. HEA x40.

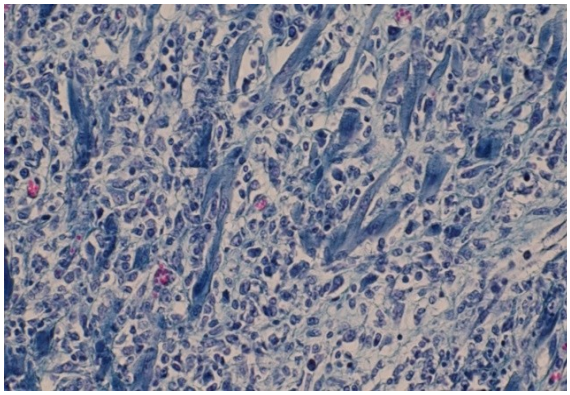

Fig. 4. Lymphohistiocitary myocarditis: lymphohistiocitary hyperplasia, located perifibrilar and perifascial fallowed by atrophies, dystrophies and necrosis. Col. HEA x40.

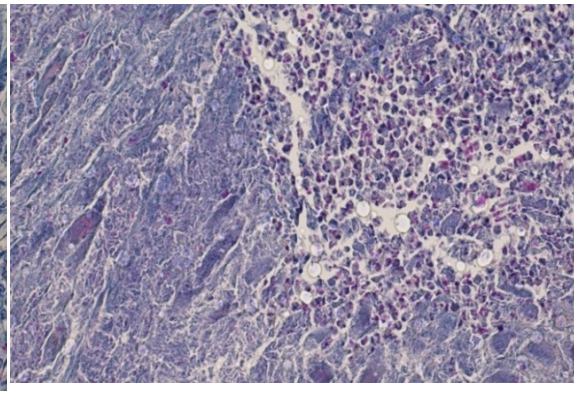

Fig. 5. Fibrous interstitial myocarditis and eosinophilic: interstitial fibro-conjunctive and eosinophilic hyperplasia which lead to atrophies, dystrophies, and necrosis. Col. HEA x20.

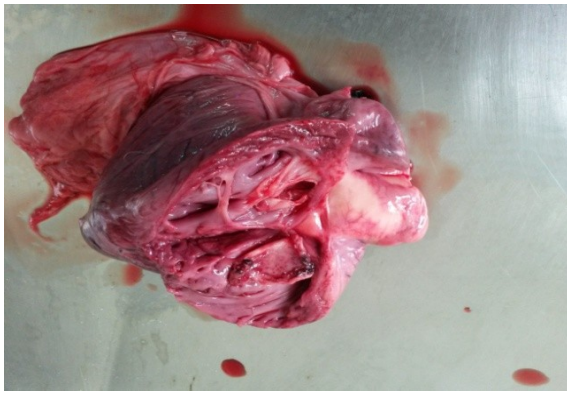

Fig. 6. Verrucous endocarditis (thrombotic): deposits with an irregular surface, isolated or confluated on the tricuspid valvular endocardium.

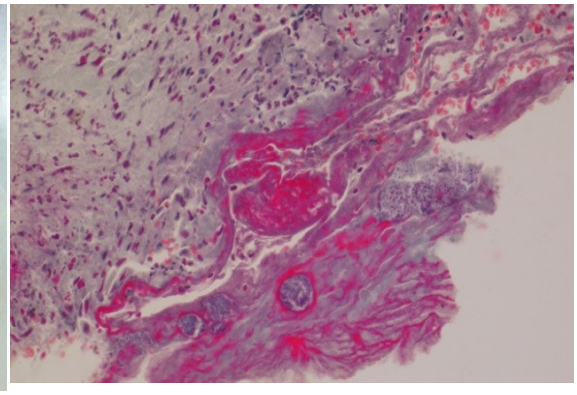

Fig. 7. Verrucous endocarditis (thrombotic): thrombus attached to the swollen and edematous endocardus. Col. HEA x40.

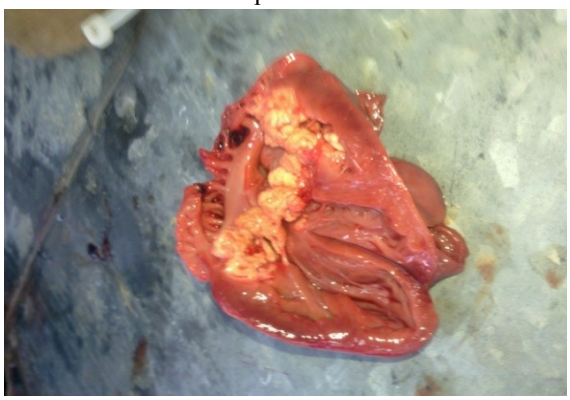

Fig. 8. Ulcero-polypous endocarditis and myocardial steatosis.

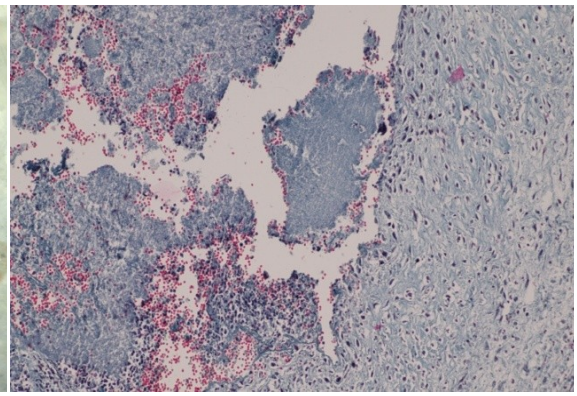

Fig. 9. Ulcero-polypous endocarditis: vegetation attached to the edematous endocardium infiltrated with inflammatory cell elemets. Col. HEA x 20.

Fig. 10. Dirofilaria in cardiac cavities and pulmonary artery.

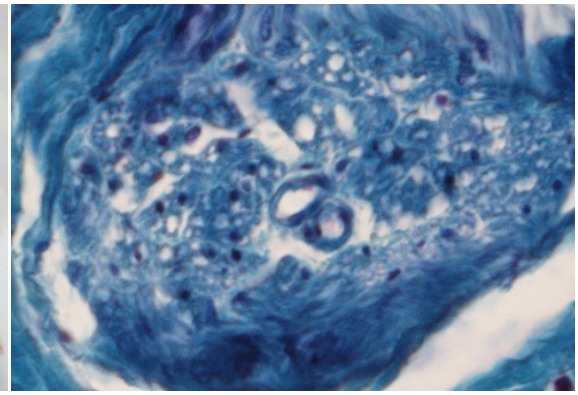

Fig. 11. Vermin pulmonary arteritis (dirofilaria): endothelial denudation and larval thromboembolisms. Col. HEA x 100.

CONCLUSIONS

Out of 19 cases presented, which have shown lesions of the heart, 8 cases were diagnosed with inflammatory cardiopathies.

The hearts belonging to the examined cases have shown inflammatory lesions (42, 09%), proving a big implication in the cardiac pathology of this species.

The diagnosed cardiac lesions, of the cases taken into study were multiple and complex, they developed at the same time or successively in several structures (pericardium, myocardium, endocardium and blood vessels) exteriorized through pericarditis (5.26%), myocarditis (21.5%), endocarditis (10.52%) and pulmonary arteritis (5.26%). The inflammatory myocardiopathies are on the first place, and they are represented by parenchymatous ar acute toxic myocarditis (5.26%), lymphohistiocitary myocarditis (10.52%) and fibrous myocarditis (5.26%), lymphohistiocitary myocarditis (10.52%) and fibrous myocarditis (5.26%) followed by thrombotic or verrucous endocarditis (5.26%), ulcero-polypous endocarditis (5.26%) and pulmonary verminous arteritis (5.26%).

The vascular lesions are represented by the verminous thrombo-arteritis of the pulmonary artery, caused by dirofilaria.

REFERENCES

1. BRĂSLAȘU, C.M., (2011)- Bolile cordului în medicina internă a animalelor, coordonator FALCĂ,C, Editura Eurostampa, Timișoara, cap XXIV,582-643.
2. CALIARI, M.V., MACHADO, R. DO., LANA, M. DE., CAJÂ, R.A.F., CARNEIRO, C.M., BAHIA, M.T., SANTOS, C. A. B. DOS., MAGALHÃES, G. A., SAMPAIO, I. B. M., TAFURI, W.L., (2002) - Quantitative analysis of cardiac lesions in chronic canine chagasic cardiomyopathy. Rev. Instituto de Med. Tropical de Sao Paulo, 44, 5, 273-278.
3. HERMAN, V., MOGA MĂNZAT, R., RĂMNENŢU, M., (2008) – Diagnosticul în boli infecţioase comune mai multor specii de animale, Ed. Mirton Timişoara.
4. McGAVIN, M.D., CARLTON, W.W., ZACHARY, J.F., (2001) - Special veterinary pathology, Ed. Mosby, USA.
5. OLARIU-JURCA, I., (2006) – Diagnostic necropsic şi medicină legală veterinară, Ed. Brumar, Timişoara.
6. OPREAN, O.Z., (2002) – Diagnosticul necropsic la carnivorele de companie, Edit. ''Ion Ionescu de la Brad'', Iasi.
7. PAUL, I., (1990) - Morfopatologia aparatelor şi sistemelor organice. Bul Inf. al SMV nr. 23-24, Bucureşti.

8. ROBINSON W. F., HUXTABLE C. R., PASS D. A., (1980) - Canine parvoviral myocarditis: A morphologic description of the natural disease. Vet Pathol. 17, 282-293.
9. ROBINSON WF, MAXIE MG., (1993) - The cardiovascular system. In: Jubb KVF, Kennedy PC, Palmer N, eds. Pathology of Domestic Animals. Vol. 3. 4th ed. New York: Academic Press, 1-100.
10. VLEET, V.J.J., FERRANS,J., (2001)- Cardiovascular system, In Special veterinary pathology, Edit.by.GAVIN, M.D., CARLTON, W.W., Zachary, F.J., MOSOY, SUA Edition 3, 4, 197-333.

MORPHOPATHOLOGICALL QUANTIFICATION OF UNINFLAMMATORY PNEUMOPATHIES IN DOGS

ADRIAN OLARIU-JURCA
Banat's University of Agricultural Sciences and Veterinary Medicine „King Michael I of Romania" from Timisoara, Romania
olariujurca_adrian@yahoo.com

Abstract: *Uninflammatory pneumopathies were microscopically and macrospically diagnosed in 22 cases (73.33%) out of a total of 30 necropsied dogs. A chronic evolution of the essential alveolar emphysema was morphopathologically diagnosed in 3 cases (13,63%). Macroscopically, the lungs were enlarged, with a tense pleura, pale, crepitant with a negative docimasy while microscopically, we could enhance the accentuated distension of the alveoli which presented flat pneumocytes and were accompanied by the rupture of the alveolar walls. Thrombosis of the pulmonary vein was noticed in one case (4,54%), with parietal thrombi present, microscopically, in the lumen of the vessel. A pulmonary red infarction was also diagnosed in one case (4,54%). Macroscopically, at inspection and section, we notice compact dense, dark-red areas, of triangular shape, with the base headed towards the pleura and the top pointed towards the pulmonary parenchyma, towards the obstructed vessel. Microscopically, a hemorrhagic infiltrate could be noticed in the area of necrosis and of coagulation of the pulmonary parenchyma.*
In 7 cases (31,81%) we have set the diagnosis of active pulmonary congestion. Microscopically we could notice the ectasis of the alveolar capillaries and the congestion of the blood vessels, as well as the presence of well-individualized and intensely stained erythrocytes in the lumen. The passive congestion was identified in 3 cases (13,63%) and it was morphologically expressed through the presence in the capillary lumen and in the lumen of the blood vessels, of glued erythrocytes, accompanied by hemolytic phenomena, septal, mezenchymal reactions, reduction of the respiratory space and beginning of lung sclerosis. The pulmonary edema was morphpathologically identified in six cases (27,27%). Two cases (9,09%) had stasis pulmonary edema microscopically expressed through dilation of the pulmonary alveoli caused by transudate and ectasis of the alveolar capillaries; four cases (18,18%) were diagnosed with inflammatory pulmonary edema-showing leukocytes in the edema liquid and in the lumen of the alveoli and of the bronchi as well as capillary ectasis and desquamated endothelial cells. In one case, (4,54%) with pulmonary dirofilariosis, a calcification of the aorta media could be noticed and microscopically, the disorganization of the media through dilacerations and fragmentation of the elastic fibers, alongside precipitated calcium granules, could be distinguished.

Keywords*: circulatory pneumopathies, morphopathologicall, dog*

The modifications of the pulmonary circulation in dogs are exteriorized through passive and active congestions, pulmonary hemorrhages, thrombosis of the pulmonary vein, infarctions and pulmonary edema. They are the consequence of the singular or combined action of biotic and abiotic factors which directly or indirectly affect the respiratory apparatus (1, 5, 7, 10). The congestion or the pulmonary hyperemia presents itself differently from a morphopathological point of view, depending on the affected circulatory segment, arterial or venous. Thus, we mention the active or artherial congestion and the venous or passive congestion as well as the hypostatic pulmonary congestion. The pulmonary hemorrhages, from a morphoclinical point of view, may be intratisular, intraluminal and exteriorized (4, 9, 10). The pulmonary infarction micro-and macroscopically presents itself as a red infarction (hemorrhagic necrosis), frequently located in the diaphragmatic lobes (9).

The pulmonary edema may be a stasis edema in right heart failure, inflammatory edema in infectious diseases (tetanus, monocytic ehrlichiosis of dogs, etc.), toxic edema (intoxications with antifreeze, herbicides, etc.) (2, 5, 6, 8).

MATERIALS AND METHODS

The research of the present study was conducted during the period October 2013-May 2015, through anatomopathological examination of lungs coming from 30 dog corpses of different ages, sexes and breeds, belonging to private owners, kennels or animal protection associations. The corpses were necropsied at the Veterinary Medicine Faculty in Timisoara, at Forensics.

The bodies were places in dorsal position and then necropsied according to the technique used for this species.

After a detailed examination of the lung, trachea and tracheobronchial lymph node, samples were taken for a histopathological exam. Subsequently, the pieces were prepared for the paraffin method. The obtained blocks were sectioned using a microtome at 6 micrometers and the sections were stained using the trichromatic method- hematoxylin eosin methylene blue (HEA) in order to enhance the modified structures. After staining, the sections were dehydrated and mounted in an anhydrous environment using Canada balm.

The histopathological preparations thus obtained were examined and photographed using an Olympus CX41 microscope.

RESULTS AND DISCUSSIONS

Exterior exam. The bodies were in mediocre towards good shape, the skin lacked elasticity, and they presented enophtalmos, anemia and/or cyanosis of the apparent mucosae and skin. The fat tissue and the skeleton muscles were more or less developed, depending on the age and maintenance status.

Interior exam. The presence of a serosanguinolent liquid in variable quantities, in the thoracic cavity was noticed in 6 cases (80-120ml).

Lung exam. The research regarding the pulmonary lesions was systemized in two groups: volumetric pneumopathies and circulatory pneumopathies (Table 1, Fig.1.).

Three cases which were dogs aged 9, 11 and 14 years, presented enlarged lungs, with a tense pleura, pale color, crepitant and with negative docimasy. Microscopically, and accentuated distension of the alveoli could be noticed, with flat pneumocytes, accompanied by the rupture of the alveoli walls-essential alveolar pulmonary emphysema with a chronic evolution (Fig. 2.).

One case, the corpse of a three year old dog, was identified with thrombosis of the pulmonary vein which is a circulatory modification characterized by the formation of intravascular clots, during lifetime, due to blood constituents. Parietal thrombi were observed in the lumen of the vein. Macroscopically, on inspection, the affected venous segment is more dilated, presenting a dark red color and high consistency. On longitudinal section, the thrombus was adherent to the wall, dry, harsh, friable, and on transversal section the vascular lumen occupied by the thrombus could be seen.

Microscopically, the thrombus had an elongated shape, represented by a fibrin clot, red blood cells, leukocytes and altered platelets. It was adherent to the venal wall (Fig. 3.). The

parietal thrombi produce ischemia of different degrees which, if not compensated by the collateral circulation, causes the appearance of serious processes, infarctions or gangrenes.

The red pulmonary infarction was diagnosed in one of the cases, the body of a five year old dog. Macroscopically on inspection and on section, compact dark red areas could be noticed. They were dense, of triangular shape with the base towards the pleura and the top in the pulmonary parenchyma, towards the obstructed vessel. Microscopically, hemorrhagic infiltrates could be observed, with a triangular aspect in the area of pulmonary necrosis (Fig. 4.). In seven cases, macroscopically, the lungs were enlarged in volume and weight, with a tense pleura and on inspection and section, the pulmonary parenchyma was intense red, with a moist aspect, pasty consistency and negative docimasy-active pulmonary congestion (Fig. 5.). Microscopically, we noticed ectasis of the alveolar capillaries and congestion of the interstitial blood vessels with the presence of well individualized and intensely colored erythrocytes in their lumen-active pulmonary congestion (Fig. 6.).

Three cases, the body of a 14 month old, a 15 month old and of 1.7 year old dogs, were diagnosed with passive congestion. Microscopically, glued erythrocytes were noticed, in the lumen of the capillaries and blood vessels, alongside hemolytic phenomena, septal mezenchymal reactions, reduction of the respiratory space and pulmonary sclerosis.

In two cases, macroscopically, the lungs were enlarged in volume, of pink-yellowish color, expressing a foamy liquid on section, similar to whisked egg white. The same foamy liquid was seen in the airways (trachea and bronchi). Microscopically, we notice the dilation of the alveoli due to transudate and more or less accentuated hyperemia of the alveolar capillaries-pulmonary stasis edema (Fig. 7.).

In four cases, macroscopically the lungs were enlarged in volume, the pleura was tense, transparent, the parenchyma had a dark red color and on section, we noticed the same color and the presence of a foamy, dark red liquid (serous exudate) in the parenchyma, bronchi and trachea. The docimasy was between waters- inflammatory pulmonary edema (serous bronchopneumonia) (Fig. 8.). Microscopically, in the interstitium of the pulmonary lobules, we noticed an oxyphile mass that represents the edema liquid. In the lumen of the alveoli and bronchi we noticed the presence of leukocytes in the edema liquid which appears as a homogenous oxyphile mass. These morphological modifications define, in a histopathological plan, the inflammatory pulmonary edema (Fig. 9.).

The calcification of the aorta was signaled in one case- a 13 year old dog with cardio-pulmonary dirofilaria. Macroscopically, the wall of the aorta is rigid and the consistency is rough and highly friable. On section, in the media of the artery, we noticed the presence of white, hard grains and a reduction of the lumen. Microscopically, necrosis is enhanced and the desquamation of the endothelial cells, disorganization of the media due to dilaceration and fragmentation of the elastic fibers accompanied by precipitation of oxyphile calcium grains in the HEA staining method (Fig. 10.).

Table 1

Quantification of uninflammatory pneumopathies

Nr. Crt	Necropsied dogs	**Uninflammatory pneumopathies**							
1.	30	Volumetric		Circulatory				Dystrophic	%
		Atelectasis	Emphysema	Congestion	Edema	Trombosis	Infarct	Calcification	73,33%
		-	3 (13,63%)	10 (45,45%)	6 (27,27%)	1 (4,54%)	1 (4,54%)	1 (4,54%)	

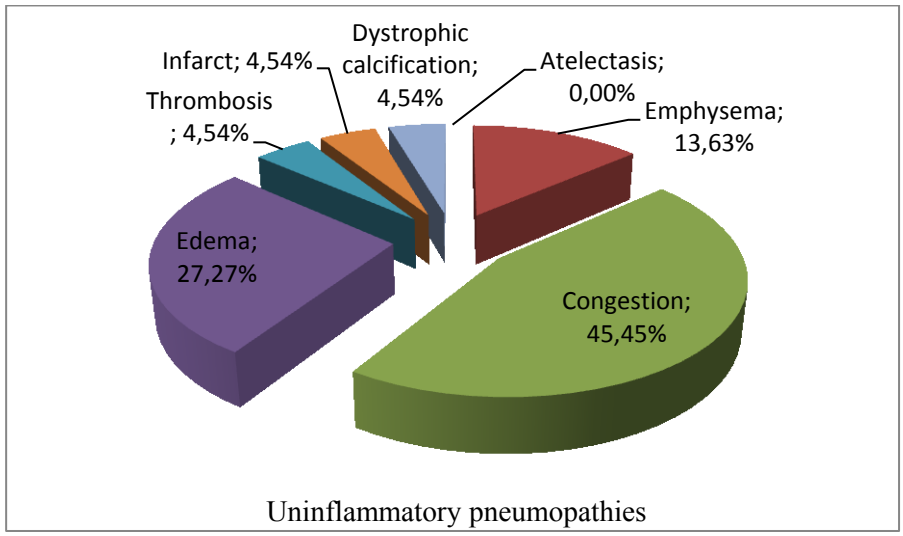

Fig. 1. Graphical representation of uninflammatory pneumopathies in dogs.

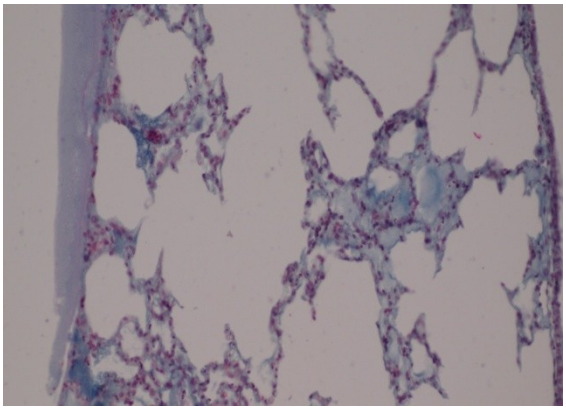

Fig. 2. Accentuated distension of the alveoli, with flat pneumocytes, accompanied by the rupture of the alveoli walls - essential alveolar pulmonary emphysema. Col. HEA x20

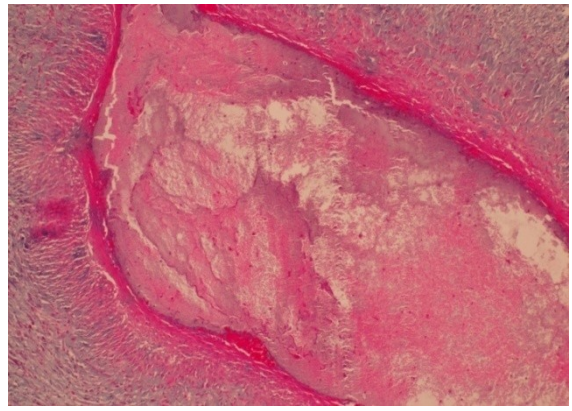

Fig. 3. Pulmonary vein – venous parietal thrombus. Col. HEA x10

Fig.4. Red pulmonary infarction - hemorrhagic infiltrates with a triangular aspect in the area of pulmonary coagulation necrosis. Col. HEA x4

Fig. 5. Dog corpse: active pulmonary congestion.

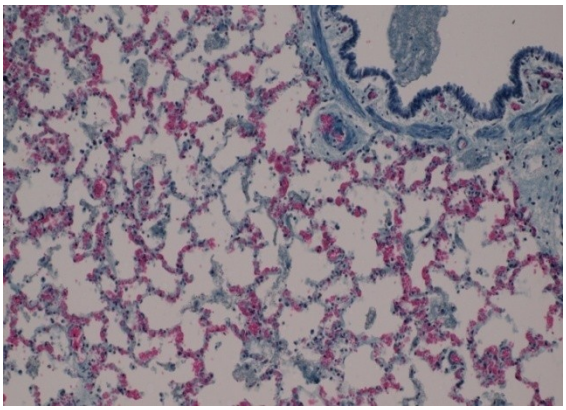

Fig. 6. Active pulmonary congestion : ectasis of the alveolar capillaries with the presence of well individualized and intensely colored erythrocytes . Col. HEA x 20.

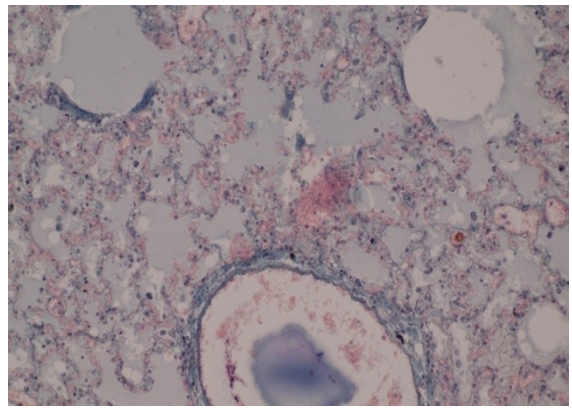

Fig. 7. Pulmonary stasis edema: the presence of edema fluid, basophil, in the lumen of the alveoli, bronchi and trachea. Col. HEA x 20.

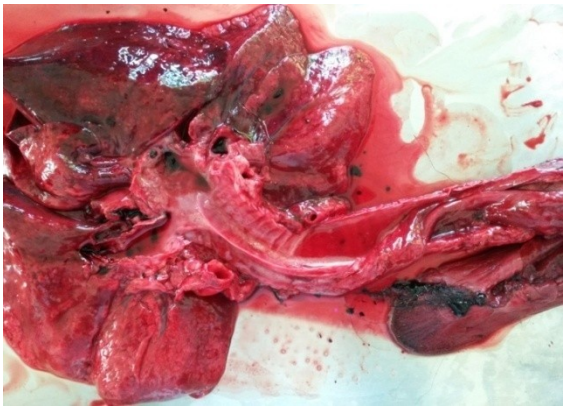

Fig. 8. Inflammatory lung edema: a red foamy liquid in the tracheal lumen, bronchi and lung parenchyma.

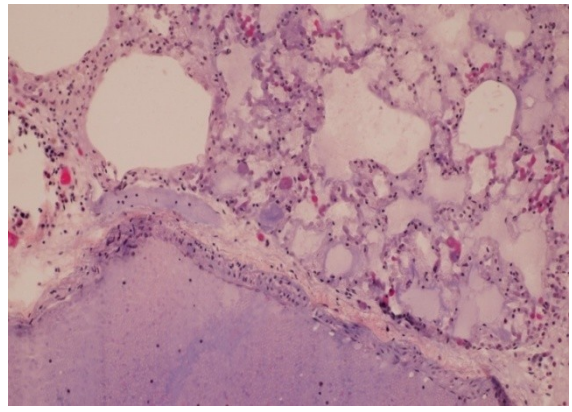

Fig.9. Inflammatory pulmonary edema: the presence of oxyphile mass that represents the edema liquid in the lumen of the alveoli and bronchi. Col. HEA x 20.

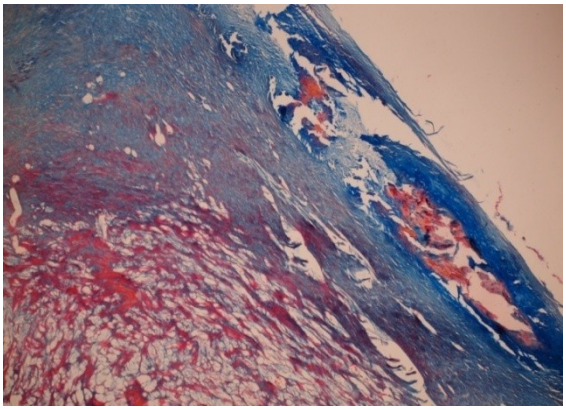

Fig.10. Calcificarea mediei aortei: desquamation of the endothelial cells, disorganization of the media, dilaceration and fragmentation of the elastic fibers, presence of oxyphile calcium grains. Col. HEAx4

CONCLUSIONS

Out of a total of 30 necropsied dog corpses, 22 cases were morphopathologically diagnosed with uninflammatory pneumopathies (73,33%).

The following were diagnosed morphopathologically: volumetric pneumopathies, essential alveolar emphysema with a chronic evolution in three cases (13,63%); circulatory pneumopathies- thrombosis of the pulmonary vein, one case (4,54%), red pulmonary infarction, one case (4,54%), active pulmonary congestion (31,81%), passive pulmonary congestion (13,63%); stasis pulmonary edema, two cases (9,09%), inflammatory pulmonary edema-four cases (18,18%). Dystrophic calcification of the aorta media was signaled in one case which presented cardio-pulmonary dirofilaria.

Out of the circulatory pneumopathies, the most numerous were the active and passive congestions followed by the stasis edema and inflammations.

The dystrophic pneumopathies translated through calcifications of the aorta media were frequently signaled in dogs aged over 9 years.

The uninflammatory pneumopathies expressed through vascular thrombosis, infarctions, congestions, edema and pathological calcifications, which were macro and microscopically diagnosed in the examined cases, correspond to the pneumopathies signaled in the consulted specialty literature (4, 8, 9, 10).

In this paper, we made a prevalence of the uninflammatory pneumopathies of the cases taken into study, respecting the morphopathological presentation criteria of the fundamental pathological processes unanimously acknowledged in our country and abroad.

BIBLIOGRAPHY

1. BONCA, GH., CĂTANĂ, N., DĂRĂBUŞ, GH., MOŢ, T., ŢIBRU, I., (1995) – Patologie canină, Ed. Mirton, Timişoara.
2. BRIGHAM, KL., STAUB,NC., (1998) – Pulmonary edema and acute lung injury research, Am J Respir Crit Care Med. 147, 109-113.
3. BUCHANAN, J.W., (2001) - Pathogenesis of single right corona-,y artery and pulmonic stenosis in English Bulddogs, J. Vet. Int. Med., 2001, 15, 2, 101-104.
4. DUNGWORTH, DL., (1993) - The respiratory system. In: Jubb, KVF., Kennedy, PC., Palmer, N., eds. - Pathology of domestic Animals, 3rd ed., Academic Press, Toronto, 2, 539.
5. EGENVALL, A., HANSSON, K., SÂTERI, II., LORD, P.P., JONSSON, L., (2003) - Pulmonary oedema in Swedish hunting dogs. Small Animal Practice, 44, 5, 209-217.
6. GREENE, C.E., (1998) – Infectious diseases of the dog and cat 2-ed , by W.B. Sounders Company.
7. JOHNSON, L.R., LAPPIN, M.R., BAKER, D.C., (1999) – Pulmonary thromboembolism in 29 dogs: 1985-1995. J. Vet. Intern. Med., 13, 338-345.
8. Mc GAVIN, M. D., CARTLON, W.W., JAC HARY, T.F., (2001) - Special Veterinary Pathology, Ed. Mosby, Inc., Missuri, USA.
9. OPREAN, O.Z., (2002) – Diagnostic necropsic la animalele de companie, Ed. Ion Ionescu de la Brad, Iaşi.
10. PAUL, I., (1990) – Morfopatologia aparatelor şi sistemelor organice. Bul. Inf. al SMV. Nr. 23-24, Bucureşti.
11. POP, M., VASIU, C., OLARIU-JURCA, I., OLARIU-JURCA, A., (2011) – Diagnostic epidemiologic şi morfoclinic în boli infecţioase la animale, Ed. Eurobit, Timişoara.

OPTIMIZATION OFFERMENTATION PARAMETERS FOR VEGETABLE JUICES WITH NITRATE CONTENT TO OBTAIN NATURAL NITRITES

NICOLETA CORINA PREDESCU, CAMELIA PAPUC, VALENTIN NICORESCU, MIMI DOBREA
University of Agronomic Sciences and Veterinary Medicine of Bucharest, Romania
durduncorina@yahoo.com

Abstract: *The aim of this study was to obtain a nitrites-containing juice by fermentation of plant materials that contain nitrates, and finding the best parameters of fermentation to obtain the highest concentration of nitrite.*
Celery and parsnip vegetable juices were obtained by manually pressing of chopped material plants. Staphylococcus carnosus and Staphylococcus xylosus used for vegetable juice fermentations were isolated and then identified from a starter culture. The nitrate and nitrite concentration (ppm) was determined before and after 20 hours and 30 hours of fermentation at different concentration of NaCl (0, 5.0, 7.5, 10.0, wt. %), different temperatures (4°C, 35°C, 45°C) and different pH value (5.0, 6.0, 7.0) for each composition. For nitrates and nitrites determination, colorimetric methods were used.
After 20 hours of incubation at 35°C, in the absence of NaCl and pH 7.0, it was obtained a concentration of 897.3±7.3 ppm nitrites in the presence of Staphylococcus xylosus, comparative with 799.3±6.7 ppm nitrites in the presence of Staphylococcus carnosus.
The highest nitrate concentration was determined for raw parsnip juice, while nitrites were not detected in fresh vegetable juices of celery and parsnip. Fermentation formulas without added salt showed the highest concentration of nitrites, optimum temperature for juices fermentation was 35°C, and optimum pH value for juices fermentation was 7.0.

Keywords: *vegetable juice, nitrate reductase*, *Staphylococcus carnosus, Staphylococcus xylosus, fermentation parameters.*

INTRODUCTION

Nitrate and nitrite are water soluble compounds containing nitrogen and oxygen. Nitrites and nitrates arise from the microbial degradation of nitrogen-containing materials, such as organic human, animal and vegetable wastes, but also fertilizers and pollutants. The ammonium ion, NH_4^+, generated from different types of decomposition, is oxidized to yield NO_2^- and NO_3^- (Scheurwater et al., 1997).

Nitrate is a major form of nitrogen available to plants in soil. Before the NO_3^- is taken up by the plant and assimilated into organic nitrogen, it must first be reduced to NO_2^- and then to NH_4^+. The reduction of NO_3^- to NO_2^- is catalyzed by nitrate reductase. Nitrite reductase catalyzes the reduction of NO_2^- to NH_4^+ (Scheurwater et al., 2002).

The nitrate ion, NO_3^-, is negatively charged, and, in general, is not absorbed by soil until it is taken up by plant roots. Nitrates are essential for the healthy growth of plants. High nitrate concentrations are found in vegetables especially if excessive amounts of nitrogen have been added in fertilizers as manures (Scheurwater et al., 1997).

Leafy vegetables, such as lettuce, spinach, silverbeet, have been found to accumulate nitrate at higher concentration than root or fruit vegetables. Plant variety is also a major consideration when assessing nitrate levels (Reuter and Robinson, 1997).

The aim of this study was to obtain a nitrites-containing juice by fermentation of plant materials containing nitrates, and finding better methods of fermentation to obtain the

highest concentration of nitrite. Fermented juice containing nitrites can be used in food industry to obtain uncured products.

Fermented juice made from plants has been obtained using microorganisms (*Staphylococcus carnosus* and *Staphylococcus xylosus*) capable to produce nitrate reductase to reduce nitrate in the nitrite. The process of converting nitrate to nitrite using microorganisms requires time in order to find favorable conditions (pH, temperature, NaCl concentration) for optimal yield in regarding to the quantity of nitrite produced (Scheurwater et al., 2002). The study had several steps: (1) selecting a plant material that contains an important amount of nitrate, (2) choosing a bacterial microorganism used in the meat industry, able to produce the nitrate reductase in order to reduce nitrate to nitrite, and (3) choosing the best conditions (temperature, pH, concentration of NaCl) to get the best conversion efficiency of NO_3^- in NO_2^-. Most strains of *S. xylosus* and *S. carnosus*, like other meat-associated staphylococci, have a nitrate reductase activity (García-Varona et al., 2000; Mauriello et al., 2004). *S. xylosus* and *S. carnosus* are commonly used as starter culture in meat fermentation (Talon and Leroy, 2011).

MATERIALS AND METHODS

Vegetable materials. Selected plants were the celery root and parsnip root. Celery and parsnip were bought from a local market and then were washed. Plant materials were cut into pieces and chopped in a laboratory blender. Vegetable juices were obtained by manually pressing of chopped material plants.

Bacterial strains. *S. carnosus* and *S. xylosus* used for vegetable juice fermentations were isolated and then identified from a starter cultures. The two staphylococcus strains were determined by microbiological analysis. The isolates were confirmed as gram positive, catalase positive, non-motile, coagulase-negative, non-toxigenic, non-spore-forming, aerobic cocci, and were biochemically identified. All the isolates with that profile confirmed were subjected to further analyses.

Sample preparation. The working scheme used to determine the optimum fermentation conditions are presented in Table 1. Each composition contained celery or parsnip juice concentrate that was diluted 1: 10 in distillated water to which 0.3 wt. % yeast extract was added. The pH of each composition was adjusted with 1 M sodium hydroxide. The compositions were sterilized at 121°C for 15 minutes. Each composition was then inoculated with either *S. xylosus* or *S. carnosus*. The strains of *S. carnosus* and *S. xylosus* used for vegetable juice fermentations are coagulase-negative and non-toxigenic. The nitrate and nitrite concentration (ppm) was determined before and after 20 hours and 30 hours of fermentation for each composition.

Table 1. Sample preparation in order to find the optimal conditions for reduction of nitrates to nitrites

Sample	NaCl (wt. %)	Temperature (°C)	pH
1	0	35	7.0
2	5.0	35	7.0
3	7.5	35	7.0

4	10.0	35	7.0
5	0	4	7.0
6	0	45	7.0
7	0	35	5.0
8	0	35	6.0

Determination of nitrate in vegetable juice. For nirates determination, it was used a colorimetric method described by Cataldo et al. (1975). The complex formed by nitration of salicylic acid under highly acidic conditions absorbs maximally at 410 nm in basic (pH>12) solutions. Absorbance of the chromophore is directly proportional to the amount of nitrate-N present. Ammonium, nitrite and chloride ions do not interfere. It was pipetted an aliquot of 0.200 mL of extract or standard into a 50 mL Erlenmyer flask. It was added 0.8 mL of 5% (w/v) salicylic acid in concentrated H_2SO_4 and the reaction mixture was gently homogenized. After 20 minutes at room temperature, it was added 19 mL of 2 N NaOH to raise the pH above 12, and the tubes were left to cool at room temperature. In parallel it was prepared a blank of 0.200 mL extractant (H_2O) with the same reagents. The absorbance was measured at 410 nm.

Determination of nitrite in fermented juice. Nitrite ions react with a Griess reagent (sulphanilamide and N-(1-naphltyl) ethylenediamine hydrochloride (NED)) for color formation and the purple color that developed after 20 min was read spectrophotometrically at 538 nm (AOAC, 1990). 10 mL of extracted solution were pipetted into a 50 mL volumetric flask and water was added to make up to 30 mL. 5 mL of sulphanilamide solution followed by 3 mL of concentrated HCl were then added and the solution was left in the dark for 5 min. After adding of 1 mL of NED solution, the mixture was left for 15 min. in the dark and then it was diluted to mark with water. The absorbance of the solution was measured in a 1 cm cell using a spectrophotometer at a wave length of about 538 nm (Giustarini et al. 2008). Absorbance values of the samples were compared with absorbance values for standard solutions containing 0.00, 0.20, 0.40, 0.60, and 0.80 ppm nitrite.

RESULTS AND DISCUSSIONS

Determination of nitrates and nitrites in vegetable juices. Nitrate concentration was determined for each vegetable juice, celery and parsnip. It can be observed that the highest nitrate concentration was determined for parsnip juice (Table 2). Also, nitrites were not detected in vegetable juices of celery and parsnip.

Table 2. Nitrate concentrations in vegetable juices of celery and parsnip

Vegetable juice	**Nitrates (ppm)**	**Nitrites (ppm)**
Celery	956.7± 10.1	0
Parsnip	1054±11.9	0

The nitrate concentrations in plants greatly differ depending on soil, fertilizers, growing conditions, etc. From the obtained results it can be noted that fresh untreated juices contain no nitrites. Similar results were obtained and Nabrzyski and Gajewska (1994).

Nitrate concentrations in vegetables depend on the biological properties of the plant culture, sun light intensity, type of soil, temperature, humidity, frequency of plants in the field, plant maturity, vegetation period, harvesting time, size of the vegetable unit, storage time and source of nitrogen (Tamme et al., 2006). Even among different samples of the same vegetable varieties, the nitrate concentration may vary in a wide range (Prasad and Chetty, 2008; Thomson et al., 2007). Environmentally, nitrite is formed from nitrate or ammonium ions by certain microorganisms that produce nitrate reductase.

Determination of nitrite in fermented juice

The effect of NaCl on nitrite concentrations. In Table 3, it can be observed that NaCl concentration shows an important influence on fermentation process of vegetable juices of celery and parsnip.

Table 3. NaCl effect on the fermentation process

Fermented juice	**NaCl (wt %)**	***Staphylococcus xylosus***		***Staphylococcus carnosus***	
		Nitrites (ppm) 20 h	**Nitrites (ppm) 30 h**	**Nitrites (ppm) 20 h**	**Nitrites (ppm) 30 h**
Celery	**0**	897.3±7.3	756.6±7.3	799.3±6.7	598.5±3.3
	5.0	647.2±6.1	435.4±3.4	547.2±4.5	323.5±7.4
	7.5	93.2±2.1	56.9±1.1	43.2±1.8	11.4±1.5
	10.0	0	0	0	0
Parsnip	**0**	987.6±10.2	867.4±8.1	898.3±10.2	765.5±8.5
	5.0	564.4±4.2	354.2±3.2	432.7±4.7	356.4±3.1
	7.5	90.5±1.2	34.9±0.9	65.7±1.5	23.3±1.1
	10.0	0	0	0	0

For both extracts, fermentation formulas without added salt showed the highest concentration of nitrites. It can be noticed that increasing salt concentration reduces the nitrate concentration obtained for both types of vegetable juices. Also, from the obtained results it can be noticed that a concentration of 10% salt inhibit the reducing reaction of nitrates to nitrites. Results indicate that after 20 hours of fermentation it is obtained the highest concentration of nitrites, while after 30 hours of fermentation, nitrite concentration starts to decrease. The results obtained indicate that after 30 hours of fermentation, nitrites begin to decompose.

Fermented juices in the presence of *S. xylosus* showed higher concentration of nitrites compared to the nitrite concentration obtained in the presence of *S. carnosus*.

The effect of temperature on nitrite concentrations. The obtained results indicate that the optimum temperature for fermentation of juices is 35° C.

On the other hand, at 35°C nitrite concentrations achieved after 20 hours of fermentation are higher than those measured after 30 hours of fermentation. Also, for both of vegetable juices, the reduction reaction of nitrite to nitrate is slow at 4°C. At 45°C it can be seen that the reaction stops at 30 hours (Table 4), probably due to distortion of nitrate reductase enzyme produced by the staphylococci. Fermented juices in the presence of *S. xylosus* achieved higher concentration of nitrites compared to the nitrite concentration obtained in the presence of *S. carnosus*.

Table 4. Temperature effect on fermentation process

Fermented juice	Temperature (°C)	*Staphylococcus xylosus*		*Staphylococcus carnosus*	
		Nitrites (ppm) 20 h	Nitrites (ppm) 30 h	Nitrites (ppm) 20 h	Nitrites (ppm) 30 h
Celery	**4**	39.2± 1.1	67.5±1.4	42.2± 0.9	54.7±1.6
	35	897.3±7.3	756.6±7.3	799.3±6.7	598.5±3.3
	45	9.3±0.4	0	10.2±0.7	0
Parsnip	**4**	45.2±1.2	72.2±1.3	37.5±0.7	66.3±1.1
	35	987.6±10.2	867.4±8.1	898.3±10.2	765.5±8.5
	45	11.3±1.0	0	12.7±1.3	0

The temperatures used for these cultures vary with the strain. Casaburi et al. (2005) demonstrated that staphylococcus strains were able to reduce nitrate to nitrite at temperatures as low as 15°C but the activity increased as temperature increased, with maximum activity at temperatures over 30°C. It is recommended that commercially available strains used for nitrate reduction should be used at temperatures of 38-42°C. Recent research has shown that time is a critical factor for the conversion of nitrate to nitrite.

Sindelar et al. (2007) concluded that incubation time (at 38°C) was more critical than the amount of vegetable juice powder to produce no nitrate/nitrite added emulsified cooked sausages that had characteristics similar to a nitrite cured control.

The effect of pH on nitrite concentrations. Table 5 shows the concentrations of nitrites obtained at different pH values. Optimum pH value is 7.0, after 20 hours of fermentation when the maximum concentration of nitrites is achieved. For the other two pH values, 5.0 and 6.0, the reaction happens more slowly.

Table 5. pH effect on fermentation process

Fermented juice	pH	*Staphylococcus xylosus*		*Staphylococcus carnosus*	
		Nitrites (ppm) 20 h	Nitrites (ppm) 30 h	Nitrites (ppm) 20 h	Nitrites (ppm) 30 h
Celery	**5,0**	585.2±3.2	433.4±4.5	478.6±4.3	378.3±4.5
	6,0	675.4±6.4	501.5±8.5	412.4±2.9	453.3±4.9
	7,0	897.3±7.3	756.6±7.3	799.3±6.7	598.5±3.3
Parsnip	**5,0**	603.6±8.6	573.6±6.3	678.3±7.8	557.2±3.5
	6,0	731.1±6.9	612.3±4.6	625.2±5.7	597.3±3.9
	7,0	987.6±10.2	867.4±8.1	898.3±10.2	765.5±8.5

In the presence of *S. xylosus,* fermented juices achieved higher concentration of nitrites compared to the nitrite concentration obtained in the presence of *S.carnosus*.

CONCLUSIONS

The highest nitrate concentration was determined for raw parsnip juice, while nitrites were not detected in fresh juices of celery and parsnip.

NaCl concentration had an important influence on the fermentation process of celery and parsnip vegetable juices. For both extracts, fermentation formulas without added salt showed the highest concentration of nitrites.

The optimum temperature for juices fermentation is 35°C. At 4°C, the reduction reaction of nitrite to nitrate is slow; at 45°C, the reaction stops after 30 hours.

The optimum pH value was determined as 7.0, after 20 hours of fermentation when the maximum concentration of nitrites was achieved.

In the presence of *Staphylococcus xylosus,* fermented juices achieved higher concentration of nitrites compared to the nitrite concentration obtained in the presence of *Staphylococcus carnosus*.

ACKNOWLEDGMENTS: This work was carried out through Partnerships in priority areas Program – PN II, implemented with the support of MEN – UEFISCDI (Romania), project nr. 149/2014.

REFERENCES

1. Association of Official Analytical Chemists [AOAC]. (1990). Nitrites in cured meat. Official Method 973.31. Official Methods of Analysis. 15th ed. Arlington, Va: AOAC.
2. Casaburi A, Blaiotta G, Mauriello G, Pepe O & Villani G. (2005). Technological activities of Staphylococcus carnosus and Staphylococcus simulans strains isolated from fermented sausages. Meat Science 71:643-650.
3. Cataldo DA, Haroon LE, Schrader LE, Youngs VL (1975) Rapid colorimetric determination of nitrate in plant tissue by nitration of salicylic acid. Communications in Soil Science and Plant Analysis 6, 71–80.
4. García-Varona, M., Santos, E. M., Jaime, I., Rovira, J. (2000). Characterisation of Micrococcaceae isolated from different varieties of chorizo. Int. J. Food Microbiol. 54, 189–195.
5. Giustarini D, Rossi R, Milzani A, Dalle-Donne I. (2008). Nitrite and nitrate measurement by Griess reagent in human plasma: evaluation of interferences and standardization. Methods Enzymol.440:361-80.
6. Klaassen, C.D., Casarett and Doull's (2001). Toxicology: The Basic Science of Poisons, Sixth Edition, ed. McGraw-Hill Publishing Co., Inc.
7. Mauriello, G., Casaburi, A., Blaiotta, G., Villani, F. (2004). Isolation and technological properties of coagulase negative staphylococci from fermented sausages of Southern Italy. Meat Sci. 67, 149–158. doi:10.1016/j.meatsci.2003.10.003
8. Nabrzyski M, Gajewska R. (1994). The content of nitrates and nitrites in fruits, vegetables and other foodstuffs. Rocz Panstw Zakl Hig, 45(3):167-80.
9. Prasad, S., Chetty, A. A. (2008). Nitrate-N determination in leafy vegetables: study of the effects of cooking and freezing. Food Chemistry, 106(2), 772-780.
10. Reuter D., Robinson JB, (eds), (1997). Plant Analysis: An Interpretation Manual, Melburn CSIRO Publishing.
11. Scheurwater I, Cornelissen C, Dictus F, Welschen R, Lambers H.(1998). Why do fast- and slow-growing grass species differ so little in their rate of root respiration, considering the large differences in rate of growth and ion uptake? Plant, Cell and Environment 21, 995–1005.
12. Scheurwater I, M. Koren, H. Lambers, O. K. Atkin, (2002). The contribution of roots and shoots to whole plant nitrate reduction in fast- and slow-growing grass species, J. Exp. Bot., 53 (374): 1635-1642.

13. Sindelar JJ, Cordray JC, Sebranek JG, Love JA & Ahn DU. (2007). Effects of vegetable juice powder concentration and storage time on some chemical and sensory quality attributes of uncured, emulsified cooked sausages. Journal of Food Science 72(5):S324-S332.
14. Talon, R., and Leroy, S. (2011). Diversity and safety hazards of bacteria involved in meat fermentations. Meat Sci. 89, 303–309. doi:10.1016/j.meatsci.2011.04.029
15. Tamme, T., Reinik, M., Roasto, M., Juhkam, K., Tenno, T., & Kiis, A. (2006). Nitrates and nitrites in vegetables and vegetable-based products and their intakes by the Estonian population. Food Additives and Contaminants, 23(4), 355-361.
16. Thomson, B. M., Nokes, C. J., & Cressey, P. J. (2007). Intake and risk assessment of nitrate and nitrite from New Zealand foods and drinking water. Food Additives and Contaminants, 24(2), 113-121.

THE CONSIDERATIONS ON HEAD AND NECK LYMPHOCENTERS MORPHOTOPOGRAPHY IN GUINEA PIG

ANCA ŞEICARU, G. PREDOI, C. BELU, VALERICA DĂNACU, PETRONELA ROŞU

Abstract:*Lymph from head and neck regions is collected,filtered and drained from towards through the afferent and efferent vessels of main lymphcenters: thebuccal, facial, submandibular, auricular, superficial cervical and deep cervical.The lymph centers are characteristically organized in lymph nodes groups in a different way,depending from a series of factors, depending on the head and neck length and the conformation of the salivary glands. In guinea pigs the lymphcenters are included in a great amount of adiposetissue. In the center of this tissue we reveal the lymphcenterwhich are gray colored. The lymph centers in the guinea pig are spread in more numerous groups.The buccal lymph center consist of a single lymph node and it is close of the superior molar glands which are characteristic in rodents. The parotid lymphcenter consist of a three lymph nodes.*

The anterior auricular lymph center consists of two lymphnodes groups: round and kidney shaped. The posterior auricular lymph center is covered by parotidoauricular muscle. The mandibular lymph center is kidney shaped in aspect and is covered by the platysma muscle.The superficial cervical lymphcenter is characterized by ventral superficial cervical lymph nodes situated between the caudal border of the parotid gland and the cleidoocipital muscle. The deep cervical lymphcenter (cranial, middle and caudal) is situated at the caudal pole of the submandibulary gland or on the lateral side of the sternothyroid muscle.

Key words: *guinea pig, lymph, lymph node, lymph center*

MATERIAL AND METHOD

Six mature guinea pigs from each sex were injected with a 0.1 ml dose ofChina ink in physiologicalserum solution. The injection's purpose was to visualize the lymph nodes and the path of the lymphatic vessels. The colorific substance was injected intradermic, subcutaneous, intratracheal, intraperitoneal. The chosen spot was represented by the caudal face of the auricular concha, the tip of the nose, the inferior lip. Animal scarification was performed 24 hours later through profound narcosis with ethylic ether. Stratigraphic and regional dissection applied, using the Nikon stereomicroscope.

RESULTS AND DISCUSSIONS

The head lymph centers

- The mandibular lymph center: a group of 2-3 obvious lymph nodes, representing the rostral mandibular lymph centerand a single lymph node, representing the aboralmandibular lymph center. The rostral mandibular lymph nodes are covered by the platysma muscle in relation to the rostral edge of the mandibular gland. Theaboral mandibular lymph nodes are placed behind the previous ones, parallel to the horizontal branch of the mandible and to the external maxillary vein. The efferent lymphatic vessels drain themselves through the lateralretropharyngeal lymph nodesand into the tracheal conduct.

Figure nr. 1 Figure nr. 2

1 – aboral mandibular lymph node
1 – rostral mandibular lymph node
2 – oral parotid lymph node
2 –parotid lymph nodes
3 – facial lymph node

- The buccal lymph center: situated on the lateral face of the buccinator muscle, in relation to the superior molar glands. The efferent vessels collect the lymph from the facial region, the tip of the nose, the superior lip, the musculature of the cheeks, the eyelids and from the masseterianregion.
- The facial lymph center: a single lymph node on the lateral face of the buccinator muscle, dorsal from the buccal lymph center. The afferent vessels collect the lymph from the oral portion of the buccal cavity, the efferent vessels being tributary of the mandibular lymph center.
- The parotid lymph center: three nearly spherical lymph nodes, a lymphonodular group on the surface of the superior edge of the masseter muscle. Another lymphonodular group, on the temporal muscle's surface, right behind the caudal auricular vein and artery. Another lymphonodular group at the base of the auricular concha. The lymph is collected from the parotid gland and from the ear pavilion. The efferent vessels reach into the mandibular lymph center and into the cervical collector canal.
- The auricular lymph center: anterior – two lymph nodes, on the path of the rostral auricular artery

Posterior – behind and lateral from the base of the ear, on the path of the caudal auricular artery.

- The retropharyngeal lymph center: represented by the medial retropharyngeal lymph nodes–arranged on the dorsal side of the pharynx, on the path of the ascending palatine artery – and the lateral retropharyngeal lymph nodes, placed on the path of

the occipital artery, under the sternocephalic and cleidomastoid muscle, on the caudal edge of the parotid gland.

Cervical lymph centers

- The superficial cervical lymph center – cranial superficial cervical lymph nodes: two lymph nodes situated on the confluence angle between the jugular and the maxillary veins. The afferent vessels collect the lymph from the anterior cervical region and from the larynx.
- Caudal superficial cervical lymph nodes – situated on the angle between the cleidocephalic and cleidooccipital muscles, on the path of the superficial cervical artery, the ascending branch.

Profound cervical lymph center

- Cranial profound cervical lymph nodes: on the path of the external maxillary artery, at the posterior pole of the mandibular gland.
- Middle profound cervical lymph nodes: situated in the middle third of the neck, lateral to the sternothyroid muscle.
- Caudal profound cervical lymph nodes: situated about 4 mm away from the brachiocephalic trunks's origin.

Figure nr. 3
1 – Ventral cervical lymph nodes

Figure nr. 4
1 – Caudal profound cervical lymph nodes

CONCLUSIONS

1. The muscular lymph centers are found in a variable quantity of fat, being visible thanks to their grey coloring.
2. There is a notable variability of the lymph nodes' shape in the head region: globular, reniforme.
3. The mandibular lymph center was spotted in 85% of the cases.
4. The lymph nodes from the head and neck regions have an appreciable development in relation to the size of the animal.
5. The profound cervical lymph nodes appear very close to each other because of the cervical region's reduced length.

REFERENCES

1. Gabriel Predoi, Bogdan Georgescu, Cristian Belu, Iulian Dumitrescu, AncaȘeicaru, PetronelaRoșu, Comparative Anatomy of domestic mammals. Osteology, Artrology, Miology, CERES editure, Bucharest, ISBN – 978-973-40-0906-0, pg. 286, 2011.
2. Șeicaru, Anca – Comparative morphology of the lymphatic system in laboratory rodents. Thesis, F.M.V. Bucharest, 2001.
3. Gheție, V. – Contributions to the study of lymphatic vessels in the horse bladder. Thesis, F.M.V. Bucharest, 1928.
4. Dănacu, Viorel – Comparative pathologic researches regarding the leporidae lymphatic system. Thesis, F.M.V. Bucharest, 2000.

THE MORPHOTOPOGRAPHY OF NASAL MUCOSA VASCULARITY IN SHEEP

ANCA ȘEICARU, G. PREDOI, C. BELU, VALERICA DĂNACU, PETRONELA ROȘU

Abstract: *The nasal mucosa membrane is supplied by the sphenopalatine artery (a branch of the descending palatine artery) which forms an arterial network before entering the sphenopalatine conduct. In the nasal cavity, the artery divides into four branches, each one of them reaching the floor and the walls of the nasal cavity. These branches give birth to some verybranched arterial networks. These networks are arranged on a superficial and a profound layer. The fact that the majority of the arteries in the nasal cavity are oriented towards its roof is remarkable. Histologically speaking, a developed muscular layer is to be observed. This layer diminishes the arterial lumen, thus controlling the speed and blood quantity going through these vessels.*

Key words: *sheep, nasal mucosa, vascularity*

MATERIAL AND METHOD

10 specimens (ovine and caprine) of different ages, races and sexes were used. In view of highlighting the nasal mucosa vascularity, a plastic substance of AGO contrast was injected. The substance was bilaterally administered in the external carotid artery. In order to observe the microscopic smears and to study the arterial walls, the hematoxylin-eosin, Azan and the orzein-nitrate colorations were used. After sacrificing the animals, the stratigraphic and regional dissection method was used.

RESEARCH RESULTS

Regarding the ruminants, the commune carotid artery does not end with the internal carotid artery, only an intracranial portion formed of epidural networks being noticeable.

The ethmoidal artery goes into the cranium through the ethmoidal aperture, emits the internal ethmoidal artery and spreads into the olfactory labyrinth.The infraorbital artery: its first side can be the malar artery. Inside the infraorbital canal, it emits branches for the premolars, the superior molars, but also smooth branches for the maxillary sinus.

The descending palatine artery: it emits the sphenopalatine artery, thereupon narrows itself. The sphenopalatine artery has a medially oriented path, going into the aboral portion of the nasal cavities, through the sphenopalatine aperture. Once inside the nasal cavities, it emits the caudal septal artery and several caudolateral nasal arteries. The caudal septal arteries branch within the mucosa of the nasal septum, and the caudolateral nasal arteries spread within the mucosa of themaxiloturbinal cornet and within the mucosa of the ventral nasal meatus.

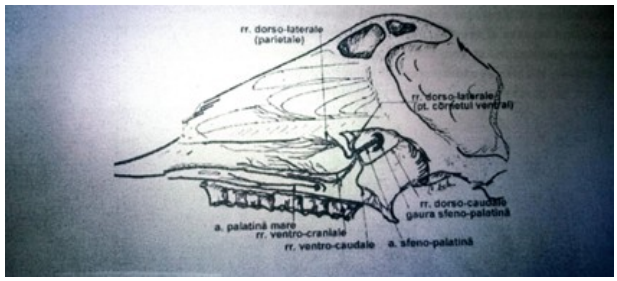

Sphenopalatine artery distribution in ovine

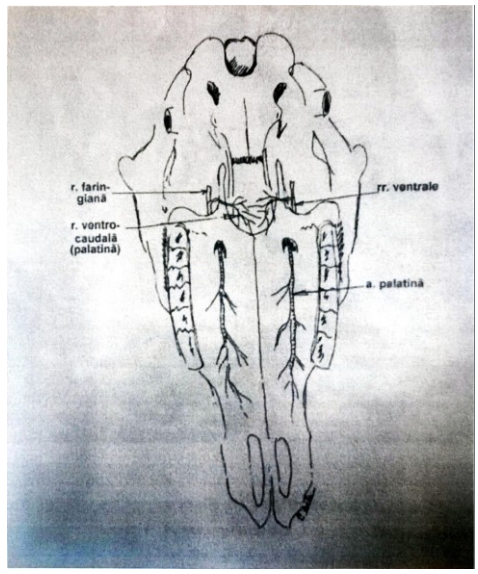

Greater palatine artery in ovine

The descending palatine artery emits in the medial surface of the maxillary tuberosity the small palatine artery (ascending path towards the palatine wave) and the greater palatine artery (reaches the palatine canal through the aboral palatine aperture, accompanied by the homonymous nerve). The greater palatine artery exits through the oral palatine aperture and emits small branches within the palate mucosa. The most rostral branches make a connection (anastomosis) with the ones behind the incisive burelet. In this region, small branches cross the interincisive fissure, irrigating the rostral portion of the nasal cavity's mucosa.

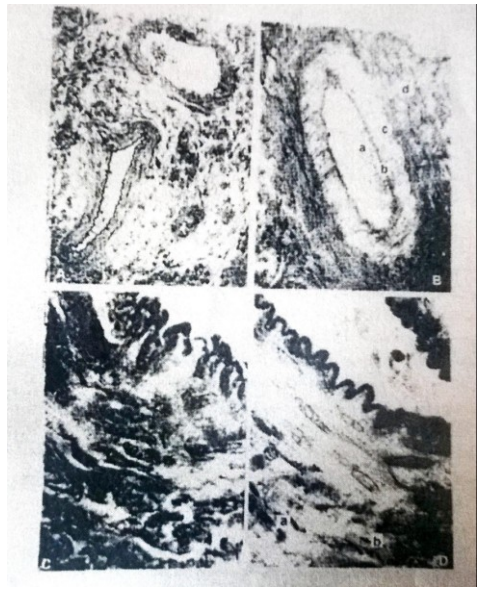

A.The section from nasal mucosa (ob.x40).B.The section from artery (a.lumenb.intimac.mediad.external layer).C.Arterial wall (color Azan).D.Arterial wall (orzein-nitrat).
a.elastic fibers. b.colagen fibers.

CONCLUSIONS

1. The olfactory labyrinth is irrigated by the internal ethmoidal artery after smooth branches cross the ethmoid's riddled blade.
2. The infraorbital artery's caliber is about 1.5-2 mm. It emits as a first side the malar artery (unspecified in some major writings).
3. The rostral portion of the nasal cavity is irrigated by the greater palatine artery.
4. Histologically speaking, the vessels in the nasal cavity (branches of the sphenopalatine artery) posses the same structure without being influenced by the harvesting area in the nasal mucosa. By comparison to the arteries, the walls of the veins in the nasal mucosa are much thinner and the muscular layer is much more undeveloped.

REFERENCES

1. Bacha, W.J., Linda Wood – Color atlas of Veterinary Hystology. Lea &Febiger Comp., Philadelphia – London, 1990.
2. CristianBelu – Cercetari comparative morfotopograficeprivindvascularizatia si inervatiaregiunii cervico-cefalice la rumegatoarelemici.PhDthesis, FMV, Bucharest, 2000.
3. Bancroft, J.D., Stevens, A. – Theory and practice of histological techniques. Fourth edition – Churchill Livingstone – Hong Kong, 1996.
4. Anatomie compare des mammifères domestiques. Tome V, EDITION VIGOT, Paris, 1996.
5. B. Georgescu, G. Predoi, C. Belu, N. Cornila, I. Dumitrescu, PetronelaRosu, Carmen Bitoiu, AncaSeicaru – RESEARCH ON THE MORPHOLOGY OF THE CAROTIDE ARTERY AT GOAT (Capra hirscus), Lucraristiintifice, MedicinaVeterinara, Universitatea de StiinteAgricolesiMedicinaVeterinara ‹‹ Ion Ionescu de la Brad››, Iasi, 53 12(3) 418-421. ISSN 1454-7406, 2010.

RABBITS AND CHINCHILLAS AS EXPERIMENTAL MODELS

FLORIN STAN
Faculty of Veterinary Medicine Cluj - Napoca,
University of Agricultural Sciences and Veterinary Medicine, , Romania,
florin.stan@usamvcluj.ro

Abstract: *In biomedical research, the rabbits are the most commonly used laboratory animal for the production of polyclonal antibodies, in toxicity and drugs safety studies. Rabbit offers many advantages over other species. The relatively large size gentle disposition and ease of maintenance in the laboratory condition are characteristics that ensure the continued use of rabbits as valuable and essential animal model for many diseases. Anatomical and functional particularities of rabbits are appropriate and sometimes unique to the study of human diseases. The main studies that rabbits are the model of choice are those related to atherosclerosis, Alzheimer's disease, osteoarthritis, tuberculosis and ophthalmic disease in addition to the familiar models of neoplastic investigations.*
Chinchillas are the traditional animal model in research related to the ear, especially hearing loss and otitis. Although some studies used mice and guinea pigs in the same area, due to special anatomical features the chinchillas remain the ideal model in this area. The chinchilla inner ear anatomy and ear physiology are similar with the humans. Other areas include the use of chinchillas to study renal anatomy, cardiovascular anatomy, arterial blood supply of the brain and ear, ovarian endocrine activity besides gastrointestinal motility studies, and respiratory infections.
This paper provides a review of the main areas in which those species are used as experimental model with emphasis of anatomical characteristics that make them compatible and suitable with specific areas of research.

Keywords: *rabbit, chinchilla, animal model*

INTRODUCTION

The key to using animal models is to select ones that have similarities to human anatomy and physiology or have the same disease states. Researchers should be guided by the ethical principles contained in the Guide for the Care and Use of Laboratory Animals () and the use of animals as models must be scientifically justified and approved by the local Institutional Bioethics Committee. Small animals have been extensively used in medical research. The choice of an animal model should take into consideration: 1) scientific hypothesis; 2) the degree of species similarity to the human anatomy; 3) the institutional capability to ensure the optimal and safety laboratory conditions to the chosen specie. Most of the proper animal models can be expensive to maintain and the funding must be appropriate to achieve the required number of animals which is need to accomplish a statistically significant result.

Rodents comprise the largest mammalian order with over 1800 species representing 40% of all mammals being found worldwide from the arctic to tropical and temperate regions. Lagomorphs differ from rodents in that they have four incisors and a different jaw structure, but otherwise they share many similar behavioural and anatomical characteristics. But the digestive strategy (non ruminant herbivores) of the species belonging the Rodent and Lagomorph orders is common (Stan, 2013 ,2014). Both rabbits and chinchillas possess anatomical particularities and similarities which makes them suitable and valuable models in biological research.

MATERIAL AND METHOD

A PubMed search using key search "rabbit" from 2010 to 2015 return over 27 500 items in which rabbits was not only species used in research but this demonstrate continued used of rabbits as experimental models. The main fields in which rabbit were used as animal models were atherosclerosis, ophthalmic disease, infectious disease, orthopedic procedures and neoplastic disease. Regarding the rodents, same method of PubMed search, using key word "rodent", return over 368000 articles demonstrating high use of rodents as experimental models, but only 459 items in which chinchillas were involved. The main field in which chinchillas have been used was ear related research. In this paper we will not summarize the 27500 or 368000 articles in which rabbits or rodents were used, instead we will provide an overview of the main fields of research in which rabbits and chinchillas are continuously used with emphasis of the anatomical particularities of the systems involved and due to which these small animals are experimental models of choice.

RESULTS AND DISCUSSIONS

Fundamental ethical concepts of using animals as experimental models

In this respect have appeared numerous directives for use of animal models in research, teaching and testing but the simplest with the greatest impact is the ethical concept "The 3Rs". This concept announced early in the 1956 by Russell and Burch is a call to apply, whenever is possible the alternatives of replacement of animals used in medical research, reduction of number of used animals in testing purposes and the refinement in procedures used on animals in research.

Replacing defines total replacement of animals with computerized programs or relative replacements with animals that are lower on phylogenetic scale. But development of total replacement programs it is a slow process. In accordance with the topic of this paper is worth to be mentioned two areas where the use of rabbits has been replaced. One is eye toxicity (the Draize experiment) in which rabbits were replaced by the bovine corneal opacity and permeability test using a slaughtered cow eye or the isolated chicken eye test or a device the Cytosensor microphysiometer (Molecular Devices, Inc. USA). The Draize test was based on rabbit unique nasolacrimal anatomy namely the presence of a single lacrimal punctum and a tortuous nasolacrimal duct. The second domain is represented by the replacement of rabbits with the aquatic species (e.g horseshoe crabs) in tests which required injection of drugs, biologics or raw materials into rabbits to look for a febrile response as an indication of contamination with endotoxins.

Reduction involves a reduced number of animals used in research or obtaining maximum scientific information from a small number of animals. This approach is based on careful choice of experimental design, improved selection of an animal model including selection of animals with the most appropriate health and genetic status, use of new technologies, improved statistical design, and statistical analysis along a careful control of environment in order to obtain proper care conditions.

Refinement is related to the modifications and use of the least invasive experimental procedures in order to eliminate pain and distress which involved accurate recognition of pain and the use of analgesics and supportive care, enhanced housing and husbandry.

Another redoubtable concept enunciated in 1979 and resumed in 1993 is the concept of the 5 freedoms created by the United Kingdom Farm Animal Welfare Advisory Council. The principles of this concept are often coordinating rules in the enunciation of the ethical principles in medical research. The five freedoms (revised in 1993) include: 1) freedom from hunger and thirst by assuring ready access to fresh water and a sufficient diet to maintain full health and vigor; 2) freedom from discomfort, by providing an environment including shelter and a comfortable resting area; 3) freedom from pain, injury and disease by preventive means or rapid diagnosis and treatment; 4) freedom from fear and distress, by ensuring conditions to avoid mental suffering; 5) freedom to express normal behaviour, by providing sufficient space, proper facilities, and company of the animals own kind (Webster 2001).

Therefore, it is recognized that animal welfare is a core concern of veterinary ethics. This subject is of a major importance of society and the main professional category involved is veterinarians as the first line of care. In the European Union, the basis for the ethical rules of biomedical research on the protection of animals used for scientific purposes is "European Union Parliament and Council Directive 2010/63/EU, revised in 2010 (European Union 2010). One of the goals of this Directive, besides the statement of ethical guidelines in medical research is to minimize the discrepancies between member states which were present in 1986 Directive. In research often occur conflicts of interest among scientists, technicians, veterinarians and research institute on the one hand and on the other hand the nongovernmental companies that require compliance with animal rights. According to Tannenbaum, (1995) the simplest rules of ethics must follow the simplest principles of what is good and what is bad, what is right and what is wrong and looks for the correct norms for veterinary professional behaviour and attitude to respect the moral imperative to treat animals decently. The Guide for the Care and Use of Laboratory Animals (2011) states that "Humane care means those actions taken to assure that laboratory animals are treated according to high ethical and scientific standards".

Rabbits as experimental models

In biomedical research, the rabbits are experimental model of choice used in the production of monoclonal (Fortunato et al., 2014; Yam et al., 2014; Quin et al., 2015; Pan et al., 2015) and polyclonal antibodies (Hu et al., 2013; Nan et al 2015) and in recombinant protein production (Bősze et al 2003; Bősze and Houdebine 2006; Houdebine 2009). Comparing to monoclonal antibodies, the polyclonal antibodies are more heterogeneous having the ability to bind the specific antigen by binding several different epitopes. Rabbits have a high responsiveness to a great variety of antigens having only one immunoglobulin G isotype and combined with ready availability of secondary reagents these specie is the primary specie used in polyclonal antibody production. The procedure for the immunization of rabbits for polyclonal antibody production is dependent upon the immunogen, adjuvant and the purpose for which the antibodies are produce and are well documented (Lagatie et al 2015). Due to the relative large body size compare to the smallest rodents, easily access of the marginal ear vein rabbits remain the suitable species used in this immunologic research domain. Recently, in some studies, rabbits were largely replaced by some rodent with a short life span, a large number of offspring after a short gestation period, advanced and well documented genomics and proteomics and wide availability of reagents (Park et al 2015). Therefore, rabbits remain the linking model used in the early stages of research being an

important niche between laboratory mouse and domesticated animals having a major importance in preclinical translational research. This statement is supported by the low costs of purchasing, maintenance and regulation of research bioethics committees (Fisher 2010).

Rabbits have much closer phylogenetic features to primate compare to inbred rodent strains, providing a much broader genetic material. Moreover, the rapid advancement of genomics and proteomics knowledge of rabbits led to selection of specific lines of research available targets. But the most important aspect is related to the characteristics of the specific human diseases, which often is impossible to be replicated in other rodent experimental models. A topical example is seen in AIDS where infection with HIV-1 in rodent specie is not possible. Instead, rabbits seem to develop and replicate human disease pathogenesis like chimpanzees and gibbons ape, but not with the same consistent symptoms as in humans. It was suggested that rabbit CD4 (RaCD4) like receptor is the counterpart of human CD4 (HuCD4) the principal receptor of HIV-1 in human (Pan et al 2015; Hatziioannou 2012; Tervo et Kleper 2010)

Anatomical and functional particularities of rabbits are appropriate and sometimes unique to the study of human diseases. The main studies that rabbits are experimental model of choice are those related to atherosclerosis, Alzheimer's disease, osteoarthritis, tuberculosis and pharmacologic ocular research besides well known neoplastic models.

Although rabbits being herbivores do not spontaneously develop hypercholesterolemia (like man, several non human primate and pigs), which is considered the main factor to atherosclerosis developement, a diet rich in cholesterol lead to vascular lesions deposition of atheromatous plaques occurrence within a few weeks (Priyadharsin et al., 2015. Atherosclerosis is a chronic progressive inflammatory disease characterized by intimal arterial wall accumulation of lipids (especially LDL), enhancement of endothelial permeability and accumulation of inflammatory cells (monocytes, lymphocytes) leading to appearance of lesions and subsequent thickening of the arterial wall which compromise the residual lumen and ischemic event apparition (Konya 2008) The pathogenesis is complex and mediated by adhesion molecules, inflammatory cells, and smooth muscle cells. In the rabbit the atheromatous plaques are located in the vascular wall of the aortic arch and on the thoracic aorta at the origins of intercostal arteries with a less extent in abdominal aorta as in humans. The anatomical and functional explanation is the turbulent blood flow in these locations and a higher vascular permeability of LDL as a focal response of the artery wall to local vascular injury.

The model of diet-induced hypercholesterolemia in rabbits it is well known in the field. Hypercholesterolemia, in particular LDL fractions (low density lipoprotein) is a major risk to the occurrence of atherosclerotic lesions. Similar to the humans, rabbits show the same metabolism of the cholesterol fractions. In comparison, rodents show high levels of HDL (high density lipoprotein), which makes them unsuitable for this type of research. A natural and spontaneous occurrence of hyperlipidemia is found in Wantanabe heritable hyperlipidemic (WHHL) strain of rabbit which is the first animal model with endogenous hypercholesterolemia due to the lack of LDL receptors. (Wantanabe 1980). This inbreed strain develop more severe lesions located in the thoracia aorta, coronary arteries and abdominal aorta and adjacent branching vessels as humans. In this condition the WHHL rabbit inbred strain is the model of choice in atherosclerosis research. Another animal model

used in familial combined hyperlipidemia is the St. Thomas Hospital strain which show high level of VLDL, intermediate density lipoproteins-IDL, and high level of LDL (Taylor 1997).

Probably the only specie that could surpass the rabbit in those specified above in atherosclerosis experimental model is pigs**.** Alzheimer's disease is another condition in which due to the fact that its appearance is not spontaneous in animals (induction in animals is done either through diet, pharmacological or genetic manipulation) research was focused on developing the rabbit as experimental model due to spontaneous occurrence of atherosclerosis (Woodruff-Pak 2008). Furthermore, physiologically, at cellular and molecular level, rabbits show similarities with neuropathology of Alzheimer's disease in human**.** In rabbits affected by brain disease, the brain shows increased level of cholesterol and β amyloid, low levels of acetylcholine, Aß plaques in the extracellular space, increased permeability of the haematoencephalic barrier, with high population of glial cells and neural population decrease. Rabbits phylogenetic similarity with humans is reflected in a high percentage (97% of Aß protein amino acid sequence is conserved). Anatomically rabbits possess a suitably sized brain so the cognitive tests are relevant. From a cognitive point of view, rabbits show neurological deficiencies with the coming of age, similar to humans.

Using rabbits as experimental model in ophthalmologic research is due to an anatomical characteristic: the eye has an optimal size related to body size, which allows maneuvers of intraocular injection, histopathological examination. Moreover because of the physiological similarities of the visual apparatus, the rabbit is often the model of choice in this type of research (Gwon 2008). The main areas in which the rabbit is used as experimental model are related to eye surgery: remedying cataract (Woodruff-Pak 2008), corneal transplantation, insertion of intraocular lenses, procedures for refractive laser (Kang and Grossniklaus 2011), implantation of shunts in glaucoma (Albrecht 2008), retinal detachment and vitreous transport of medication. The most suitable strains of transgenic rabbits that are appropriate for ophthalmic research are the New Zealand White Rabbit (NZWR) breed (Kondo 2009). The use of young rabbits in pediatric ophthalmology research is justified by prompt and strong inflammatory response after surgery, similar to that seen in children.

Another condition that is idiopathic or post traumatic in humans, in which rabbits are the ideal model, is osteoarthritis, which leads to tissue changes in joint cartilage, subchondral changes of the bone and synovial ligaments and subordinated muscles (Poole 2010). Although several species of mammals have been used (mice, guinea pigs, dogs and even horses), none of them offer specific advantages of rabbit as an experimental model. An example is the morphology of the femoral-tibial-patellar joint (knee) of rabbits being very similar to that of humans. Moreover, rabbit joints are sufficient size for collecting histopathological samples, compared to small animals (Laverty et al. 2010). Another aspect is related to the skeletal ossification that in humans, like in rabbits, at adult ages is complete, which does not happen for small rodents, hence the difficulty of extrapolating translational research findings from these species.

In research related to the pathogenesis of human tuberculosis there are three species which are commonly used: rabbits, guinea pigs and mice because all can be infected by inhalation, develop an antibody response and in general have a mechanism to control the disease before being fatal, like humans (Dharmadhikari and Nardelli 2008). However, only rabbits, like humans, develop tuberculosis cavities and may develop a localized infection.

Curious, it is that man can present spontaneous reactivation of the disease, while rabbits require immunosuppression for the disease to be reactivated.

The use of rabbits in cancer research is essential in finding and understanding of fundamental mechanisms of malignancies and metastasis process in order to improve prevention, obtaining an accurate and early diagnosis and to develop advanced treatments. Even the use of rabbits as models in mammary carcinomas is low (Stan 2014) the following cancers are studied using rabbits as experimental model: VX-2 tumors, endometrial adenocarcinoma, monoclonal gammopaties, nephroblastoma, lymphoblastic leukemia and malignant fibroma. The Shope papilloma virus which was first isolated in cottontail rabbits show substantial sequence similarities to HPV1a and due to this feature it has been used as a model to human papillomaviruses (Willer et.al., 1999). This finding has a great importance in HPV vaccine producing and establishing new antiviral therapies. The VX-2 tumor induced anaplastic squamos cell carcinoma played a crucial role in using rabbits as cancer models of liver, pancreas, lung, kidney, urinary bladder, uterus, bone and even brain (Gaba et al.,2012).

As a general rule for all studies involving animals used as experimental model in cancer research it should be apply ethical principles of biomedical research. The main considerations that must be fulfilled are: a careful choice of study design and statistical methods; correct choice of tumour models - genetically modified, metastatic, orthotopic; the possibility of applying the therapy and stopping the experiment – human endpoints- if the cancer affects multiple systems.

Chinchillas as experimental models

Chinchillas are the traditional model of research related to the ear canal. Although some studies used mice and guinea pigs in the same area (Salvi and Boettcher 2008), due to special anatomical features, chinchillas remain the ideal model in this field of research.

These considerations are based on anatomical similarities of the inner ear – including the cochlea with that of humans. Chinchilla ear has three rounds of cochlea and the tympanum similar to that as described in humans. Easily accessible cochlea, large tympanic membrane together with an easy approach of the middle ear through a large and thin tympanic bullae are just some substantial and consistent anatomical attributes that support the above statements (Songer et al., 2007, Lim et al., 2005). The main diseases of the ear for which chinchillas are used as an experimental model are: hearing loss (Dun et al 1991; Salvi et al. 2008), otitis media (Lim et al., 2002, 2005; Giebink, 1999), tinnitus, perforation of the tympanic membrane (Downey and colab.2003), cochlea implants (McFaden et al. 2002; Naito et al. 2004), perilymph fistulas (Wall and Casselbrandt 1992), cholesteatoma (Masaki et al. 1989), implantation of electrodes, superior canal dehiscence (Songer and al. 2007).

Another anatomical feature on which numerous studies on drug ototoxicity are based, is the thinness and smoothness of the round window of the ear (10-14μm) - compared to humans (40-70μm) - that allows easy penetration of drugs (Daniel et al. 2008). Also, on this anatomical characteristic are based pharmacokinetic studies of otic antibiotics administration. The average lifespan of chinchillas -15 years- compared to mice -2 years - offers safety research without interference of senescence phenomenon of auditory system during the study period (Giebink 1982; Bakaletz 2009). The audiogram conducted on chinchillas is closer to that of humans than the ones achieved in other rodents given that the frequency ranges from 20 MHz to 30 MHz (Miller 1970; Giebink 1999; Heffner and Heffner 1991).

Immunologically and genetically chinchillas have many advantages as an experimental model. Mucous membranes (digestive, respiratory, genital, urinary) are the most vulnerable structures, their main characteristic being the prompt answer on contact with antigens. These structures represent not only an anatomical entity, but also an immunologically functional one, with protective role against infections coming through the mucosa. The mucosal structures most involved are the respiratory and digestive mucosa. In the structures above mentioned the immune system is represented anatomically and functionally by: BALT (lymphoid tissue Associated bronchus) and GALT (gut lymphoid tissue Associated). In most rodents the BALT system is well developed compared to humans in which BALT structures are not developed being replaced by palatine tonsils and those nasopharyngeal (Waldeyer ring) representing the NALT barrier (Associated nasal lymphoid tissue). NALT equivalence is well developed in chinchillas compared to other rodents, dogs, cats and rabbits in which the presence of nasal branched turbinates are not suitable for research in this direction (Barone 1996; Quesenberry and Carpenter 2012; McGilvary et al.2008). Anatomically, chinchillas are the ideal candidates in the studies on transport and responsiveness of nasally administered vaccines and the possibility of establishing therapy in this way for otitis of the median ear (Bakaletz 2009).

Chinchilla's immune response can be easily studied because they can use human-based reagents based on the fact that the cytokines involved in the immune response cross-react (Giebink 1999; Sato and colab.1999). Human cytokines stimulate maturation of dendritic cells derived from bone marrow and such human immunoglobulin antibodies cross-react with immunoglobulins of chinchillas. There are no studies at the molecular level due to a lack of a synthesized anti-chinchilla serum, as is done with mice and other laboratory rodents (Lim colab.2005). However, there is sufficient similarity at the genetic level between the genes encoding the formation of mucin, the effectors of innate immunity and epithelial cell receptor (Bakaletz 2009). Therefore immunology is another area of wide interest where chinchilla can be used as an experimental model due to diversity of immune response.

Other areas of study where chinchillas can be used as an experimental model include renal micro-anatomy, cardiovascular anatomy, arterial blood supply of the brain and ovarian endocrine activity besides gastrointestinal motility studies, and respiratory system diseases.

CONCLUSIONS

Animal models are and will remain necessary in both basic and applied research projects. The value of these models lies in proper knowledge of the anatomy of the specie involved and the ability to manipulate anatomical systems and apply rigorous scientific methods to discover the underlying mechanism of the disease and to develop the most advanced treatments.

REFERENCES

1. Albrecht May, C., (2008). Comparative anatomy of the optic nerve head and inner retina in non primate animal models used for glaucoma research. *Open Opthalmol. J*. 2, 94–101.
2. Bakaletz, L., (2009). Chinchilla as a robust, reproducible and polymicrobial model of otitis media and its prevention. *Expert. Rev. Vaccines,* 8 (8), 1063–1082.
3. Barrone, R., (1996). *Anatomie Comparee des Mammiferes Domestiques. Vol I, 1-428. VigotFeres Paris*.

4. Bosze, Z. and Houdebine, L.M. (2006) Application of rabbits in biomedical research: a review. World Rabbit Sci. 14:1-14.
5. Bősze, Z., Hiripi, L., Carnwath, J. W., &Niemann, H., (2003). The transgenic rabbit as model for human diseases and as a source of biologically active recombinant proteins. *Transgenic research*, 12(5), 541-553.
6. Daniel, S.J., Sahmkow, S.I., Munguia, R., Schloss, M.D., Akache, F., (2008).Ototoxicity of triethnolamine polypeptide (Cerumenex) in the chinchilla. *Laryngoscope* 118, 478–482.
7. Dharmadhikari, A. and Nardell, E.A., (2008).What animal models teach humans about tuberculosis. *Am. J. Respir. Cell Mol. Biol*. 39,503-508.
8. Donelly, TM. (2012). Basic anatomy, physiology and husbandry. In: Hillyer EH, Quesenberry KE, editors. *Ferrets, rabbits and rodents: clinical medicine and surgery.* Philadelphia: W.B. Saunders;. p. 147–59.
9. Downey, T., Champeaux, A., Silva, A., (2003). AlloDermtympanoplasty of tympanic membrane perforations. *Am. J. Otolaryngol*. 24 (1), 6–13.
10. Dunn, D., Davis, R., Merry, C., Franks, J., (1991).Hearing loss in the chinchilla from impact and continuous noise exposure. *J. Acoust.Soc. Am*. 90 (4 Pt. 1), 1979–1985.
11. European Union, 2010. Directive 2010/63/EU of the EuropeanParliament and of the Council on the protection of animals used for scientific purposes. Official Journal of the European Union L 276, 20 October 2010, pp. 33–79.
12. Fisher P.G., (2010). Standards of Care in the 21st Century:The Rabbit, Journal of Exotic Pet Medicine, Vol 19, 1, pp 22-35
13. Fortunato M.J., Bal,l C.E., Hollinger, K., Patel, N.B., Modi, J.N., Rajasekaran, V., Nonneman, D.J., Ross, J.W., Kennedy, E.J., Selsby, J.T., Beedle, A.M., (2014).Development of rabbit monoclonal antibodies for detection of alpha-dystroglycan in normal and dystrophic tissue.*PLoS One.* 13;9(5):e97567.
14. Gaba RC, Baumgarten S, Omene BO, et al. Ethiodized oil uptake does not predict doxorubicin drug delivery after chemoembolization in VX2 liver tumors. J Vasc Interv Radiol 2012; 23:265−273.
15. Giebink, G., (1999). Otitis media: the chinchilla model. *Microb. Drug Resist*. 5 (1), 57–72.
16. Gwon, A., (2008). The rabbit in cataract/IOL surgery. In: *Tsonis, P.A. (ed.) Animal models in eye research*. Elsevier, 184-204.
17. Hatziioannou, T., & Evans, D. T., (2012). Animal models for HIV/AIDS research. *Nature Reviews Microbiology*, 10(12), 852-867.
18. Houdebine, L. M., (2009). Production of pharmaceutical proteins by transgenic animals. *Comparative immunology, microbiology and infectious diseases*,32(2), 107-121.
19. Hu FJ, Uhlen M, Rockberg J.N., (2013). Generation of HER2 monoclonal antibodies using epitopes of a rabbit polyclonal antibody.*Biotechnol.* 25;31(1):35-43.
20. Kang, S.J. ,Grossniklaus, H.E., (2011). Rabbit model of retinoblastoma. *J. Biomed. Biotechnol*.2011:394730.
21. Katherine Quesenberry, Carpenter J.W.,(2012). Ferrets, Rabbits, and Rodents: *Clinical Medicine and Surgery 3rd ed*. ISBN-10: 1416066217
22. Kondo, M., (2009). Generation of a transgenic rabbit model of retinal degeneration.*Invest. Ophthalmol. Vis. Sci.* 50(3)1371-1377.
23. Kónya, A., (2008). Animal models for atherosclerosis, restenosis, and endovascular aneurysm repair. In: *Conn, P.M. (ed.) Sourcebook of models for biomedical research*. Humana Press, 369-384.
24. Lagatie O, Tritsmans L, StuyverLJ., (2015). Characterization of Rabbit Antibodies Against the Immunogenic JC Polyomavirus Peptide JCPyV_VP2_167-15mer Viral Immunol. 2015 Jun 15. [Epub ahead of print]
25. Laverty, S.,(2010). The OARSI histopathology initiative – recommendations for histological assessments of osteoarthritis in the rabbit. *Osteoarthritis Cartilage* 18 (Suppl. 3) 53-65.
26. Lim, D., Hermansson, A., Hellstrom, S., Hussl, B., Alper, C., Iino, Y., et al., (2005). Recent advances in otitis media 3. Animal models; anatomy and pathology; pathogenesis; cell biology and genetics. *Ann. Otol. Rhinol. Laryngol*. (Suppl. 194), 31–41.

27. Masaki, M., Wright, C., Lee, D., Meyerhoff, W., (1989).Experimental cholesteatoma.*ActaOtolaryngol*. (108), 113–121.
28. Miller, JD.,(1970). Audibility curve of the chinchilla. *J. Acoust. Soc. Am*. (48), 513–523.
29. Naito, Y., Nakamura, T., Nakagawa, T., Iguchi, F., Endo, T., Fujino, K., (2004).Transplantation of bone marrow stromal cells into the cochlea of chinchillas. *Neuroreport*15 (1), 1–4.
30. Nan Fang Yi Ke Da XueXue Bao., (2015). Preparation and identificationof rabbit polyclonal antibodies against vacuolar proton pyrophosphatase type I of Toxoplasma gondii 2015 Aug 20;35(8):1137-42. Chinese.
31. National Research Council., (2011). *Guide for the Care and Use of Laboratory Animals.Washington*, DC: National Academies Press.
32. Nordestgaard, B. G., Tybjærg-Hansen, A., and Lewis, B., (1992). Influx in vivo of low density, intermediate density, and very low density lipoproteins into aortic intimas of genetically hyperlipidemic rabbits. Roles of plasma concentration, extent of aortic lesion, and lipoprotein particle size as determinants. *Arterioscler. Thromb*. (12), 6–18.
33. Pan R, Chen Y, Vaine M, Hu G, Wang S, Lu S, Kong XP., (2015). Structural analysis of a novel rabbit monoclonal antibody R53 targeting an epitope in HIV-1 gp120 C4 region critical for receptor and co-receptor binding. *Emerg Microbes Infect*. 4 (7), 44.
34. Park, S. H., Kim, A. Y., Ma, S. H., Kim, H. M., Kang, H. S., Maeng, J. S., ... &Joung, Y. H., (2015). Purification of human carcinoma antigen GA733-2 expressed in Escherichia coli and production of its polyclonal antibody in rabbit. *Animal Cells and Systems*, (ahead-of-print), 1-6.
35. Poole, R., (2010). Recommendations for the use of preclinical models in the study and treatment of osteoarthritis. *Osteoarthritis Cartilage,* 18 (Suppl. 3), 10-16.
36. Priyadharsini, R. P., (2015). Animal models to evaluate anti-atherosclerotic drugs. *Fundamental & Clinical Pharmacology*, (29) 329–340.
37. Russell WMS, Burch RL., (1959).*The Principles of Humane Experimental Technique*. London: Methuen;
38. Salvi, R., Boettcher, FA.,(2008). Animal models of noise-induced hearing loss. In: *Conn, P.M. (Ed.), Sourcebook of Models for Biomedical Research. Human Press*, Totowa, NY, 289–304.
39. Songer, J., Rosowski, J., (2007).A mechano-acoustic model of the effect of superior canal dehiscence on hearing in chinchilla. *J. Acoust. Soc. Am*. 122 (2), 943–951.
40. Stan, F. (2014). Morphological study of lymphatic drainage and lymph nodes of mammary glands in doe. . *Bulletin of University of Agricultural Sciences and Veterinary Medicine Cluj-Napoca. Veterinary Medicine, 71*(1), 213-219
41. Stan, F., (2014). Anatomical Particularities of the Cecum in Rabbits and Chinchillas. *Bulletin of University of Agricultural Sciences and Veterinary Medicine Cluj-Napoca. Veterinary Medicine*, *71*(2), 406-412.
42. Stan, F.,(2013). Comparative study of the stomach morphology in rabbit and chinchilla. *AgroLife Scientific Journal*, 2 (2), 73-78.
43. Tannenbaum, J., (1995). *Veterinary Ethics: Animal Welfare, Client Relations, Competition, and Collegiality*. Mosby, St. Louis.
44. Taylor, J. M., (1997). Transgenic rabbit models for the study of atherosclerosis. *Front. Biosci*. (2**)** 298–308.
45. Tervo H.M., Keppler O.T., (2010). High natural permissivity of primary rabbit cells for HIV-1, with a virion infectivity defect in macrophages as the final replication barrier. *J. Virol*. (84) 12300-12314.
46. Wall, C., Casselbrant, M., (1992).System identification of perilymphatic fistula in an animal model. *Am. J. Otol*. 13 (5), 443–448.
47. Webster, A.J.F., (2001). Farm animal welfare: the five freedoms and the free market. *Vet. J*. 161, 229–237.
48. Willer DO, McFadden G, , Evans DH (1999). The complete genome sequence of Shope (rabbit) fibroma virus. *Virology* 264:319–343
49. Woodruff-Pak, D.S.,(2008). Animal models of Alzheimer's disease: therapeutic implications. *J. Alzheimers Dis*. 15(4)507-521.
50. Yam, P. C., and K. L. Knight.,(2014). Generation of rabbit monoclonal antibodies. *Methods Mol. Biol*. 1131: 71-79

RESEARCH REGARDING THE DENSITY OF THE MYOCYTES AND THE RATIO OF THE MAIN TISSUE CATEGORIES FROM THE LATERAL MUSCLE OF THE *POLYODON SPATHULA* SPECIES

TEUȘAN VASILE[1], ANCATEUȘAN[2]
CRAUS STEFAN[3]
[1]University of Applied Life Sciences and Environment, Iasi
[2] Acad. "IoanHaulica" Research Institute, "Apollonia" University, Iasi
[3] Acad. "Ioan Haulica" Research Institute, "Apollonia" University, Iasi
vasile.teusan@yahoo.com

Abstract: *Histological samples were taken from the lateral muscle (dorsal epaxial) (ML-ED), from ten four year old sturgeon (Polyodon spathula) male specimens (Ps3+). These samples were processed with the paraffin sectioning technique and 20 slides with transversal sections of the lateral muscle were obtained. The slides where colored according to the HEA method. They were analyzed with an optic microscope (OM), type MC3. Both diameters (long and short) were measured in the microscopic field for the myocytes and the primary muscular fibers (PMB). Also in the microscopic field the myocytes from the PMB were counted. Through calculations, the average diameter, the circumference and the values for the shape and profile index were determined, at the PMB level. Afterwards the myocytes density and the ratio of the two tissue categories (muscle tissue and conjunctive tissue) at PMB and SMB level were determined. The following results were obtained: the average thickness of the PMB, from the 5 secondary muscle bundles (SMB) studied it varied between 318μ and 452.5μ, with a mean of 383.85μ. The average circumference of the PMB was 1206μ, the shape is a cylindroid with a flattening tendency (If=1,768/1)(Ip=59,19%). The PMB myocyte number oscillated between 34.2 and 72.33, the average being 50.76 muscle fibers. The myocyte density varied between 444.282fm/mm² and 489.166fm/mm², with a mean of 467.383fm/mm². The muscle tissue ratio varied between 64.10% and 75.0%, with a mean of 68.72%. The differences between the means of the five SMB, in accordance with the 11 studied parameters, were tested for statistical purposes, ascertaining that 99.09% of them are insignificant.*

Keywords: *Polyodon spathula; dorsal epaxial; myocytes; density; muscle tissue.*

INTRODUCTION

The rapid human population growth on our planet and the increase in quality and quantity demands regarding food, has determined the introduction of new animal species into consumption, as well as the improvement of their bio-economic performances. Apart from mammals and birds, humans also eat the meat and roe from different species of fish or other aquatic animals. In Romania, pisciculture has a very old tradition, our waters being known as highly productive in this field. Many fish species are bred in mono or mixed culture, ensuring large quantities of meat and roe for the food industry and for direct human consumption. Existing literature data specifies that 12-15% of our diet consists of fish and fish-based products (from the total of proteins consumed), with major differences according to geolocation. Fish meat is widely known for its distinct organoleptic properties; for its high digestibility rate and for its nutritional and superior biological value, due to the high content of proteins and essential aminoacids; the high percentage of unsaturated fats and the high quantity of vitamins and minerals. Sturgeons are among the oldest species to inhabit the waters of the Northern hemisphere and because their meat and roe (caviar) are in high

demand, it almost lead to the extinction of this taxonomic order. This is one of the many reasons that lead to breeding sturgeons in stock ponds (aquaculture). In Romania it began in 1992, when the Nucet research station, imported *Polydon spathula* larvae from the USA. In this article, some quality aspects of the *Polydon spathula* meat were studied, specifically the histological structure of the muscles, by analyzing a series of parameters at the myocytes level and muscle fibers from the lateral muscle (dorsal epaxial muscle).

MATERIALS AND METHODS

The manner in which our research took place demanded the use of several categories of materials (biological and nonbiological) and working methods. The biological material consisted of 10 four year old Polydon spathula males (Ps3+). The studied species has the following taxonomy: Kingdom - **Animalia**; Phylum - **Chordata**; Subphylum - **Vertebrata;** Class - **Actinopterygii**; Order - **Acipenseriformes;** Family - **Polyodontidae**; Genus – **Polyodon** (Lacepede - 1797); Species - P. **Spathula.** The Paddlefish (*Polyodon spathula*) is a sturgeon native to the Mississippi (from the Great Lakes to Florida)[2]. It is a large fish, reaching up to 1.5-2 meters in length when mature and with a body weight of 30-50-80 kg (in optimal feeding conditions). Paddlefish can live up to 30 years. The skin is smooth (with microscopic scales); lateral-oriented small eyes; large mouth, with a very long rostrum (one third of the body length) and flattened like a paddle or spatula. This rostrum is part of the cranium structure [2]. This species has two very important bio-economic advantages: it eats plankton (it feeds with zoo and phytoplankton and also with aquatic insects) and it has a rapid growth rhythm. In aquaculture it does not necessarily need supplemental feeding with concentrated fodder, although this aspect has been studied and applied in the US for several decades.

From the 10 sacrificed fish, histological samples were collected from the lateral muscles, more specifically from the dorsal epaxial muscles (ML-ED). These samples were processed according to the paraffin sectioning method [12][13]. Specific anatomy tools were used for the sample collection (forceps, scalpels, scissors, dissection needles, retractors, etc.). Twenty slides with transversal sections of the lateral muscle were obtained. The slides where colored according to the HEA method [12][13].They were analyzed with an optic microscope (OM), type MC3, which was calibrated in advance.The calibration was done for three types of eyepieces: OC10xOB6; OC10xOB10 and OC10xOB20. The micrometric values (MV) from the calibration of the MO-MC3 were: VM=15,000μ, for OC10xOB6; VM=9,011μ, for OC10xOB10 and VM=4,441μ, for OC10xOB20 [9][10]. For the study of the slides the following were also used: an eyepiece micrometer, a calibration blade, a myocyte numbering grate, a digital camera and other instruments. After the best images were identified in the microscopic field, the two diameters of the myocytes and of the primary muscle fascicles (PMF) were measured (big and small) and all myocytes from the PMF were counted. Through calculus the average diameter of the myocytes and PMF was determined; the perimeter of the muscle structures; the shape and profile indices; the transversal section surface of the myocytes and of the PMF, as well as the myocyte density. Also the ratio of the two main tissue categories, the muscle tissue and conjunctive tissue, was measured. For these measurements the following mathematical equations were used:

(1) Dx = (LD+Sd)/2, where: LD = large diameter of myocytes and of PMF, in microns (μ); Sd = small diameter of myocytes and of PMF (μ); Dx = average diameter (μ).
(2) P = (LD+Sd)/2x π, where: P = myocytes perimeter and of PMF (μ); π=calculation coefficient for the lenght and surface of the circle, with the value of 3,141592656.
(3) If = LD/Sd, where: If = format index of myocytes and of PMF (x/1).
(4) Ip = (Sdx100)/LD, where: Ip = Profile index of myocytes and of PMF (%).
(5) C.s.s. = [(DMxDM)/4]xπ, where: C.s.s. = cross-section surface of myocytesn and PMF (μ^2)
(6) Dmf = (nx1000000)/C.s.s.PMF, where: n = number of myocytes from PMF; Dmf = density of muscular fibers (myocytes) (mf/mm^2); C.s.s.PMF =cross-section surface of PMF (μ^2)
(7) MTP = (C.s.s.mf.x100)/ C.s.s.PMF, where: MTP = muscle tissue proportion (%); C.s.s.mf. = cross-section surface of the muscular fibers (μ^2)
(8) CTP = 100-MTP, where: CTP = connective tissue proportion (%).

All the data resulted from the micrometric measurements and from the calculus were statistically analyzed, starting with the general statistical estimators (the statistical mean, the standard deviation of the mean; standard deviation, the variant and the variant coefficient)[4]. Then the Fischer (F) and Tukey (W) values were measured [4] to test the statistical implications of the differences between the eleven parameters, that were the object of the measurements and calculus done for this article, for the five secondary muscle bundles (SMB) taken into study. For the statistical calculus the ANOVA Single Factor (ASF) algorithm (integrated in the Microsoft Excel software) was used.

RESULTS AND DISCUSSIONS

In fish the somatic muscles are structured in muscle fibers of the fourth order (quaternary); third order (tertiary); second order (secondary) and first order (primary). The latter contain a variable number of myocytes or muscle fibers. In the current study, five SMF were investigated from the lateral – dorsal epaxial muscle (ML-ED) which contain 3 to 5 PMFs. For these SMB the parameters taken into study are presented in table 1 through 5. The diameters (big, small and medium), the PMF perimeter, the myocyte number, the transversal section surface of the PMF and their profile were determined. The variability of the raw data was not accentuated for SMF1 (v=6-15%) and SMF2 (v=7-29%), but the specific coefficient (v %) is greater for the other SMFs (tab.3, 4, 5). Table 6 presents the statistical analysis made for the 5 SMFs. Thereby, the big diameter of the PMF from the studied muscle has values between 300 and 675μ, with an average of 477.5±25.212μ (v=22.4%). The small diameter values of the PMB range between 195 and 360μ, with an average of 272.5±11.456μ (v=17.84%) (tab.6). The average thickness values of the primary muscle bundles ranged from 277.5μ to 517.5μ and the average of the 18 primary data was of 375±16.122μ (v=18.24%). The perimeter of these PMBs varied between 871.792μ and 1625.774μ and the statistical mean value was 1178.097±50.65μ (v=18.24%) (tab.6). Regarding the shape index, the variation limits are broad (1.176/1,respectively 2.500/1), with an average of1.779/1 (v=21.67%). The profile index has an average of 58.96±3.22%. These data imply that the PMF from each of the five studied SMB have a cylindroid aspect with a tendency towards flattening.

Table 1.

Statistical indicators for some morphological parameters of the first muscular fascicle ofthe *Polyodon spathula* lateral muscle

Specification					MU	n	Statistical indicators			Variation limits	
Species	Age	Sex	Muscle	Parameter studied at PMF level			$\bar{x}\pm s\bar{x}$	s	V(%)	Min.	Max.
Polyodon spathula	The fourth summer (ps 3+)	Male	Dorsal epaxial muscle	Large diameter (LD)	µ	3	575±36,055	62,450	10,86	525	645
				Small diameter (Sd)	µ	3	330±15	25,981	7,87	315	360
				Average diameter ($D\bar{x}$)	µ	3	452,5±17,5	30,311	6,70	420	480
				PMF* perimeter	µ	3	1421,571	95,224	6,70	1319,469	1507,964
				Format index (If)	x/1	3	1,752±0,152	0,264	15,04	1,542/1	2,048/1
				Profile index (Ip)	%	3	57,90±4,74	8,218	14,19	48,837	64,865
				Number of myocytes	n	3	72,33±2,96	5,132	7,09	68	78
				Transversal section surface of PMF	μ^2	3	148793,682±9485,2	16428,755	11,04	129885,221	159573,272

*PMF = primary muscular fascicle

Table 2.

Statistical indicators for some morphological parameters of the second muscular fascicle ofthe *Polyodon spathula* lateral muscle

Specification					MU	n	Statistical indicators			Variation limits	
Species	Age	Sex	Muscle	Parameter studied at PMF level			$\bar{x}\pm s\bar{x}$	s	V(%)	Min.	Max.
Polyodon spathula	The fourth summer (ps 3+)	Male	Dorsal epaxial muscle	Large diameter (LD)	µ	5	399±28,3	63,285	15,86	300	450
				Small diameter (Sd)	µ	5	237±16,02	35,812	15,11	195	285
				Average diameter ($D\bar{x}$)	µ	5	318±11,275	25,212	7,93	277,5	345
				PMF* perimeter	µ	5	999,027±35,421	79,205	7,93	871,792	1083,849
				Format index (If)	x/1	5	1,735±0,213	0,476	27,43	1,176/1	2,308/1
				Profile index (Ip)	%	5	61,533±8,036	17,969	29,20	43,333	85,00
				Number of myocytes	n	5	34,2±1,685	3,768	11,02	30	38
				Transversal section surface of PMF	μ^2	5	73407,24±4775,1	10677,422	14,55	60082,96	84823,00

*PMF = primary muscular fascicle

Table 3.

Statistical indicators for some morphological parameters of the third muscular fascicle ofthe *Polyodon spathula* lateral muscle

Specification					MU	n	Statistical indicators			Variation limits	
Species	Age	Sex	Muscle	Parameter studied at PMF level			$\bar{x}\pm s\bar{x}$	s	V(%)	Min.	Max.
Polyodon spathula	The fourth summer (ps 3+)	Male	Dorsal epaxial muscle	Large diameter (LD)	µ	3	545±78.102	135.277	24.82	405	675
				Small diameter (Sd)	µ	3	310±26.46	45.826	14.78	270	360
				Average diameter ($D\bar{x}$)	µ	3	427.5±51.96	90.000	21.05	337.5	517.5
				PMF* perimeter	µ	3	1343.031±163.242	282.743	21.05	1060.288	1625.774
				Format index (If)	x/1	3	1.742±0.121/1	0.210	12.04	1.500/1	1.875/1
				Profile index (Ip)	%	3	58.02±4.33	7.500	12.93	53.333	66.667
				Number of myocytes	n	3	59.333±10.10	19.036	32.08	41	79
				Transversal section surface of PMF	μ^2	3	135834.612± 30407.46	52667.272	38.77	85883.289	190851.754

*PMF = primary muscular fascicle (B=bundle)

The number of PMF myocytes varies a lot (v=34.38%) and the variation limits are far from one another (30-79) and the statistical mean for this parameter is 48.444±3.925 mf (tab.6). From the total number of muscle fibers (mf) (myocytes), on average 71.89% were counted (with variations from 42.65% to 100%) (tab.6), which offers credibility and precision for the data that can be analyzed from this characteristic (density and muscle tissue ratio.). The transversal section surface of the PMF varied between 60082.96 μ² and 190851.754 μ², with a statistical mean of 104016.17±8833.73μ² (v=36.03%) (tab.6).

Table 4.

Statistical indicators for some morphological parameters of the fourth muscular fascicle ofthe *Polyodon spathula* lateral muscle

Specification					MU	n	Statistical indicators			Variation limits	
Species	Age	Sex	Muscle	Parameter studied at PMF level			$\bar{x}\pm s\bar{x}$	s	V(%)	Min.	Max.
Polyodon spathula	The fourth summer (ps 3+)	Male	Dorsal epaxial muscle	Large diameter (LD)	μ	4	476.25±42.59	85.184	17.89	405	600
				Small diameter (Sd)	μ	4	236.25±15.462	30.923	13.09	195	270
				Average diameter ($D\bar{x}$)	μ	4	356.25±24.78	49.561	13.91	300	420
				PMF* perimeter	μ	4	1119.192±77.85	155.699	13.91	942.478	1319.469
				Format index (If)	x/1	4	2.030±0.178	0.355	17.51	1.667	2.500/1
				Profile index (Ip)	%	4	50.37±2.111	8.446	16.77	40	60
				Number of myocytes	n	4	43.5±5.38	10.755	24.72	30	54
				Transversal section surface of PMF	μ^2	4	88843.26±10672.7	21345.374	24.03	62026.820	113097.335

*PMF = primary muscular fascicle

Table 5.

Statistical indicators for some morphological parameters of the fifth muscular fascicle ofthe *Polyodon spathula* lateral muscle

Specification					MU	n	Statistical indicators			Variation limits	
Species	Age	Sex	Muscle	Parameter studied at PMF level			$\bar{x}\pm s\bar{x}$	s	V(%)	Min.	Max.
Polyodon spathula	The fourth summer (ps 3+)	Male	Dorsal epaxial muscle	Large diameter (LD)	μ	3	445±77.621	134.443	30.21	360	600
				Small diameter (Sd)	μ	3	285±8.66	15.000	5.26	270	300
				Average diameter ($D\bar{x}$)	μ	3	365±35	60.62	16.61	330	435
				PMF* perimeter	μ	3	1146.682±109.96	190.449	16.61	1036.726	1366.593
				Format index (If)	x/1	3	1.579±0.323	0.560	35.44	1.200/1	2.222/1
				Profile index (Ip)	%	3	68.11±11.75	20.347	29.87	45.0	83.33
				Number of myocytes	n	3	44±7.0	12.124	27.56	37	58
				Transversal section surface of PMF	μ^2	3	98665.645±14286.71	24745.301	25.08	83939.429	127234.503

*PMF = primary muscular fascicle

Table 6.

Statistical indicators for some morphological parameters of the all five secundary muscular fascicles of the *Polyodon spathula* lateral muscle

Specification					MU	n	Statistical indicators			Variation limits	
Species	Age	Sex	Muscle	Parameter studied at PMF level			$\bar{x}$±s$\bar{x}$	s	V(%)	Min.	Max.
Polyodon spathula	The fourth summer (ps 3+)	Male	Dorsal epaxial muscle	Large diameter (LD)	µ	18	477.5±25.212	106.967	22.40	300	675
				Small diameter (Sd)	µ	18	272.5±11.456	48.606	17.84	195	360
				Average diameter (D$\bar{x}$)	µ	18	375±16.122	68.401	18.24	277.5	517.5
				PMF* perimeter	µ	18	1178.097±50.65	214.887	18.24	871.792	1625.774
				Format index (If)	x/1	18	1.779±0.091	0.385	21.67	1.176/1	2.500/1
				Profile index (Ip)	%	18	58.958±3.217	13.648	23.15	40	85
				Total number of myocytes from PMF	n	18	48.444±3.925	16.653	34.38	30	79
				Number of myocytes measured from PMF	n	18	33.444±2.201	9.338	27.92	20	54
				Proportion of myocytes measured from their total number	%	18	71.89±3.61	15.307	21.29	42.65	100.00
				Transversal section surface of PMF	µ²	18	104016.169±8833.733	37478.353	36.03	60082.96	190851.754

*PMF = primary muscular fascicle

Regarding the thickness and the density of the myocytes from the 18 PMFs, the data presented in table 7 shows that these myocytes have an average diameter of 43.502±0.493µ and a transversal section surface of 1486.523±34.848µ².

Table 7.

Statistical indicators for myocytes density and the proportion of the two tissue categories from primary muscle fascicles of lateral muscle of *Polyodon spathula* fish

Specification						MU	n	Statistical indicators			Variation limits	
Species	Age	Sex	Muscle	Morphological parameters of myocytes and of PMF*				$\bar{x} \pm s\bar{x}$	s	V (%)	Min.	Max.
Polyodon spathula fish	Fourth summer	Male	Lateral muscle (Epaxial muscle)	In the myocytes	Large diameter	µ	18	51.641±0.644	2.732	5.29	46.099	56.071
					Small diameter	µ	18	35.361±0.515	2.186	6.18	31.662	39.680
					Average diameter	µ	18	43.502±0.493	2.092	4.81	38.835	47.146
					Cross-sectional area	µ²	18	1486.523±34.848	147.847	9.95	1177.553	1770.941
				In the PMF	Myocytes density (m.f.**/mm²)	mf/ mm²	18	468.911±9.12	38.690	8.25	405.054	551.374
					Muscle tissue proportion	%	18	69.565±1.835	7.787	11.19	57.558	81.782
					Connective tissue proportion	%	18	30.435±1.835	7.786	25.58	18.218	42.442

*PMF=Primay Muscle Fascicle (B=Bundle), **m.f.=muscle fibers (myocytes)

Table 8.

Average statistical values for the thickness and profile of primary muscle fascicles as well as for the density of myocytes and for muscle tissue proportion and connective tissue proportion in

lateral muscle of *Polyodon spathula* fish

Specification		Secundary muscle fascicles studied for lateral muscle (average statistical values)					Average value of the five SMF** studied
Morphological parameters studied for PMF*	MU	SMF_1	SMF_2	SMF_3	SMF_4	SMF_5	
Large diameter (LD)	μ	575.0	399.0	545.0	476.25	445.0	**488.05**
Small diameter (Sd)	μ	330.0	237.0	310.0	236.25	285.0	**279.65**
Average diameter ($D\bar{x}$)	μ	452.5	318.0	427.5	356.25	365.0	**283.85**
PMF perimeter (P)	μ	1421.571	999.027	1343.031	1119.192	1146.682	**1205.9006**
Format index of PMF	x/1	1.752/1	1.735/1	1.742/1	2.030/1	1.579/1	**1.7676/1**
Profile index of PMF	%	57.90	61.533	58.02	50.37	68.11	**59.1866**
Total number of myocytes from PMF	n	72.33	34.20	59.333	43.50	44	**50.6726**
Cross-sectional area from PMF	μ^2	148793.682	73407.240	135834.612	88843.260	98665.645	**109108.8878**
Density of myocytes from PMF	mf***/mm^2	488.265	470.248	444.952	489.166	444.282	**467.3826**
Proportion of muscle tissue from PMF	%	64.098	74.998	65.070	71.376	68.059	**68.7202**
Proportion of connective tissue from PMF	%	35.902	25.002	34.930	28.624	31.941	**31.2798**

*PMF=Primary Muscle Fascicle, **SMF=secundary muscle fibers (myocytes), ***m.f.=muscle fibers (myocytes).

The myocyte density varies between 405.054 mf/mm² and 551.374 mf/mm² and the statistical mean for this characteristic is 468.911±9.12mf/mm² (v=8.25%) (tab.7). For the pure muscle tissue ratio in the 18 PMFs, the values ranged between 57.558% and 81.782%, with a statistical mean of 69.565±1.835% (v=11.19%) (tab.7).The conjunctive tissue ratio was on average of 30.435±1.835% (tab.7). The average values of the studied parameters (for the PMFs) where then compared between the 5 SMFs, as shown in table 8. Also in table 8 the arithmetic mean of the 5 SMFs was calculated for each of the 11 parameters taken into study. It can be observed that the big diameter values of the PMF vary between 399μ and 575μ and the average of the 5 SMF is 488.05μ.

Table 9.

Statistical significance of the differences between the five (5) secundary muscular fascicles of the lateral muscle of *Polyodon spathula*, regarding the thickness and profile of myocytes from PMF.

Studied parameters of PMF* from SFM**	Differences between average values of the 5 SMF compared	Tukey values(W'=0,01)	Statistical significance	At 4; 13 LL (liberty levels), for:			
				P	p≤0.05	p≤0.01	p≤0.001
				Fα	3.180	5.200	9.070
Large diameter of PMF(μ)	SMF_1-SMF_2= 176,0	235,3117	n.s.	$\hat{F}$	2,092000		
	SMF_1-SMF_3=30,0	306,3163	n.s.				
	SMF_1-SMF_4=98,75	311,9512	n.s.				
	SMF_1-SMF_5=130,00	353,8695	n.s.				
	SMF_2-SMF_3=146,00	235,3116	n.s.				
	SMF_2-SMF_4=77,25	251,6648	n.s.				
	SMF_2-SMF_5=46,00	298,2824	n.s.				
	SMF_3-SMF_4=68,75	246,0948	n.s.				
	SMF_3-SMF_5=100,00	306,3163	n.s.				
	SMF_4-SMF_5=31,25	246,3491	n.s.				
Small diameter of PMF (μ)	SMF_1-SMF_2=93,00	106,9252	n.s.	$\hat{F}$	6,074270		
	SMF_1-SMF_3=20,00	139,1896	n.s.				

	SMF_1-SMF_4=93,75	141,7501	n.s.		
	SMF_1-SMF_5=45,00	160,7976	n.s.		
	SMF_2-SMF_3=73,00	106,9252	n.s.		
	SMF_2-SMF_4=0,75	114,356	n.s.		
	SMF_2-SMF_5=48,00	135,539	n.s.		
	SMF_3-SMF_4=73,75	111,825	n.s.		
	SMF_3-SMF_5=25,00	139,1896	n.s.		
	SMF_4-SMF_5=48,75	111,8251	n.s.		
Average diameter of PMF (μ)	SMF_1-SMF_2=134,50	150,472	n.s.	$\hat{F}$	4,073117
	SMF_1-SMF_3=25,00	195,8765	n.s.		
	SMF_1-SMF_4=69,25	199,478	n.s.		
	SMF_1-SMF_5=87,50	226,2847	n.s.		
	SMF_2-SMF_3=109,50	150,4720	n.s.		
	SMF_2-SMF_4=38,25	160,9292	n.s.		
	SMF_2-SMF_5=47,00	190,7391	n.s.		
	SMF_3-SMF_4=71,25	157,3674	n.s.		
	SMF_3-SMF_5=62,50	195,8765	n.s.		
	SMF_4-SMF_5=8,75	157,3674	n.s.		
Perimeter of PMF (μ)	SMF_1-SMF_2=422,544	472,7215	n.s.	$\hat{F}$	4,073123
	SMF_1-SMF_3=78,540	615,3639	n.s.		
	SMF_1-SMF_4=302,379	626,6839	n.s.		
	SMF_1-SMF_5=274,889	710,8942	n.s.		
	SMF_2-SMF_3=344,004	472,7215	n.s.		
	SMF_2-SMF_4=120,165	505,5736	n.s.		
	SMF_2-SMF_5=147,655	599,2244	n.s.		
	SMF_3-SMF_4=223,839	494,384	n.s.		
	SMF_3-SMF_5=196,349	615,3639	n.s.		
	SMF_4-SMF_5=27,490	494,384	n.s.		
Format index of PMF (Fi)(x/1)	SMF_1-SMF_2=0,017	0,8478	n.s.	$\hat{F}$	0,588310
	SMF_1-SMF_3=0,010	1,1036	n.s.		
	SMF_1-SMF_4=0,278	1,1239	n.s.		
	SMF_1-SMF_5=0,173	1,2749	n.s.		
	SMF_2-SMF_3=0,007	0,8478	n.s.		
	SMF_2-SMF_4=0,295	0,9067	n.s.		
	SMF_2-SMF_5=0,156	1,0747	n.s.		
	SMF_3-SMF_4=0,288	0,8866	n.s.		
	SMF_3-SMF_5=0,163	1,1036	n.s.		
	SMF_4-SMF_5=0,451	0,8876	n.s.		
Profile index of PMF (Pi)(%)	SMF_1-SMF_2=3,633	30,023	n.s.	$\hat{F}$	0,737192
	SMF_1-SMF_3=0,120	39,0823	n.s.		
	SMF_1-SMF_4=7,530	39,8012	n.s.		
	SMF_1-SMF_5=10,210	45,1495	n.s.		
	SMF_2-SMF_3=3,513	30,023	n.s.		
	SMF_2-SMF_4=11,163	32,1094	n.s.		
	SMF_2-SMF_5=6,577	38,0573	n.s.		
	SMF_3-SMF_4=7,650	31,3988	n.s.		
	SMF_3-SMF_5=10,090	39,0823	n.s.		
	SMF_4-SMF_5=17,74	31,3987	n.s.		

Table 10.

Statistical significance of the differences between the five (5) secundary muscular fascicles of the lateral muscle of *Polyodon spathula*, regarding the number and density of myocytes and the proportion of
muscular and connective tissue from PMF

Studied parameters of PMF* from SFM**	Differences between average values of the 5 SMF compared	Tukey values(w=0,01)	Statistical significance	At 4; 13 LL (liberty levels), for:			
				P	p≤0.05	p≤0.01	p≤0.001
				Fα	3.180	5.200	9.070
Total number of myocytes from PMF	SMF_1-SMF_2=38,130	36,634	**	$\hat{F}$	7,13688144		
	SMF_1-SMF_3=12,997	47,6883	n.s.				
	SMF_1-SMF_4=28,830	48,5655	n.s.				
	SMF_1-SMF_5=28,330	55,0915	n.s.				
	SMF_2-SMF_3=25,133	36,634	n.s.				
	SMF_2-SMF_4=9,300	39,1800	n.s.				

	SMF_2-SMF_5=9,800	46,4375	n.s.		
	SMF_3-SMF_4=15,833	38,3128	n.s.		
	SMF_3-SMF_5=15,333	47,6883	n.s.		
	SMF_4-SMF_5=0,500	38,3128	n.s.		
Cross section of PMF (μ^2)	SMF_1-SMF_2=75386,442	82446,961	n.s.	$\hat{F}$	5,245366
	SMF_1-SMF_3=12959,070	107325,111	n.s.		
	SMF_1-SMF_4=59950,422	109299,426	n.s.		
	SMF_1-SMF_5=50128,037	123986,469	n.s.		
	SMF_2-SMF_3=62427,372	82446,961	n.s.		
	SMF_2-SMF_4=15436,020	88176,683	n.s.		
	SMF_2-SMF_5=25258,405	104510,232	n.s.		
	SMF_3-SMF_4=46991,352	86225,103	n.s.		
	SMF_3-SMF_5=37168,967	107325,111	n.s.		
	SMF_4-SMF_5=9822,385	86225,232	n.s.		
Density of myocytes from PMF (m.f./mm^2)***	SMF_1-SMF_2=18,017	89,9886	n.s.	$\hat{F}$	0,927429
	SMF_1-SMF_3=43,313	117,1425	n.s.		
	SMF_1-SMF_4=0,901	119,2974	n.s.		
	SMF_1-SMF_5=43,983	135,3279	n.s.		
	SMF_2-SMF_3=25,296	89,9886	n.s.		
	SMF_2-SMF_4=18,918	96,2425	n.s.		
	SMF_2-SMF_5=25,966	114,0701	n.s.		
	SMF_3-SMF_4=44,214	94,1124	n.s.		
	SMF_3-SMF_5=0,670	117,1425	n.s.		
	SMF_4-SMF_5=44,884	94,1124	n.s.		
Proportion of muscular tissue (MT)(%) from PMF	SMF_1-SMF_2=10,90	17,1293	n.s.	$\hat{F}$	1,448594
	SMF_1-SMF_3=0,972	22,2980	n.s.		
	SMF_1-SMF_4=7,278	22,7082	n.s.		
	SMF_1-SMF_5=3,961	25,8945	n.s.		
	SMF_2-SMF_3=9,928	17,1293	n.s.		
	SMF_2-SMF_4=3,622	18,3197	n.s.		
	SMF_2-SMF_5=6,939	21,7132	n.s.		
	SMF_3-SMF_4=6,306	17,9143	n.s.		
	SMF_3-SMF_5=2,989	22,2980	n.s.		
	SMF_4-SMF_5=3,317	17,9143	n.s.		
Proportion of connective tissue (CT)(%) from PMF	SMF_1-SMF_2=10,90	17,1293	n.s.	$\hat{F}$	1,448594
	SMF_1-SMF_3=0,972	22,2980	n.s.		
	SMF_1-SMF_4=7,278	22,7082	n.s.		
	SMF_1-SMF_5=3,961	25,8945	n.s.		
	SMF_2-SMF_3=9,928	17,1293	n.s.		
	SMF_2-SMF_4=3,622	18,3197	n.s.		
	SMF_2-SMF_5=6,939	21,7132	n.s.		
	SMF_3-SMF_4=6,306	17,9143	n.s.		
	SMF_3-SMF_5=2,989	22,2980	n.s.		
	SMF_4-SMF_5=3,317	17,9143	n.s.		

*PMF=Primary Muscle Fascicle, **SMF=secundary muscle fibers (myocytes), ***m.f.=muscle fibers (myocytes).

The small diameter values are between 236.25µ and 330µ, with a mean of 279.65µ (tab.8). The average thickness of the 5 SMFs is 383.85µ, with limits between 318µ and 452.5µ. The PMF perimeter values from the 5 SMFs ranges from 999.027µ to 1421.671µ (tab.8). The shape index values range from 1.579/1 to 2.030/1, with a mean of 1.768/1, which highlights an accentuated cylindroid aspect (shape) of the SMF. This is confirmed also by the values of the profile index (Ip=50.37-68.11%; Ip=59.19%) (tab.8). Regarding the total number of myocytes, it varied between 34.20 and 72.33mf/mm², with a mean for the 5 SMFs of 50.67mf/mm². For the transversal section surface of the PMF, the mean for the 5 SMF was of 109108.888µ², with values between 73407.24µ² and 148793.682µ² (tab.8). The myocyte density varied less in the 5 SMFs, with values ranging from 444.282mf/mm² to 489.166mf/mm² and the arithmetic mean was 467.383mf/mm² (tab.8). The muscle tissue ratio in the SMF varied between 64.098% and 74.998%, with a mean for the 5 SMFs of 68.72%

(tab.8). The conjunctivetissue ratio values ranged from 25% to 35.90%, with a mean for the 5 SMFs of 31.28% (tab.8). The existing differences for the five secondary muscle bundles (regarding the 11 parameters analyzed) are notable, with smaller or bigger values, yet these differences are not significant from a statistical point of view. Thus, for the small, average and big diameter values of the PMB, the F values are lower than Fα=0,01 at 4;13 GL, and Tukey (w'=0,01) values are greater than the tested differences (tab. 9). The same can be observed regarding the differences between the perimeters; shape indices; profile indices; the transversal section surfaces; myocyte densities and the muscle and conjunctive tissue ratios (tab.9) (tab.10). Only in the case of the myocyte number values, the difference between SMF1 and SMF2 was statistically significant (F>Ftab.α=0,01, at 4;13 GL) (w'<dif.test.) (tab.10). Regarding the thickness of the myocytes from the lateral-dorsal epaxial muscle of Polyodon Spathula, the values found are comparable with the ones obtained by other authors [7], yet smaller than for other species of fish, for example trout (47-67µ). Also, the pure muscle tissue ratio found in the studied muscle is greater in *Polyodon spathula*, when compared to other species of animals (chicken, pork, and beef). The small ratio of conjunctive tissue from the analyzed muscle, positively correlates with the reduced percentage of collagen in this meat, which in Ps3+ fish was of 4.21% [7], determining a higher tenderness to the meat from this species of fish.

CONCLUSIONS

1. The average thickness of the primary muscle bundles (PMF), from 4 year old Polyodon Spathula lateral-dorsal epaxial muscle was of 383.85µ.
2. The perimeter of these structural muscle units (PMF), for the species and for the studied muscle is 1205.9µ.
3. The primary muscle bundles (PMF) from this muscle have an accentuated cylindroid shape (If=1,768/1) (Ip=59,19%).
4. The myocyte number of the PMF, in the studied muscle is 50.67mf, for the four year old Polyodon Spathula (Ps3+).
5. The transversal section surface of the PMF from the studied muscle (ML-ED) is 109108.888µ².
6. The PMF myocytes have an average thickness of 43.502µ; a transversal section surface of 1486.523µ² and a density of 467.38mf/mm².
7. The pure muscle tissue ratio, for the Polyodon Spathula species, in the lateral-dorsal epaxial muscle is of 68.72% and positively correlates with the myocyte density.
8. The conjunctive tissue ratio for the same species and muscle is 31.28% and it correlates positively with the low ratio of collagen (4.21%) from the meat obtained from Polyodon Spathula.

REFERENCES

1. Carla Hassan-Williams, Timothy H. Bonner (2007). "Polyodon spathula". Fishes of Texas Project and Online Database. Texas National History Collection, a division of Texas Natural ScienceCenter, University of Texas at Austin. Retrieved June 19, 2014
2. Cecil A. Jennings, Steven J. Zigler (2009). Craig P. Paukert, George D. Scholten, ed. "Distribution, Ecology, and Life History; Biology and Life History of Paddlefish in North America: An Update" -Paddlefish Management, Propagation, and Conservation in the 21st Century (American Fisheries Society) **66** (1): 1–22. ISBN 978-1-934874-12-7.-June 18, 2014.

3. Cotea C.V., 2014 – Biologiecelulara, HistologieșiEmbriologiegeneralășispecială, EdituraTehnopress, Iaşi.
4. SanduGh., 1995 – MetodeexperimentaleînZootehnie, Editura Coral Sanivet, Bucureşti, 134-139, 300-302, 317-319.
5. Simeanu, Cristina; Păsărin, B.; Simeanu, D.-2010 „The study of some morphological characteristic of the sturgeon species of Polyodon spathula in different development stages".Lucr. Științ.SeriaZootehnie, USAMV Iași, vol. 53, pg. 244-247.
6. Simeanu, Cristina; Simeanu, D.; Nistor, C.; Păsărin, B.-2011" Evaluation of quantitative particularities of meat production at Polyodon spathula specie", Lucr.Științ.SeriaZootehnie, USAMV Iași, vol. 55, pg. 593-596.
7. Simeanu Cristina-2012-„Contribuții la cunoaștereacalitățiicărniiobținută de la specia de sturioni Polyodon spathula, crescutăînbazinelepiscicole din Moldova",Teză de Doctoratelaboratășisusținută la USAMV Iași, februarie 2012.
8. Spătaru, Mihaela-Claudia, 2009 – Anatomiacomparatăaanimalelor, Editura Alfa, Iași, pg. 22-31; 121-127.
9. Teușan, V.;Anca, Teușan; A.A.Prelipcean, 2012 –" Research regarding the surface on transversal section and density of superficial pectoral muscle of meat-type hybrid COBB-500, at different age stages", 2012, University of Agricultural Sciences and Veterinary Medicine - LucrăriştiinţificeSeriaMedicină-Veterinară, Editura "Ion Ionescu de la Brad", Iaşi, vol. 55 (1-2), pg. 133-143, ISSN 1454-7406
10. Teuşan V., AncaTeuşan, 2013 –" Research on the thickness and profile of profound pectoral muscle myocites of meat-typehybrid hen COBB-500, slaughtered at different ages", LucrăriŞtiinţificeU.S.A.M.V.Iaşi, SeriaMedicină-Veterinară, vol. 56, ISSN 1454-7406,pg.45-54.
11. Teușan, V.; Anca, Teușan, 2013 –" Investigations on the histological structure of the pectoralissuperficialis muscle in COBB-500 meat-type hybrid hen, slaughtered at different ages", 2013 , University of Agricultural Sciences and Veterinary Medicine, LucrăriştiinţificeMedicină-Veterinară, Editura "Ion Ionescu de la Brad", Iaşi, vol. 56 (1-2), pg. 30-44, ISSN 1454-7406,
12. Teuşan,Anca; Teuşan, V. 2014-„Research on the histological structure of the deep pectoral muscle, of meat-type commercial hybrid Cobb-500, slaughtered at different ages". First International Congress-"Life Science- A Challenge for the Future", held in Iasi(Romania),at " Ion Ionescu de la Brad" University of Agricultural Science and Veterinar Medicine, 23-24 October, 2014. Lucr.Științ.SeriaMedicinăVeterinară, USAMV Iași, vol.56(4), pg.174-185, ISSN 1454-7406.
13. Teușan, Anca-2014-"Research regarding the fineness and density of myocytes as well as the proportion of main tissue categories from the lateral gastrocnemius muscle of avian hybrid COOB-500,by sex and age of slaughter" . First International Congress-"Life Science- A Challenge for the Future", held in Iasi(Romania),at " Ion Ionescu de la Brad" University of Agricultural Science and Veterinar Medicine, 23-24 October, 2014. Lucr.Științ.SeriaMedicinăVeterinară, USAMV Iași, vol.56(4), pg., ISSN 1454-7406.
14. Tudor,Despina; Constantinescu,Gh.M., 2002 –„NominaAnatomicaVeterinaria", Ediţiebilingvă, EdituraVergiliu, Bucureşti.
15. Tudor,Despina; Constantinescu, Gh.M.; Constantinescu, Ileana;Cornilă, N., 2010 – „NominaHistologica et EmbriologicaVeterinaria", Ediţiebilingvă, EdituraVergiliu, Bucureşti.
16. *** Tehnicahistopatologică, Editura de Stat-RSR, pentruliteraturăștiințifică, 1953.
17. ***Investigațiahistologicăîn diagnostic veterinar, Ediția-a-I-a București,1995, L.C.S.V. deDiagnostic- uz intern.

RESEARCH REGARDING THE MYOCYTES THICKNESS AND PROFILE OF THE LATERAL MUSCLE IN *POLYODON SPATHULA* SPECIES

TEUȘAN VASILE[1], ANCATEUȘAN[2], CRISTINA SIMEANU[3]
CRAUS STEFAN[4]
[1]University of Applied Life Sciences and Environment, Iasi
[2] Acad. "Ioan Haulica" Research Institute, "Apollonia" University, Iasi
[3] University of Applied Life Sciences and Environment, Iasi
[4] Acad. "Ioan Haulica" Research Institute, "Apollonia" University, Iasi
vasile.teusan@yahoo.com

Abstract: *Histological samples from the lateral muscle (dorsal epaxial) were collected from ten, four year old, male sturgeon (PolyodonSpathula) specimens. These samples were processed in accordance with the paraffin sectioning method. Twenty histological slides were obtained with transversal sections from the above mentioned muscle. HEA coloration method was used and the slides were analyzed with a MC3 type optical microscope. Through microscopy, in the microscopic field, the small and big diameters of the primary muscle bundle (PMB) myocytes were determined. Calculations were made for the average diameter; perimeter and the values for the two indices that characterize the myocyte profile. The analysis was made on five secondary muscle bundles (SMB) and the obtained results were compared. The big myocyte diameter from the five SMB varied between48.397µ and52.605µ, with a mean of 51.363µ.Regarding the small myocyte diameter, it varied between 32.582µ and 37.119µ, with a mean of 35.238µ. The average thickness of the myocytes from the five SMB was between 40.489µ and 44.866µ, with a mean of 43.300µ. The average perimeter of the myocytes taken into this study was 136.048µ and the profile and shape index had average values of 70.303%, 1,512/1 respectively, which characterizes a cylindroid format with a tendency towards cylindrical. Most differences (95%) between the five SMB, for the 6 studied parameters are insignificant from a statistical point of view.*

Keywords:*Polyodon Spathula; epaxial muscle; thickness; myocyte; profile.*

INTRODUCTION

The rapid growth of human population across the globe, as well as the increase in food quality demands, led animal breeders to supply a diversified range of animal species for human consumption. Although continental and sea waters provided man since ancient times with a constant supply of food (proteins), semi-intensive and intensive breeding of fish (pisciculture) is a relatively new practice. Many species of fish are bred for their meat and roe, yet they vary according to the country's development in this field of animal husbandry. In Romania, pisciculture is an old tradition, but it did not have a significant growthas compared with poultry farms. Fish meat can compete successfully with poultry, due to its dietary, nutritional and sanogenous qualities. Regarding the trade and human consumption of fish meat and roe, as well as other fish products, there are major differences across the globe. In the last decades, from the many fish species bred for consumption, a rise in sturgeon farms has been observed, due to their high value market price of meat and roe (caviar). The sturgeon species taken into study in the present article is *Polyodon spathula* (Paddlefish), which has recently been introduced in mono and mixed cultures in Romania (Nucet Research Station - 1992)[7]. This plankton-eating freshwater fish has a rapid growth, but the qualitative characteristics of its somatic muscles are not known. The structural aspects of the lateral dorsal epaxial muscles are the object of this study.

MATERIALS AND METHODS

At least two categories of materials and a few methods were used to organize and conduct the research for the present study. Biological samples were used from the lateral dorsal epaxial muscles (L-ED), from ten four years old male paddlefish (Ps3+)[7]. The samples were processed according to the paraffin sectioning method [12][13], in the pathological anatomy laboratory of the Faculty of Veterinarian Medicine, UASVM Iasi. Twenty sample slides were obtained with transversal muscle sections from the afore mentioned muscles, which were coloured according to the HEA technique. The slides were then observed with a photonic microscope, MO-MC3 type (calibrated in advance)[9]. The calibration was done for three types of eyepieces: OC10xOB6; OC10xOB10 and OC10xOB20. The micrometric values (MV) from the calibration of the MO-MC3 were: VM=15,000μ, for OC10xOB6; VM=9,011μ, for OC10xOB10 and VM=4,441μ, for OC10xOB20 [10]. For the study of the slides the following were also used: an eyepiece micrometer, a calibration blade, a myocyte numbering grate, a digital camera and other instruments. After the best images were identified in the microscopic field, the myocyte and primary muscle bundle (PMB) diameters were measured. The best images are shown in the present article. The following were determined through measurements: the average diameter, the perimeter, the shape index, the profile index and the myocyte transversal section surface from the 18 PMB found in the structure of the five secondary muscle bundles (SMB). The following mathematical equations were used:

(1) Dx=(LD+Sd)/2, where: Dx=average diameter (μ); LD=large diameter (μ); Sd=small diameter (μ).
(2) P=[(LD+Sd)/2]xπ, where: P=Perimeter of myocytes (μ); π=calculation coefficient for the lenght and surface of the circle=3,141592656.
(3) If=LD/Sd, where: If= format index of myocytes (x/1).
(4) Ip=(Sdx100)/LD, where: Ip=Profile index of myocytes (%)
(5) C.s.s.=[(LDxSd)/4]xπ, where: C.s.s.= Cross-section surface of myocytes (μ^2).

The obtained data from the measurements and calculus were interpreted statistically in two steps. In the first step all the general statistical indices were calculated: the statistical mean, the standard deviation of the mean; standard deviation, the variant and the variant coefficient) [4]. The second step consisted of the variation analysis, estimating the Fischer (F) and Tukey (w') values [4], to test the differences between the five SMBs of the studied muscle (L-ED) for the six morphological parameters that were studied. For the statistical calculus the ANOVA Single Factor (ASF) algorithm (integrated in the Microsoft Excel software) was used[4]; [9]; [10].

RESULTS AND DISCUSSIONS

In fish, the somatic muscle structure is not that much different than the one of mammals or birds. Therefore the fundamental morphological structure of the lateral dorsal epaxial muscle is the myocyte (rhabdocyte), which through association, form larger and larger muscle structures called bundles (primary, secondary, tertiary, quaternary). In the present study, five secondary muscle bundles (SMB) were investigated from the dorsal lateral epaxial muscle (ML-ED), which contained in their structure 18 primary muscle bundles

(PMB) and 602 myocytes. Regarding the latter, a series of parameters that characterize their finesse and profile were determined. In the structure of the first secondary muscle bundle (SMB1) three PMBs were found, which had 40, 29 and 51 myocytes. (tab. 1), totaling to 120 muscle fibers (myocytes).

Table 1.

Statistical indicators for thethickness and profile of the myocytes from the firstsecundary muscular bundle (SMB1)**, ofthe *Polyodon spathula* lateral muscle.

Specification						MU	n	Statistical indicators			Variation limits	
Species	Age	Sex	Muscle	PMB studied	Parameterstudied at myocytes level			$\bar{x}\pm s_{\bar{x}}$	s	V (%)	Min.	Max.
Polyodon spathula	The fourth summer(ps 3+)	Male	Dorsal epaxialmuscle	PMB1*	Large diameter (LD)	µ	40	48,929±2,222	14,051	28,72	27,033	90,100
					Small diameter (Sd)	µ	40	32,845±1,486	9,395	28,61	18,022	58,572
					Average diameter ($D\bar{x}$)	µ	40	40,887±1,699	10,746	26,28	23,428	74,336
					PMB* perimeter	µ	40	128,45±5,338	33,758	26,28	73,601	233,533
					Format index (If)	x/1	40	1,533±0,062	0,392	25,55	1,000/1	3,000/1
					Profile index (Ip)	%	40	68,666±2,332	14,747	21,48	33,33	100,0
				PMB2*	Large diameter (LD)	µ	29	51,86±2,865	15,431	29,76	27,033	81,099
					Small diameter (Sd)	µ	29	33,838±1,508	8,123	24,00	22,527	54,066
					Average diameter ($D\bar{x}$)	µ	29	42,849±1,916	10,320	24,08	27,033	67,582
					PMB* perimeter	µ	29	134,613±6,02	32,421	24,09	84,927	212,315
					Format index (If)	x/1	29	1,563±0,081	0,437	27,95	1,000/1	2,667/1
					Profile index (Ip)	%	29	68,505±3,222	17,352	25,33	37,50	100,00
				PMB3*	Large diameter (LD)	µ	51	46,009±1,395	9,962	21,65	27,033	72,088
					Small diameter (Sd)	µ	51	31,662±0,986	7,045	22,25	18,022	45,055
					Average diameter ($D\bar{x}$)	µ	51	38,835±1,075	7,675	19,76	22,527	56,318
					PMB* perimeter	µ	51	122,005±3,38	24,112	19,77	70,771	176,928
					Format index (If)	x/1	51	1,483±0,041	0,292	19,70	1,050/1	2,174/1
					Profile index (Ip)	%	51	69,873±1,819	12,988	18,59	46,000	95,240

*PMB= primary muscular bundle;**SMB=secondary muscular bundle.

In table 1 the general statistical indicators (the mean and its deviation; standard deviation; variation coefficient) and the variation limits for the 6 parameters are shown. These parameters characterize the myocyte thickness and profile. It has been observed that the variability of the raw data, for these parameters, is accentuated (v=18.59%-29.76%) (tab.1).

Similarly in tables 2, 3, 4 and 5 the general statistical indicators for the six parameters are shown for the secondary muscle bundles 2, 3, 4 and 5. The same observation can be made for these SMBs as well: the primary data variability is also accentuated (v=21.07%-34.05%) (v=14.24%-25.42%) (v=21.93%-35.68%) (v=20.41%-26.47%).

In the second secondary muscle bundle (SMB2) five primary muscle bundles (PMB) were found, each having: 28, 22, 30, 24 and respectively 20 myocytes, totaling 124 muscle fibers (tab. 2). In SMB 3, there were three PMBs with 40, 35 and respectively 41 myocytes, totaling 116 muscle fibers (tab. 3). In SMB 4, four PMBs were found, with 30, 28, 26 and respectively 40 myocytes, totaling 124 muscle fibers (tab. 4). Lastly, in SMB 5 there were 3 PMBs, with 32, 32 and respectively 54 myocytes, totaling 118 muscle fibers (tab. 5).

After the statistical analysis for each of the PMBs, the values of the 6 studied myocyte parameters were analyzed for each SMB and the results are shown in table 6.

Hence, the big diameter of the SMB 1 myocytes has values ranging from 27.033 to 90.10µ, and the statistical mean of the 120 values is 48.397±1.183µ (v=26.77%). For the small diameter of these myocytes, the variation limits were 18.022µ and 58.572µ, with a mean of 32.582±0.742µ (v=24.95%) (tab.6).

The average diameter of the SMB 1 myocytes ranges between 22.527µ and 74.336µ, with a statistical mean for the 120 values of 40.489±0.867µ (v=23.46%) (tab.6). The myocytes from this SMB have a mean perimeter of 127.2±2.724µ (v=23.46%), and aspect-wise they have a cylindroid shape with a cylindic tendency. This characteristic is backed up by the two mean values of the specific indices: the shape index(If=1.519±0.033/1) and the profile index (Ip=69.14±1.334%)(tab.6).

For the SMB 2, the myocyte's big diameter statistical mean has a value of 52.605±1.243µ(v=26.31%); a statistical mean of the small diameter of 37.119±0.956µ and a statistical mean of the average diameter of 44.866±0.97µ (v=24.08-28.69%) (tab.6). The perimeter of these myocytes measures on average 140.95±3.048µ, and the shape is also a cylindroid. (If=1.489±0.038/1) (Ip=72.3±1.532%) (tab.6).

Regarding SMB 3, the big diameter for the 116 myocytes varied between 31.538µ and 85.605µ, with a statistical mean of 51.767±1.071µ(v=22.28%)(tab.6).

The small diameter values ranged from 18,022µ to 56,066µ, with a mean for the 116 values of 35.158±0.738µ (v=22.61%) (tab.6). The average thickness of these myocytes was of 43.458±0.813µ (v=20.15%), and the perimeter average had a value of 136.602±2.56µ (v=20.18%) (tab.6). Also, the myocytes of this SMB had a cylindroid shape (If=1.511±0.032/1) (Ip=69.114±1.272%) (v=19.82-22.48%) (tab.6).

The big diameter of the fourth SMB (124 myocytes) varied between 27.033 µ and 85.604µ, with a statistical mean of 51.704±1.19µ(v=25.62%) (tab.6). The small diameter of these myocytes had a mean of 35.106±0.884µ (v=28.03%), while the average diameter mean value was 43.405±0.901µ (v=23.1%) (tab.6).

The muscle fiber perimeter from SMB 4 varied between 77,849µ şi 212,315µ, with a mean value of 136.369±2.831µ (v=24.78%) (tab.6). Regarding, the shape of these myocytes it is cylindroid (If=1.544±0.042/1) (Ip=69.775±1.588%) (tab.6).

The big diameter of the 118 myocytes that form SMB 5 ranged from 27.033µ to 81.099µ, with a mean of 52.34±1.149µ (v=23.85%) (tab.6).The small diameter varied between 18.022µ and 54.066µ, with a mean value of 36.227±0.816µ (v=24.46%). The limits of the average diameter were 27.033µ and 67.582µ, with a mean of 44.283±0.849µ (v=20.82%) (tab.6).The perimeter values ranged from 84.927µ to 212.315µ, and the mean value was 139.12±2.667µ(v=20.82%)(tab.6). Regarding the myocyte shape of SMB 5, the mean values of the specific indices show that these muscle fibers are also cylindroid shaped. The shape index has a mean value of 1.493±0.036/1, and the profile index mean value was 72.187±1.541% (tab.6).

Next, the mean values of the six studied parameters were analyzed for all of the SMBs (tab.7). The big diameter varied between 48,397µ and 52,605µ, with a mean of 51.363µ (tab.7).

Table 2.

Statistical indicators for the thickness and profile of the myocytes from the secondary muscular fascicle(SMB2), of the *Polyodon spathula* lateral muscle**

Specification						MU	n	Statistical indicators			Variation limits	
Species	Age	Sex	Muscle	PMB studied	Parameterstudied at myocytes level			$\bar{x}\pm s_{\bar{x}}$	s	V(%)	Min.	Max.
Polyodon spathula	The fourth summer (ps 3+)	Male	Dorsal epaxial muscle	PMB1*	Large diameter (LD)	µ	28	54,581±2,965	15,691	28,75	36,044	90,110
					Small diameter (Sd)	µ	28	39,68±2,299	12,168	30,66	22,527	63,077
					Average diameter ($D\bar{x}$)	µ	28	47,146±2,28	12,065	25,59	31,538	72,533
					PMB* perimeter	µ	28	148,114±7,16	37,903	25,59	99,080	227,869
					Format index (If)	x/1	28	1,468±0,094	0,500	34,05	1,000/1	3,333/1
					Profile index (Ip)	%	28	74,884±3,623	19,172	25,60	30,00	100,00
				PMB2*	Large diameter (LD)	µ	22	53,411±2,979	13,974	26,16	36,044	90,110
					Small diameter (Sd)	µ	22	34,856±1,93	9,0512	25,97	18,022	54,066
					Average diameter ($D\bar{x}$)	µ	22	44,133±2,007	9,415	21,33	31,538	63,077
					PMB* perimeter	µ	22	138,649±6,31	29,579	21,34	99,080	198,162
					Format index (If)	x/1	22	1,612±0,123	0,578	35,87	1,053/1	3,000/1
					Profile index (Ip)	%	22	67,927±3,81	17,869	26,31	33,33	95,00
				PMB3*	Large diameter (LD)	µ	30	50,552±2,171	11,894	23,53	31,538	72,088
					Small diameter (Sd)	µ	30	35,063±1,77	9,694	27,65	22,527	63,077
					Average diameter ($D\bar{x}$)	µ	30	42,802±1,764	9,661	22,57	31,538	67,582
					PMB* perimeter	µ	30	134,466±5,54	30,351	22,57	99,080	212,315
					Format index (If)	x/1	30	1,508±0,066	0,361	23,92	1,000/1	2,400/1
					Profile index (Ip)	%	30	70,74±2,925	16,024	22,65	41,67	100,00
				PMB4*	Large diameter (LD)	µ	24	53,052±2,885	14,134	26,64	36,044	90,110
					Small diameter (Sd)	µ	24	37,508±2,22	10,878	29,00	23,429	54,066
					Average diameter ($D\bar{x}$)	µ	24	45,28±2,322	11,374	25,12	31,538	65,330
					PMB* perimeter	µ	24	142,252±7,29	35,732	25,12	99,080	205,240
					Format index (If)	x/1	24	1,479±0,06	0,316	21,40	1,000/1	2,222/1
					Profile index (Ip)	%	24	71,799±3,237	15,859	22,09	45,00	100,00
				PMB5*	Large diameter (LD)	µ	20	51,498±3,177	14,209	27,59	27,033	90,110
					Small diameter (Sd)	µ	20	38,657±2,466	11,028	28,53	22,527	54,066
					Average diameter ($D\bar{x}$)	µ	20	45,077±2,61	11,672	25,89	27,033	72,088
					PMB* perimeter	µ	20	141,614±8,199	36,668	25,89	84,927	226,471
					Format index (If)	x/1	20	1,365±0,06	0,289	21,14	1,000/1	2,000/1
					Profile index (Ip)	%	20	76,433±3,60	16,101	21,07	50,00	100,00

The small diameter values ranged from 32.582µ to 37.119µ, and a mean of 35.238µ (tab.7). The average diameter of the myocytes varied between 40.489µ and 44,866µ, with a mean of 43.3µ (tab.7). The myocyte perimeter for the 5 SMBs varied between 127.2µ and 140.95µ, with a mean of 136,048µ (tab.7). Regarding the mean values of the indices that characterise the shape and profile of the myocytes forming the 5 SMBs, it can be observed that the values are very close: Shape index values ranged from 1.489/1 to 1.544/1, with a mean of 1.5112/1 (tab.7), and the profile index values were between 69.114% and 72.30%,and with a mean of 70.3032% (tab.7). Analyzing the data shown in table 7, it can be concluded that the SMB 1 myocytes are the thinnest, whilst the ones in SMB 2 are the thickest. The myocytes that form SMB 3, 4 and 5 have intermediary parameters in regards to their thickness. Regarding the shape and profile, the differences between the five SMBs are minor. The differences found among the five SMBs were statistically tested (tab.8) and the

differences between SMB 1 and SMB 2 are significant from a statistical point of view. All other differences are not statistically significant (tab.8).

Table 3.

Statistical indicators for the thickness and profile of the myocytes from the tkird muscular fascicle(SMB3), of the *Polyodon spathula* lateral muscle**

Specification						MU	n	Statistical indicators			Variation limits	
Species	Age	Sex	Muscle	PMB studied	Parameterstudied at myocytes level			$\bar{x}\pm s_{\bar{x}}$	s	V (%)	Min.	Max.
Polyodon spathula	The fourth summer (ps 3+)	Male	Dorsal epaxial muscle	PMB1*	Large diameter (LD)	µ	40	56,071±2,254	14,254	25,42	31,538	85,605
					Small diameter (Sd)	µ	40	35,864±1,38	8,725	24,33	18,022	54,066
					Average diameter ($D\bar{x}$)	µ	40	45,967±1,675	10,596	23,05	27,934	65,330
					PMB* perimeter	µ	40	144,409±5,26	33,289	23,05	87,757	205,240
					Format index (If)	x/1	40	1,593±0,05	0,340	21,34	1,125/1	2,571/1
					Profile index (Ip)	%	40	65,202±1,91	12,083	18,53	38,89	88,89
				PMB2*	Large diameter (LD)	µ	35	49,432±1,19	7,038	14,24	31,538	63,077
					Small diameter (Sd)	µ	35	34,139±1,181	6,986	20,46	18,022	49,560
					Average diameter ($D\bar{x}$)	µ	35	41,785±1,032	6,107	14,62	29,285	51,813
					PMB* perimeter	µ	35	131,272±3,24	19,187	14,62	92,002	162,813
					Format index (If)	x/1	35	1,490±0,05	0,297	19,91	1,091/1	2,500/1
					Profile index (Ip)	%	35	69,452±2,131	12,610	18,16	40,00	91,67
				PMB3*	Large diameter (LD)	µ	41	49,56±1,666	10,670	21,53	31,538	72,088
					Small diameter (Sd)	µ	41	35,341±1,254	8,031	22,72	18,923	49,560
					Average diameter ($D\bar{x}$)	µ	41	42,45±1,032	8,337	19,64	27,032	60,824
					PMB* perimeter	µ	41	133,534±4,12	26,364	19,74	84,924	191,084
					Format index (If)	x/1	41	1,448±0,057	0,365	25,18	1,000/1	2,857/1
					Profile index (Ip)	%	41	72,642±2,389	15,298	21,06	35,00	100,00

*PMB= primary muscular fascicle;**SMB=secondary muscular fascicle.

Table 4.

Statistical indicators for the thickness and profile of the myocytes from the four muscular fascicle(SMB4), of the *Polyodon spathula* lateral muscle**

Specification						MU	n	Statistical indicators			Variation limits	
Species	Age	Sex	Muscle	PMB studied	Parameterstudied at myocytes level			$\bar{x}\pm s_{\bar{x}}$	s	V(%)	Min.	Max.
Polyodon spathula	The fourth summer(ps 3+)	Male	Dorsal epaxialmuscle	PMB1*	Large diameter (LD)	µ	30	55,418±2,665	14,595	26,34	31,538	81,099
					Small diameter (Sd)	µ	30	33,671±1,618	8,862	26,32	18,022	54,066
					Average diameter ($D\bar{x}$)	µ	30	44,544±1,878	10,284	23,087	27,033	67,582
					PMB* perimeter	µ	30	139,939±5,90	32,308	23,09	84,927	212,315
					Format index (If)	x/1	30	1,710±0,09	0,491	28,69	1,000/1	3,044/1
					Profile index (Ip)	%	30	62,791±2,97	16,268	25,91	32,86	100,00
				PMB2*	Large diameter (LD)	µ	28	49,303±2,423	12,823	26,01	31,538	72,088
					Small diameter (Sd)	µ	28	35,529±1,724	9,122	25,67	18,022	63,077
					Average diameter ($D\bar{x}$)	µ	28	42,416±1,766	9,346	22,03	28,384	67,582
					PMB* perimeter	µ	28	133,252±5,55	29,361	22,03	89,171	212,315
					Format index (If)	x/1	28	1,450±0,10	0,517	35,68	1,000/1	3,500/1
					Profile index (Ip)	%	28	74,623±3,399	17,985	24,10	28,57	100,00
				PMB3*	Large diameter (LD)	µ	26	48,867±2,101	10,715	21,93	31,538	72,088
					Small diameter (Sd)	µ	26	32,509±2,001	10,201	31,38	18,022	58,571
					Average diameter ($D\bar{x}$)	µ	26	40,688±1,82	9,282	22,81	24,78	65,329
					PMB* perimeter	µ	26	127,863±5,74	29,268	22,89	77,849	206,237

					Format index (If)	x/1	26	1,603±0,096	0,489	30,52	1,000/1	3,000/1
					Profile index (Ip)	%	26	67,051±3,285	16,748	24,98	33,33	100,00
				PMB4*	Large diameter (LD)	µ	40	52,444±2,161	13,669	26,06	27,033	85,604
					Small diameter (Sd)	µ	40	37,576±1,661	10,503	27,95	22,527	63,077
					Average diameter ($D\bar{x}$)	µ	40	45,01±1,685	10,656	23,68	27,033	67,582
					PMB* perimeter	µ	40	141,402±5,29	33,478	23,68	84,927	212,315
					Format index (If)	x/1	40	1,448±0,06	0,374	25,85	1,000/1	2,333/1
					Profile index (Ip)	%	40	73,391±2,795	17,679	24,09	42,86	100,00

*PMB= primary muscular fascicle;**SMB=secondary muscular fascicle.

Table 5.

Statistical indicators for the thickness and profile of the myocytes from the fifth muscular fascicle(SMB5), of the *Polyodon spathula* lateral muscle**

Specification						MU	n	Statistical indicators			Variation limits	
Species	Age	Sex	Muscle	PMB studied	Parameterstudied at myocytes level			$\bar{x}\pm s\bar{x}$	s	V(%)	Min.	Max.
Polyodon spathula	The fourth summer (ps 3+)	Male	Dorsal epaxial muscle	PMB1*	Large diameter (LD)	µ	32	54,573±2,374	13,428	24,61	31,538	81,099
					Small diameter (Sd)	µ	32	34,157±1,299	7,350	21,52	20,725	54,066
					Average diameter ($D\bar{x}$)	µ	32	44,365±1,601	9,055	20,41	28,384	63,077
					PMB* perimeter	µ	32	139,376±5,029	28,448	20,41	89,171	198,162
					Format index (If)	x/1	32	1,629±0,069	0,392	24,05	1,000/1	2,667/1
					Profile index (Ip)	%	32	64,908±2,741	15,508	23,89	37,50	100,00
				PMB2*	Large diameter (LD)	µ	32	53,869±2,201	12,45	23,11	31,538	81,099
					Small diameter (Sd)	µ	32	36,044±1,687	9,542	26,47	18,022	54,066
					Average diameter ($D\bar{x}$)	µ	32	44,956±1,713	9,692	21,56	27,033	67,582
					PMB* perimeter	µ	32	141,234±5,382	30,447	21,56	84,927	212,315
					Format index (If)	x/1	32	1,556±0,072	0,405	26,04	1,000/1	2,400/1
					Profile index (Ip)	%	32	68,312±2,902	16,415	24,03	41,67	100,00
				PMB3*	Large diameter (LD)	µ	54	50,111±1,60	11,761	23,47	27,033	81,099
					Small diameter (Sd)	µ	54	37,562±1,248	9,169	24,41	22,527	54,066
					Average diameter ($D\bar{x}$)	µ	54	43,837±1,249	9,178	20,94	27,033	63,077
					PMB* perimeter	µ	54	137,716±3,924	28,833	20,94	84,927	198,162
					Format index (If)	x/1	54	1,374±0,05	0,343	24,95	1,00/1	2,250/1
					Profile index (Ip)	%	54	76,612±2,202	16,178	21,12	44,44	100,00

*PMB= primary muscular fascicle;**SMB=secondary muscular fascicle.

Table 6.

Statistical indicators for the thickness and profile of the myocytes, from the muscular secondary fascicle(SMB)*, of the *Polyodon spathula* lateral muscle

Specification						MU	n	Statistical indicators			Variation limits	
Species	Age	Sex	Muscle	SMB studied	Parameterstudied at myocytes level			$\bar{x}\pm s\bar{x}$	s	V (%)	Min.	Max.
Polyodon spathula	The fourth summer (ps 3+)	Male	Dorsal epaxial muscle(secondary muscular fascicles)(SMB)	SMB1*	Large diameter (LD)	µ	120	48,397±1,183	12,957	26,77	27,033	90,100
					Small diameter (Sd)	µ	120	32,582±0,742	8,129	24,95	18,022	58,572
					Average diameter ($D\bar{x}$)	µ	120	40,489±0,867	9,499	23,46	22,527	74,336
					PMB* perimeter	µ	120	127,2±2,724	29,842	23,46	70,771	233,533
					Format index (If)	x/1	120	1,519±0,033	0,364	23,93	1,000/1	3,0/1
					Profile index (Ip)	%	120	69,14±1,334	14,608	21,13	33,33	100,0
				SMB2*	Large diameter (LD)	µ	124	52,605±1,243	13,840	26,31	27,033	90,110
					Small diameter (Sd)	µ	124	37,119±0,956	10,651	28,69	18,022	63,077
					Average diameter ($D\bar{x}$)	µ	124	44,866±0,97	10,802	24,08	27,033	72,533

					PMB* perimeter	µ	124	140,95±3,048	33,936	24,08	84,927	227,869
					Format index (If)	x/1	124	1,489±0,038	0,424	28,47	1,000/1	3,333/1
					Profile index (Ip)	%	124	72,30±1,532	17,064	23,60	30	100
				SMB3*	Large diameter (LD)	µ	116	51,767±1,071	11,532	22,28	31,538	85,605
					Small diameter (Sd)	µ	116	35,158±0,738	7,948	22,61	18,022	56,066
					Average diameter ($D\bar{x}$)	µ	116	43,458±0,813	8,756	20,15	27,032	65,330
					PMB* perimeter	µ	116	136,602±2,559	27,561	20,18	84,924	205,240
					Format index (If)	x/1	116	1,511±0,032	0,340	22,48	1,000/1	2,857/1
					Profile index (Ip)	%	116	69,114±1,272	13,701	19,82	35	100
				SMB4*	Large diameter (LD)	µ	124	51,704±1,19	13,246	25,62	27,033	85,604
					Small diameter (Sd)	µ	124	35,106±0,884	9,842	28,03	18,022	63,077
					Average diameter ($D\bar{x}$)	µ	124	43,405±0,901	10,028	23,10	24,780	67,582
					PMB* perimeter	µ	124	136,369±2,831	31,522	23,12	77,849	212,315
					Format index (If)	x/1	124	1,544±0,042	0,470	30,44	1,000/1	3,500/1
					Profile index (Ip)	%	124	69,775±1,588	17,68	25,34	28,57	100,00
				SMB5*	Large diameter (LD)	µ	118	52,34±1,149	12,482	23,85	27,033	81,099
					Small diameter (Sd)	µ	118	36,227±0,816	8,862	24,46	18,022	54,066
					Average diameter ($D\bar{x}$)	µ	118	44,283±0,849	9,219	20,82	27,033	67,582
					PMB* perimeter	µ	118	139,12±2,667	28,962	20,82	84,927	212,315
					Format index (If)	x/1	118	1,493±0,036	0,387	25,95	1,000/1	2,667/1
					Profile index (Ip)	%	118	71,187±1,541	16,742	23,52	37,500	100,00

*SMB=secondary muscular fascicle.

Table 7.

Average statistical values for the thickness and profile of myocytes from secondary muscular fascicles, from lateral muscle, of *Polyodon spathula* fish

Specification		Secundary muscle fascicles studied for lateral muscle (average statistical values)					Average value of the five SMB*studied
Morphological parameters studied at myocytes level	MU	SMB_1	SMB_2	SMB_3	SMB_4	SMB_5	
Large diameter (LD)	µ	48,397	52,605	51,767	51,704	52,340	**51,363**
Small diameter (Sd)	µ	32,582	37,119	35,158	35,106	36,227	**35,238**
Average diameter ($D\bar{x}$)	µ	40,489	44,866	43,458	43,405	44,283	**43,300**
Perimeter (P)of myocytes	µ	127,200	140,950	136,602	136,369	139,120	**136,048**
Format index of myocytes	x/1	1,519/1	1,489/1	1,511/1	1,544/1	1,493/1	**1,5112/1**
Profile index of myocytes	%	69,14	72,30	69,114	69,775	71,187	**70,3032**

*FMS= secondary muscular fascicle.

Table 8.

Statistical significance of the differences between the five (5) secundary muscular fascicles of the lateral muscle of *Polyodon spathula*, regarding the thickness and profile of myocytes.

Studied parameters of myocytes	Differences between average values of the 5 SMB* compared	Tukey values(w'=0,01)	Statistical significance	At 4; 597 LL (liberty levels), for:			
				P	p≤0.05	p≤0.01	p≤0.001
				Fα	**2,370**	**3,320**	**4,620**
Large diameter of myocytes(µ)	SMB_1-SMB_2= 4,208	4,2523	**n.s.**	$\hat{F}$	**2,108297**		
	SMB_1-SMB_3=3,370	4,8939	**n.s.**				
	SMB_1-SMB_4=3,307	5,1400	**n.s.**				
	SMB_1-SMB_5=3,943	5,4400	**n.s.**				
	SMB_2-SMB_3=0,838	4,2894	**n.s.**				
	SMB_2-SMB_4=0,901	4,7734	**n.s.**				
	SMB_2-SMB_5=0,265	5,1622	**n.s.**				
	SMB_3-SMB_4=0,063	4,2894	**n.s.**				
	SMB_3-SMB_5=0,573	4,9143	**n.s.**				
	SMB_4-SMB_5=0,636	4,2705	**n.s.**				

Small diameter of myocytes (μ)	SMB_1-SMB_2=4,537	3,0536	**	$\hat{F}$	**4,174364**
	SMB_1-SMB_3=2,576	3,5144	**n.s.**		
	SMB_1-SMB_4=2,524	3,6898	**n.s.**		
	SMB_1-SMB_5=3,645	3,9069	**n.s.**		
	SMB_2-SMB_3=1,961	3,0802	**n.s.**		
	SMB_2-SMB_4=2,013	3,4278	**n.s.**		
	SMB_2-SMB_5=0,892	3,7070	**n.s.**		
	SMB_3-SMB_4=0,052	3,0802	**n.s.**		
	SMB_3-SMB_5=1,069	3,5290	**n.s.**		
	SMB_4-SMB_5=1,121	3,0667	**n.s.**		
Average diameter of myocytes (μ)	SMB_1-SMB_2=4,377	3,2264	**	$\hat{F}$	**3,6381587**
	SMB_1-SMB_3=2,969	3,7133	**n.s.**		
	SMB_1-SMB_4=2,916	3,9001	**n.s.**		
	SMB_1-SMB_5=3,794	4,1280	**n.s.**		
	SMB_2-SMB_3=1,408	3,2546	**n.s.**		
	SMB_2-SMB_4=1,461	3,6218	**n.s.**		
	SMB_2-SMB_5=0,583	3,9168	**n.s.**		
	SMB_3-SMB_4=0,053	3,2546	**n.s.**		
	SMB_3-SMB_5=0,825	3,7287	**n.s.**		
	SMB_4-SMB_5=0,878	3,2403	**n.s.**		
Perimeter of myocytes (μ)	SMB_1-SMB_2=13,750	10,1404	**	$\hat{F}$	**3,637561**
	SMB_1-SMB_3=9,402	11,6706	**n.s.**		
	SMB_1-SMB_4=9,169	12,2576	**n.s.**		
	SMB_1-SMB_5=11,920	12,9740	**n.s.**		
	SMB_2-SMB_3=4,348	10,2288	**n.s.**		
	SMB_2-SMB_4=4,581	11,3831	**n.s.**		
	SMB_2-SMB_5=1,830	12,3103	**n.s.**		
	SMB_3-SMB_4=0,233	10,2283	**n.s.**		
	SMB_3-SMB_5=2,518	11,7191	**n.s.**		
	SMB_4-SMB_5=2,751	10,1839	**n.s.**		
Format index of myocytes (Fi)(x/1)	SMB_1-SMB_2=0,030	0,1318	**n.s.**	$\hat{F}$	**0,386628**
	SMB_1-SMB_3=0,008	0,1516	**n.s.**		
	SMB_1-SMB_4=0,025	0,1593	**n.s.**		
	SMB_1-SMB_5=0,026	0,1686	**n.s.**		
	SMB_2-SMB_3=0,022	0,1329	**n.s.**		
	SMB_2-SMB_4=0,055	0,1479	**n.s.**		
	SMB_2-SMB_5=0,004	0,1600	**n.s.**		
	SMB_3-SMB_4=0,033	0,1329	**n.s.**		
	SMB_3-SMB_5=0,018	0,1523	**n.s.**		
	SMB_4-SMB_5=0,051	0,1323	**n.s.**		
Profile index of myocytes (Pi)(%)	SMB_1-SMB_2=3,160	5,2929	**n.s.**	$\hat{F}$	**0,918012**
	SMB_1-SMB_3=0,026	6,0916	**n.s.**		
	SMB_1-SMB_4=0,635	6,4775	**n.s.**		
	SMB_1-SMB_5=2,047	6,7719	**n.s.**		
	SMB_2-SMB_3=3,186	5,3391	**n.s.**		
	SMB_2-SMB_4=2,525	5,9416	**n.s.**		
	SMB_2-SMB_5=1,113	6,4255	**n.s.**		
	SMB_3-SMB_4=0,661	5,3390	**n.s.**		
	SMB_3-SMB_5=2,073	6,1169	**n.s.**		
	SMB_4-SMB_5=1,412	5,3156	**n.s.**		

*SMB=secondary muscular bundle (fascicle).

CONCLUSIONS

1. Diametrul mare al miocitelor din cele 5 FMS, ale mușchiului lateral-epaxial dorsal, la specia Polyodon spathula, are o valoaremedie de 51,363μ.
2. Diametrulmic al miocitelor din cele 5 FMS, ale mușchiului lateral-epaxial dorsal, la specia Polyodon spathula, are o valoaremedie de 35,238μ.
3. Diametrulmediu al miocitelor din cele 5 FMS, ale mușchiului lateral-epaxial dorsal, la specia Polyodon spathula, are o valoaremedie de 43,30μ.
4. Perimetrulmiocitelor din cele 5 FMS, ale mușchiului lateral-epaxial dorsal, la specia Polyodon spathula, are o valoaremedie de 136,048μ.

5. Valoareamedie a indicelui formatului, pentru miocitele din mușchiul studiat(lateral-epaxial dorsal), este de 1,5112/1, iar valoarea medie pentruindiceleprofiluluimiocitelor din acelașimușchieste de 70,303%.
6. Profilulmiocitelor din mușchiul lateral-epaxial dorsal, la specia Polyodon spathula, estecilindroid.
7. Mareamajoritate a diferențelor(95%) dintre cele 5(cinci) fascicule musculare secundare, pentru cei 6(șase) parametri studiați, la nivelul miocitelor, s-au dovedit a fi nesemnificative statistic.

REFERENCES

1. Carla Hassan-Williams, Timothy H. Bonner (2007). "*Polyodon spathula*". *Fishes of Texas Project and Online Database*. Texas National History Collection, a division of Texas Natural ScienceCenter, University of Texas at Austin. Retrieved June 19, 2014
2. Cecil A. Jennings, Steven J. Zigler (2009). Craig P. Paukert, George D. Scholten, ed. "Distribution, Ecology, and Life History; Biology and Life History of Paddlefish in North America: An Update" -*Paddlefish Management, Propagation, and Conservation in the 21st Century* (American Fisheries Society) **66** (1): 1–22. ISBN 978-1-934874-12-7.-June 18, 2014.
3. Cotea C.V., 2014 – *Biologie celulara, HistologieșiEmbriologiegeneralășispecială*, EdituraTehnopress, Iaşi.
4. SanduGh., 1995 – *Metode experimentaleînZootehnie*, Editura Coral Sanivet, Bucureşti, 134-139, 300-302, 317-319.
5. Simeanu, Cristina; Păsărin, B.; Simeanu, D.-2010 „*The study of some morphological characteristic of the sturgeon species of Polyodon spathula in different development stages".*Lucr. Științ. SeriaZootehnie, USAMV Iași, vol. 53, pg. 244-247.
6. Simeanu, Cristina; Simeanu, D.; Nistor, C.; Păsărin, B.-2011*" Evaluation of quantitative particularities of meat production at Polyodon spathula specie"*, Lucr. Științ. SeriaZootehnie, USAMV Iași, vol. 55, pg. 593-596.
7. Simeanu Cristina-2012-„*Contribuții la cunoaștereacalitățiicărniiobținută de la specia de sturioni Polyodon spathula, crescutăînbazinelepiscicole din Moldova",*Teză de Doctoratelaboratășisusținută la USAMV Iași, februarie 2012.
8. Spătaru, Mihaela-Claudia, 2009 – *Anatomia comparată a animalelor*, Editura Alfa, Iași, pg. 22-31; 121-127.
9. Teuşan V., Anca Teuşan, 2013 –"*Research on the thickness and profile of profound pectoral muscle myocites of meat-typehybrid hen COBB-500, slaughtered at different ages"*, Lucrări Ştiinţifice U.S.A.M.V.Iaşi, Seria Medicină-Veterinară, vol. 56, ISSN 1454-7406,pg.45-54.
10. Teuşan,Anca; Teuşan, V. 2014-„*Research on the histological structure of the deep pectoral muscle, of meat-type commercial hybrid Cobb-500, slaughtered at different ages".* First International Congress-*"Life Science- A Challenge for the Future",* held in Iasi(Romania),at " Ion Ionescu de la Brad" University of Agricultural Science and Veterinar Medicine, 23-24 October, 2014. Lucr. Științ. SeriaMedicinăVeterinară, USAMV Iași, vol.56(4), pg.174-185, ISSN 1454-7406.
11. Tudor Despina, Constantinescu Gh.M., 2002 – *NominaAnatomicaVeterinaria*, Ediţiebilingvă, EdituraVergiliu, Bucureşti.
12. Tudor Despina, Constantinescu Gh.M., Constantinescu Ileana, Cornilă N., 2010 – *NominaHistologica et EmbriologicaVeterinaria*, Ediţiebilingvă, EdituraVergiliu, Bucureşti.
13. *** *Tehnicahistopatologica*, Editura de Stat-RSR, pentruliteraturăștiințifică, 1953.
14. ****Investigațiahistologicăîn diagnostic veterinar*, Ediția-a-I-a București,1995, LCSV de Diagnostic- uz intern.

QUALITY EVALUATION OF FREEZE-DRIED AMMODYTES AMMODYTES VENOM BY CGE ON-A CHIP WITH LASER INDUCED FLUORESCENCE DETECTION

CAMELIA TULCAN, GEORGE TUDOR, OANA BOLDURA, MIRELA AHMADI, CALIN MIRCU, IOAN HUTU, CORNELIA MILOVANOV, MIHAI SĂRĂNDAN, SIMONA ZARCULA
Faculty of Veterinary Medicine1, University of Agricultural Sciences and Veterinary Medicine of Banat "The King of Michael I of Romania" from Timișoara Romania
calinmircu@usab-tm.ro

Abstract: *Our study represents the first attempt to develop a protocol for evaluating the quality freeze-dried venom by using current proteomics analysis techniques*
The research carried out represents the initial step in the validation of the method for protein analysis by capillary electrophoresis gel with laser induced fluorescence detection , being our first attempt in determine the impairment of protein fractions during long storage of the freeze-dried venom .
Freeze-drying was used as a method of advanced dehydration Ammodytes ammodytes venom and the yield of these procedure went up to 25.92 %.
On a long-term storage at -20 ° C freeze-dried venom of the factions protein degradation occurs , the most affected being that with the molecular weight of approx . 28 and 37 kDa , respectively identified as Vammin and phospholipase A2 , as demonstrated on the one hand, by decreasing the % of these fractions and on the other hand, by increasing the % of protein fractions obtained by degradation.

Key words*: ammodytes ammodytes venom, freeze-dry, CGE-on a chip*

The use of use of Ammodytes ammodytes viper venom in therapeutics has become a very topical subject (7,8,12), which is also exploited by the vipers farmers market in our country.

Processing by lyophilization of Ammodytes ammodytes viper venom is a preparing method for the conservation of this biological material with high value on pharmaceutical market (10, 14,17,19)..

Due to the lack of a widely accepted protocol for assessing the quality of the venom, the study proposed in this paper represents the first attempt to develop a protocol for assessing the quality of freeze-dried venom by using current techniques of proteomics analysis (2,6,15,16).

The research carried out started with the validation of the method for analysis of proteins by capillary electrophoresis in gel with detection in laser-induced fluorescence (18,21), in an attempt to first determine the impairment of protein fractions according to the duration of the storage of freeze-dried venom.

1. MATERIALS AND METHODS

1.1. Sampling

Venom samples were harvested on the farm Viperin Invest SRL Ineu, Arad county, which has a nest of 450 Ammodytes vipers and Ligia Borşanu Individual with a workstation in Marga village, Caras Severin county, with 30 Ammodytes ammodytes vipers.

Fig.1. Venom sampling

Samples were collected in sterile urine containers harvested by rubber membrane (Fig.1). The harvest period was 2013-2015, collected venom being stored at -20C until processed further. The samples were rated from 1 to 10 and their collection period is shown in Table 1.

Table 1.

Sample harvesting periods

Sample no.	1	2	3	4	5	6	7	8	9	10
Year/month of harvest	2015/ 01	2015/ 05	2015 /05	2015/ 05	2014/ 02	2014/ 06	2014/ 10	2014/ 11	2013/ 03	2013/ 06

1.2. Freeze-drying venom

Freeze drying venom samples was performed at USAMVBT Interdisciplinary Research Platform in the Biochemistry Research Laboratory.

The method includes the following steps: weighing of the initial liquid venom, freezing the vials and lyophilized, freeze-drying, homogenization of the final product, the final weighing. The freeze drying machine used was IlShin Europe, made in the Netherlands, model: Kryptonstraat 11 6718 WR EDE, lyophilization conditions are the following: -54ºC temperature, pressure of 5 mTorr for lyophilization time 48 hours.

The validation method was performed by determining the solid substance according to the standardized method at 103ºC (3).

The 10 samples were freeze-dried at the time of harvesting and were stored in a freezer at -20 ° C in Eppendorf tubes sealed with paraffin film in order to prevent the wetting of the samples. The yield of freeze-drying was calculated as a percentage of dry matter obtained based compared to the initial amount taken into it.

1.3. Determination of protein content

Protein content analysis was performed with the Thermo Scientific ™ Coomassie (Bradford) (22) protein test kit, a colorimetric method based on the property of Coomassie blue dye to bind proteins in an acidic environment with an immediate change of the absorption maximum from 465nm to 595nm and a color change from brown to blue.

Analysis was performed at the Interdisciplinary Research Platform in Biochemistry Research Laboratory using UV-VIS spectrophotometer Specord 210, Analytic Jena and data processing was performed with RidaWin software.

Protein concentrations were estimated by reference to the absorbance obtained for a dilutions series of protein standard which are analyzed together with unknown samples. Since the Coomassie color response is nonlinear with the protein concentration increases, a standard curve is required to complete each test.

The calibration curve is a 4 parameters curve type, made by 8 points, albumin concentrations in standards being 2000, 1500, 1000, 750, 500, 250, 125, 25 µg/ml.

The amount of sample used or standard is 30ul over which is 1.5ml Coomassie reagent pured and shaken. Incubate for 10 min. at room temperature and read against distilled water in the spectrophotometer set at 595nm. At the same time a blank is carried out where the sample is replaced with deionized water.

Quality control of the results was carried out with certified reference material Sigma Aldrich code A1933.

1.4. The analysis of proteins by capillary gel electrophoresis with laser-induced fluorescence detection

Analysis of samples of freeze-dried venom by capillary gel electrophoresis with laser induced fluorescence detection (CGE) was conducted in the USAMVBT`s Horia Cernescu Research Laboratories Complex - CLC-HC, in the Molecular Biology Laboratory (A2). The equipment used was a Agilent 2100 Bioanalizor and for the analysis of protein fractions a Protein 80kit kit of the same manufacturer (21) was used according to the method described by Halassy and colab. (9).

Ladder (standard fractions) has the following molecular weight values: 1.60, 3.5, 6.50, 15.00, 28.00, 46.00, 63.00, 95.00 kDa.

The steps in the test procedure are described in the insert kit and are the following: preparing the mixture of gel-dye, prepaping the discoloration solution, preparation the distortion solution, sample and the ladder preparation, charging the chip with the mixture of gel-dye and solution fade, loading the chip with ladder and testing, migration, writing of the analysis report.

2. RESULTS AND DISCUSSION

2.1. Lyophilization

Lyophilisation yield expresses the percentage of dry matter relative to the initial quantity. The water content of the samples was ranged from 78.4 to 74.08% (Figure 2). The literature indicates a variation of the parameter range between 70-80% (3, 13).

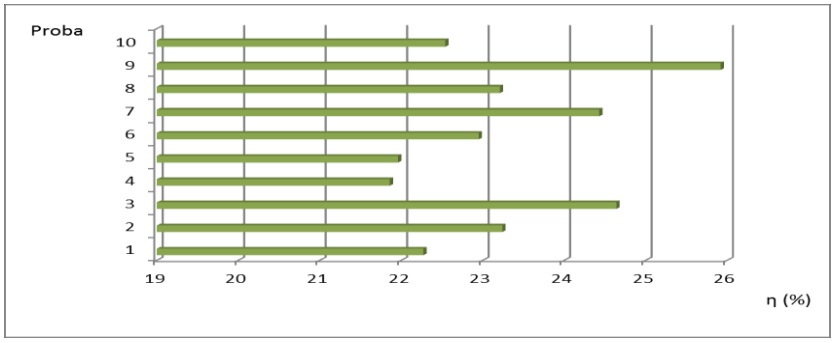

Fig. 2. Graphical representation of the variation in yield lyophilization

2.2. Analysis of protein content

The calibration curve obtained and its equation is shown in Figure 3, remarking the regression factor of the curve with a value of 0.995. Quality control of the results was ensured by using certified reference material Sigma-Aldrich, with a declared value of the protein content of over 98%. The value obtained for the reference material was 98.56%.

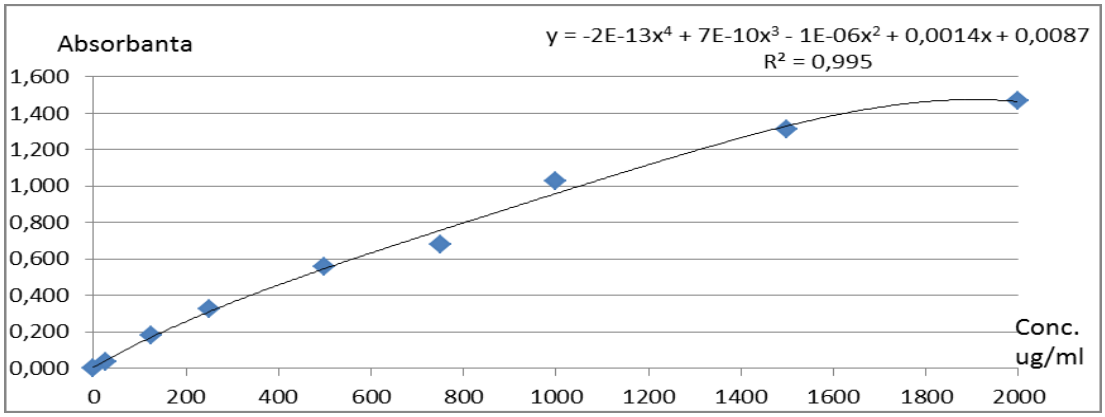

Fig 3. The calibration curve type 4 parameters - Blue Commasie method

The protein content of the analyzed samples ranged from 88.85 to 92.40 g%. Existing data in the literature on the analysis of the venom protein content of Ammodytes ammodytes indicate varying intervals depending on the method used. Thus, using the biuret method values in the range of 80-85% (3) wre obtained, while the values obtained using the Lowry method were over 95% (9).

By comparing the methods Comassie and Lowry, the values obtained were higher in the second case, this being attributed to false positives reaction of the phenolic reagent with low molecular weight phenolic compounds type from venom (11) .

The graphical representation of the variation of the protein content is given in Figure 4.

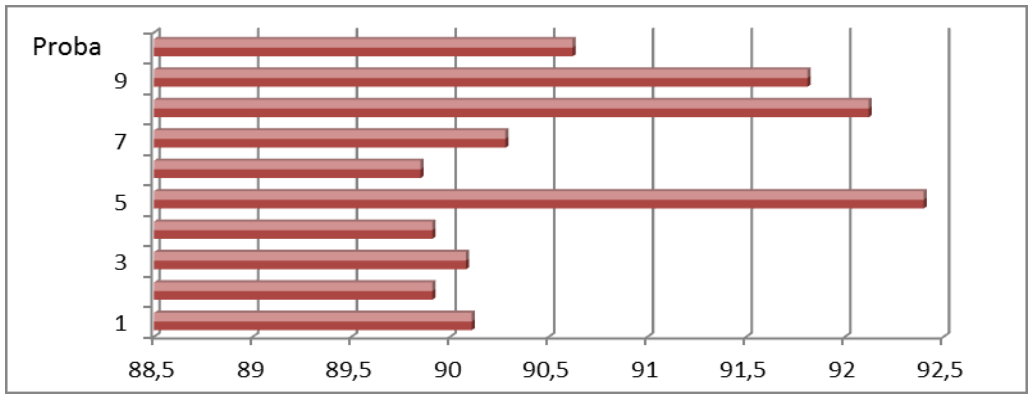

Fig. 4. Variation in protein content

2. 3. The analysis of proteins by capillary gel electrophoresis with laser-induced fluorescence detection

The gel obtained after migration is shown in Figure 5. The first position shows the ladder's migration and the next 10 correspond to the samples.

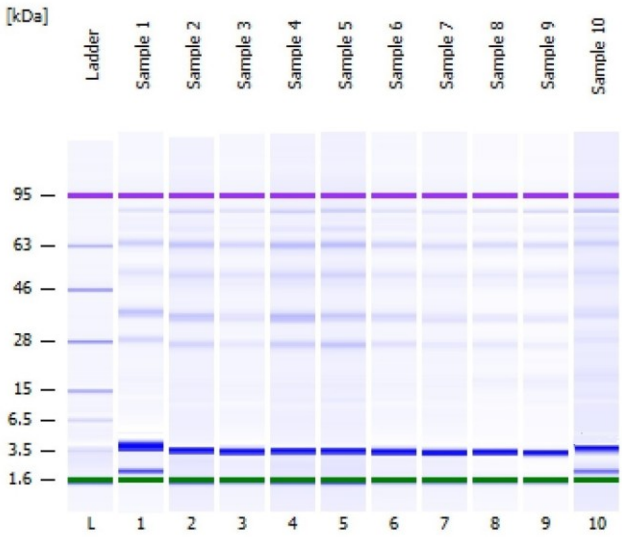

Fig5. Appearance of the gel after protein fractions migration

Percentage distribution analysis of the protein fractions identified 5 fractions of interest namely 28kDa, 37kDa, 53kDa, 64kDa and 85kDa, the difference being represented by other factions in a proportion not exceeding 3% for each of the values obtained are shown in Table 2. The marker is found at the lowest and the highest 1,6kDa to 95kDa. Peaks system are contained in the range of 2.2 and 3.5 kDa.

Table2

Protein fractions percentage distribution

Sample	Faction 28kDa	Faction 37 kDa	Faction 53 kDa	Faction 64 kDa	Faction 85 kDa	Other fractions
1	19,7	34,1	10,6	18,2	5,5	11,9
2	17,7	26,7	14,2	20,1	7,1	14,2
3	14	23,1	16,1	24,6	8,5	13,7
4	17,9	20,1	17	21	6,6	17,4
5	24,7	22,2	17,4	21,9	8,2	5,6
6	17,9	28,7	12,6	21,1	7,1	12,6
7	15	27,6	10,4	21,9	9,2	15,9
8	17,1	15,5	12,3	21,8	8,5	24,8
9	8,9	16,2	14,1	17,7	9,2	33,9
10	5,7	16,4	12,7	16,4	14,4	34,4

It is noted that the fraction of approx. 28kDa is deeply affected by storage period, the percentage of registered samples collected in 2013 were up 19% lower than the maximum value obtained from samples collected in 2015. Yamazaki and colab. have identified this fraction as V ammin (endotelio-vascular venom growth factor like) (20).

37kDa fraction corresponding to phospholipase A 2 (5, 9) also shows a decreasing trend, yielding 17.7% lower values than the maximum recorded in 2015 for freeze-dried samples.

The fraction of approximately 53kDa identified in the literature as belonging to the ammotidase (1, 2, 9), does not show any significant variation in the percentage of long-term storage. The same trend was registered and the fraction of approximately 64kDa.

In a comparative analysis of protein fractions stored from 2013 samples (Samples 9 and 10) compared to those in 2015 (samples 1-5) there is a considerable increase in the proportion of other cuts which may be an indicator of quality degradation of the venom during long storage, by proteolysis (Figure 6).

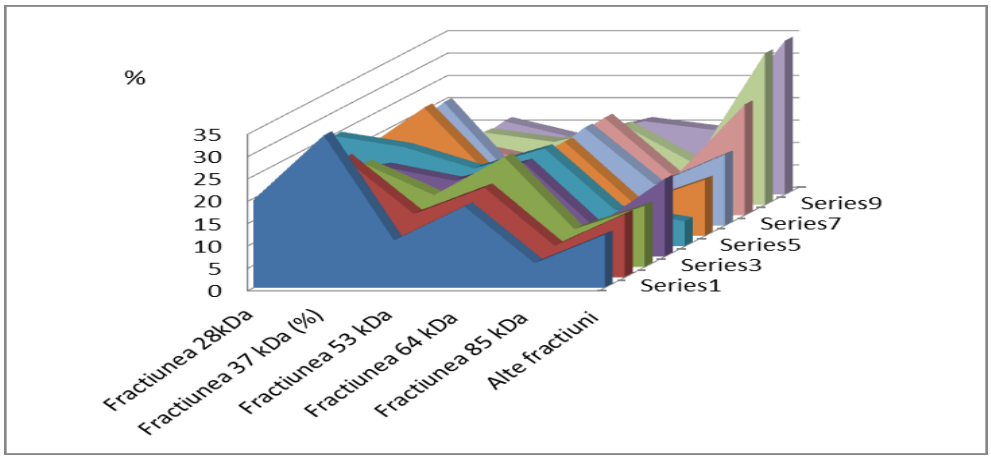

Fig 6. Comparative presentation of all factions in samples 1-10

3. CONCLUSIONS

3. 1. Freeze-drying used as a method of advanced dehydration of the Ammodytes ammodytes venom yielded a maximum of 25.92%.

3.2. The protein content of the freeze-dried venom varied in the 88.85 to 92.40 g% range.

3.3 In a long-term storage of freeze-dried venom at -20ºC, a degradation of the protein fraction appears, the most affected being the molecular weight of approx. 28 and 37 kDa, respectively identified as Vammin and phospholipase A2. After 3 years storage in this conditions, the degradation was demonstrated on the one hand by the % decrease of these fractions and on the other hand, by increasing the% of the protein fraction obtained by degradation.

REFERENCES

1. BONILLA, C., A., FAITH, M. R., MINTON, S. A. (1973) *Toxicon*, 12, 301-303.
2. BRAHMA, R.K., CLEARLY, R.J.R., KINI, M. R., DOLEY,R.(2015) *Venom gland trasncriptomics for identifying cataloging and characterizing venom proteins in snakes,* Toxicon, 93, 1-10.
3. CAPITANESCU, CRISTIAN (2001) *Cercetări privind biochimia veninului recoltat de la vipera Ammodytes ammodytes*, Editura Reduta.
4. COPLEY, A., BANERJEE, S., DEVI, A. (1973) *Studies of snake venom on blood coagulation*, Part I: *The thromboserpentin (thrombin like) enzyme În the venoms*, *Thromb. Res.* 2: 487, 508.
5. DEVI, A., (1968) *The protein and nonprotein constituents of snake venoms, Venomous Animals and Their Venoms*, vol. I, New York, Acad. Press, 119 – 165.
6. ECKERSALL, D., WHITFIELD., P.D. (2011) *Methods in Animal Proteomics,* Wiley Blackwell Ed.

7. FRY, B. (2015) Venomous Reptiles and Their Toxins: Evolution, Pathophysiology, and Biodiscovery, Oxford University Press.
8. HAVLICEK,V., SPIZEK, J. (2014), Natural Products Analysis: Instrumentation, Methods, and Applications, John Wiley and Sons Ed.
9. HALLASY, B., BRGLES, M., HABJANEC, L., BALIJA, M.L., KURTOVIC, T. (2011) Intraspecies variability in Vipera ammodytes ammodytes venom related to its toxicity and immunogenic potential, Comparative Biochemistry and Physiology, part , 153, 223-230.
10. HARVEY, A.L. (2014) Toxins and drug discovery, Toxicon 92, 193-200.
11. HOFFMAN D.R., JACOBSON R.S.(1984) Allergens in Hymenoptera venom XII:How much protein is in a sting?, Ann.of Allergy, 52, 276-278.
12. KING G. (2015) Venoms to Drugs: Venom as a Source for the Development of Human Therapeutic, The Royal Society of Chemistry, Thomas Graham House, Science Park, Milton Road, CambridgeCB4, 0WF, UK, 2015
13. MACKESSY, S. P. (2009) Handbook of venoms and toxins of reptiles, CRC Press London.
14. McCLEARY, R.J.R., KINI, MANJUNATHA, R.(2013) Non-enzymatic protein from snake venom: A gold mine of pharmacological tools and drug leads, Toxicon, 62, 56-74.
15. MEIER, J., STOCKER, K.F. (1991) Snake venom protein C activators. In: Tu, A., editor. Reptile venoms and Toxins. New York: Marcel Dekker. pp. 265–79.
16. MENEZ, A. (2002) Perspectives in molecular toxinology, Ed. John Wiley and Sons
17. PETKOVIC, D., JAVANOVIC, T., MICEVIC, D., UNKOVIC CVETKOVIC, N., CVETKOVIC, M. (1979) Action of Vipera ammodytes venom and its fractionation on the isolated rat heart. Toxicon, 17: 639–644.
18. SHERMAN, C.H. (2006) Microchip capillary electrophoresis: Methods and protocols, Ed. Springe.
19. TAN, N., H., PONNUDURAI, G. (1990) A comparative study of the biological properties of venoms from snakes of the genus Vipera (true adders) Comp. Biochem, Physiol., [B], 96, 683 – 688.
20. YAMAZAKI, Y., MATSUNAGA, Y., TOKUNAGA, Y., OBAYASHI, S., SAITO, M., MORITA, T. (2009) Snake Venomvascular endothelial growth factors (VEGF-FS)exclusively vary their structures and functions among species, J.of.Biol.Chem., 284, 15, 9885-9891.
21. *** Agilent Protein 80 kit Guide, http://www.chem.agilent.com, accesat în 23.02.2015.
22. *** Coomassie Plus™ (Bradford) Assay Kit, https://toolslifetechnologies.com accesat în data de 28.01.2013